

Recueil 2016

des activités du thème

"Archives et Traceurs"







Sommaire

Avant-Propos	1
Liste des publications 2016	3
publications de rang A	4
autres publications	7
Thèses soutenues en 2016	9
Cafés Sciences de 2016	13
Fiches illustrant les activités du thème	17
... sur la base des publications	18
... projets des thèses soutenues et des postdoctorats	71
... autres activités	79





Avant-propos

Ce recueil illustre les activités 2016 du thème "Archives et Traceurs".

Il contient la liste des publications 2016 impliquant des membres du thème, la liste des thèses soutenues et les animations scientifiques 2016 sous forme de Cafés Sciences. Il regroupe des fiches montrant les activités du thème: publications, développements technologiques et analytiques, projets portés par de jeunes chercheurs (doctorants et post-doctorants).

La mise en forme de ce recueil doit beaucoup à Célia Eschtruth, Valérie Daux, Catherine Kissel et les porteurs des activités illustrées par les fiches.



LISTE DES PUBLICATIONS 2016





Publications dans des revues de rang A

• Publication donnant lieu à une fiche ci-après

1. Antoine, P., Coutard, S., Guérin, G., Deschodt, L., Goval, E., Loch, J.-L. and Paris, C. (2016) Upper Pleistocene loess-palaeosol records from Northern France in the European context: Environmental background and dating of the Middle Palaeolithic. *Quaternary International* 411, 4-24.
2. Antoine, P., Moine, O., Rousseau, D. D., Lagroix, F., Kreutzer, S., Fuchs, M., Debret, M., Hatté, C., Gauthier, C., Svoboda, J. and Lisa, L. (2016) III. Loess-Palaeosol sequence DV-09 (Dolní Věstonice Brickyard). *Chronostratigraphy and Palaeoenvironments*, in: Svoboda, J. (Ed.), *Dolní Věstonice II – Chronostratigraphy, Palaeoethnology, Paleoanthropology*. Academy of Sciences of the Czech Republic, Institute of Archaeology at Brno, Brno, pp. 49-61.
3. Arnaud-Haond S., Van den Beld I.M.J., Becheler R., Orejas C., Menot L., Frank N., Grehan A., Bourillet J.F. (2016) Two "pillars" of cold-water coral reefs along Atlantic European margins: Prevalent association of *Madrepora oculata* with *Lophelia pertusa*, from reef to colony scale. *Deep-Sea Res. II*, doi: 10.1016/j.dsr2.2015.07.013
4. • Bazin, L., Landais, A., Capron, E., Masson-Delmotte, V., Ritz, C., Picard, G., Jouzel, J., Dumont, M., Leuenberger, M. and Prié, F. (2016) Phase relationships between orbital forcing and the composition of air trapped in Antarctic ice cores. *Climate of the Past* 12, 729-748.
5. Beckler, J.S., Kiriazis, N., Rabouille, C., Stewart, F.J. and Taillefert, M. (2016) Importance of microbial iron reduction in deep sediments of river-dominated continental-margins. *Marine Chemistry* 178, 22-34.
6. • Berger, A., Landais, A. ... Masson-Delmotte, V. et al. (2016) Interglacials of the last 800,000 years, *Reviews of Geophysics*, 54, 162-164.
7. • Boëda, E., Rocca, R., Da Costa, A., Fontugne, M., Hatté, C., Clemente-Conte, I., Santos, J.C., Lucas, L., Felice, G., Lourdeau, A., Villagran, X., Gluchy, M., Ramos, M.P., Viana, S., Lahaye, C., Guidon, N., Griggo, C., Pino, M., Pessis, A.-M., Borges, C. and Gato, B. (2016) New Data on a Pleistocene Archaeological Sequence in South America: Toca do Sítio do Meio, Piauí, Brazil. *PaleoAmerica* 2, 286-302.
8. • Bolliet, T., Brockmann, P., Masson-Delmotte, V., Bassinot, F., Daux, V., Genty, D., Landais, A., Lavrieux, M., Michel, E., Ortega, P., Risi, C., Roche, D.M., Vimeux, F. and Waelbroeck, C. (2016) Water and carbon stable isotope records from natural archives: a new database and interactive online platform for data browsing, visualizing and downloading. *Climate of the Past* 12, 1693-1719.
9. • Burckel, P., Waelbroeck, C., Luo, Y., Roche, D.M., Pichat, S., Jaccard, S.L., Gherardi, J., Govin, A., Lippold, J. and Thil, F. (2016) Changes in the geometry and strength of the Atlantic meridional overturning circulation during the last glacial (20–50 ka). *Climate of the Past* 12, 2061-2075.
10. • Caricchi, C., Cifelli, F., Kissel, C., Sagnotti, L. and Mattei, M. (2016) Distinct magnetic fabric in weakly deformed sediments from extensional basins and fold-and-thrust structures in the Northern Apennine orogenic belt (Italy). *Tectonics* 35, 238-256.
11. • Casado, M., Cauquoin, A., Landais, A., Israel, D., Orsi, A., Pangui, E., Landsberg, J., Kerstel, E., Prié, F. and Doussin, J.-F. (2016) Experimental determination and theoretical framework of kinetic fractionation at the water vapour–ice interface at low temperature. *Geochimica et Cosmochimica Acta* 174, 54-69.
12. • Casado, M., Landais, A., Masson-Delmotte, V., Genthon, C., Kerstel, E., Kassi, S., Arnaud, L., Picard, G., Prié, F., Cattani, O., Steen-Larsen, H.-C., Vignon, E. and Cermak, P. (2016) Continuous measurements of isotopic composition of water vapour on the East Antarctic Plateau. *Atmospheric Chemistry and Physics* 16, 8521-8538.
13. • Cauquoin A., Jean-Baptiste P., Risi C., Fourré E., Landais A. (2016) Modeling the global bomb tritium transient signal with the AGCM LMDZ-iso: A method to evaluate aspects of the hydrological cycle. *Journal of Geophysical Research*, 121, 12612-12129
14. • Chen, Q., Kissel, C., Govin, A., Liu, Z. and Xie, X. (2016) Correction of interstitial water changes in calibration methods applied to XRF core-scanning major elements in long sediment cores: Case study from the South China Sea. *Geochemistry, Geophysics, Geosystems* 17, 1925-1934.
15. Churakova, O.V., Shashkin, A.V., Siegwolf, R.T.W., Spahni, R., Launois, T., Saurer, M., Bryukhanova, M.V., Benkova, A.V., Kuptsova, A.V., Peylin, P., Vaganov, E.A., Masson-Delmotte, V. and Roden, J. (2016) Application of eco-physiological models to the climatic interpretation of $\delta^{13}\text{C}$ and $\delta^{18}\text{O}$ measured in Siberian larch tree-rings. *Dendrochronologia* 39, 51-59.



16. Closset, I., Cardinal, D., Rembauville, M., Thil, F. and Blain, S. (2016) Unveiling the Si cycle using isotopes in an iron-fertilized zone of the Southern Ocean: from mixed-layer supply to export. *Biogeosciences* 13, 6049-6066.
17. Coularis C., Tisnérat-Laborde N., Pastor L., Siclet F., Fontugne M., (2016) Temporal and Spatial Variations of Freshwater Reservoir ages in the Loire River watershed. *Radiocarbon*, 58(3), 549-563. DOI: <https://doi.org/10.1017/RDC.2016.36>
18. Daëron, M., Blamart, D., Peral, M. and Affek, H.P. (2016) Absolute isotopic abundance ratios and the accuracy of $\Delta 47$ measurements. *Chemical Geology* 442, 83-96.
19. Delunel, R., Blard, P.-H., Martin, L.C.P., Nomade, S. and Schlunegger, F. (2016) Long term low latitude and high elevation cosmogenic ^3He production rate inferred from a 107ka-old lava flow in northern Chile; 22°S-3400ma.s.l. *Geochimica et Cosmochimica Acta* 184, 71-87.
20. Dezileau, L., Pérez-Ruzafe, A., Blanchemanche, P., Degeai, J.-P., Raji, O., Martinez, P., Marcos, C. and Von Grafenstein, U. (2016) Extreme storms during the last 6500 years from lagoonal sedimentary archives in the Mar Menor (SE Spain). *Climate of the Past* 12, 1389-1400.
21. Dittmann, A., Schlosser, E., Masson-Delmotte, V., Powers, J.G., Manning, K.W., Werner, M. and Fujita, K. (2016) Precipitation regime and stable isotopes at Dome Fuji, East Antarctica. *Atmospheric Chemistry and Physics* 16, 6883-6900.
22. Dubois-Dauphin, Q., Bonneau, L., Colin, C., Montero-Serrano, J.-C., Montagna, P., Blamart, D., Hebbeln, D., van Rooij, D., Pons-Branchu, E., Hemsing, F., Wefing, A.-M. and Frank, N. (2016) South Atlantic intermediate water advances into the North-east Atlantic with reduced Atlantic meridional overturning circulation during the last glacial period. *Geochemistry, Geophysics, Geosystems* 17.
23. Fersi W., Bassinot F., Lézine A.-M. (2016) Past productivity variations and organic carbon burial in the Gulf of Aden since the Last Glacial Maximum. *Quaternaire*, 27/3, 213-226.
24. Fersi, W., Lézine, A.-M. and Bassinot, F. (2016) Hydro-climate changes over southwestern Arabia and the Horn of Africa during the last glacial–interglacial transition: A pollen record from the Gulf of Aden. *Review of Palaeobotany and Palynology* 233, 176-185.
25. Fournier, L., Fauquembergue, K., Zaragosi, S., Zorzi, C., Malaizé, B., Bassinot, F., Joussain, R., Colin, C., Morenon, E. and Leparmentier, F. (2016) The Bengal fan : External controls on the Holocene Active Channel turbidite activity, The Holocene, 1-14, DOI : 10.1177/0959683616675938.
26. Fournier, L., Fauquembergue, K., Zaragosi, S., Zorzi, C., Malaizé, B., Bassinot, F., Joussain, R., Colin, C., Moreno, E., Leparmentier F. (2016) The Bengal fan: External controls on the Holocene Active Channel turbidite activity. *Geochemistry, Geophysics, Geosystems*, 17, 3207–3223.
27. Freeman, E., Skinner, L.C., Waelbroeck, C., Hodell, D., (2016) Radiocarbon evidence for enhanced respired carbon storage in the Atlantic at the Last Glacial Maximum. *Nature Communications*, 7:11998. doi: 10.1038/ncomms11998.
28. Frery, E., Gratier, J.-P., Ellouz-Zimmerman, N., Deschamps, P., Blamart, D., Hamelin, B. and Swennen, R. (2016) Geochemical transect through a travertine mount: A detailed record of CO₂-enriched fluid leakage from Late Pleistocene to present-day – Little Grand Wash fault (Utah, USA). *Quaternary International*.
29. Gottschalk, J., L.C. Skinner, J. Lippold, H. Vodel, N. Frank, S. L. Jaccard, C. Waelbroeck (2016), Biological and physical controls in the Southern Ocean on past millennial-scale atmospheric CO₂ change, *Nature Communications* 7, 10.1038/ncomms11539, 2016.
30. Goude, G. and Fontugne, M. (2016) Carbon and nitrogen isotopic variability in bone collagen during the Neolithic period: Influence of environmental factors and diet. *Journal of Archaeological Science* 70, 117-131.
31. Guillou, H., V.Scao, S. Nomade (2016) Blake excursion at Vulcano (Aeolian Islands, Italy): Revised K-Ar and $^{40}\text{Ar}/^{39}\text{Ar}$ ages. *Quaternary Geochronology*, 35, 77-87.
32. Haddam, N.A., Michel, E., Siani, G., Cortese, G., Bostock, H.C., Duprat, J.M. and Isguder, G. (2016) Improving past sea surface temperature reconstructions from the Southern Hemisphere oceans using planktonic foraminiferal census data. *Paleoceanography* 31, 822-837.
33. Hamre, S.S. and Daux, V. (2016) Stable oxygen isotope evidence for mobility in medieval and post-medieval Trondheim, Norway. *Journal of Archaeological Science: Reports* 8, 416-425.
34. Hansen, J., Sato, M., Hearty, P., Ruedy, R., Kelley, M., Masson-Delmotte, V., Russell, G., Tselioudis, G., Cao, J., Rignot, E., Velicogna, I., Tormey, B., Donovan, B., Kandiano, E., von Schuckmann, K., Kharecha, P., Legrande, A.N., Bauer, M. and Lo, K.-W. (2016) Ice melt, sea level rise and superstorms: evidence from paleoclimate data, climate




- modeling, and modern observations that 2 °C global warming could be dangerous. *Atmospheric Chemistry and Physics* 16, 3761-3812.
35. Jagercikova, M., Cornu, S., Bourlès, D., Evrard, O., Hatté, C. and Balesdent, J. (2016) Quantification of vertical solid matter transfers in soils during pedogenesis by a multi-tracer approach. *Journal of Soils and Sediments* 17, 408-422.
36. Jaubert, J., Verheyden, S., Genty, D., Soulier, M., Cheng, H., Blamart, D., Burlet, C., Camus, H., Delaby, S., Deldicque, D., Edwards, R.L., Ferrier, C., Lacrampe-Cuyaubere, F., Leveque, F., Maksud, F., Mora, P., Muth, X., Regnier, E., Rouzaud, J.N. and Santos, F. (2016) Early Neanderthal constructions deep in Bruniquel Cave in southwestern France. *Nature* 534, 111-114.
37. Jean-Baptiste, P., Allard, P., Fourré, E., Bani, P., Calabrese, S., Aiuppa, A., Gauthier, P.J., Parello, F., Pelletier, B. and Garaebiti, E. (2016) Spatial distribution of helium isotopes in volcanic gases and thermal waters along the Vanuatu (New Hebrides) volcanic arc. *Journal of Volcanology and Geothermal Research* 322, 20-29.
38. Jean-Baptiste, P., Lavielle, B., Fourré, E., Smith, T., Pagel, M. (2016) Vertical distribution of helium and $^{40}\text{Ar}/^{36}\text{Ar}$ in porewaters of the Eastern Paris Basin (Bure/Haute Marne): constraints on transport processes through the sedimentary sequence. *Geological Society Special Publications* 443. Doi: 10.1144/SP443.25
39. Jones, J.M., Gille, S.T., Goosse, H., Abram, N.J., Canziani, P.O., Charman, D.J., Clem, K.R., Crosta, X., de Lavergne, C., Eisenman, I., England, M.H., Fogt, R.L., Frankcombe, L.M., Marshall, G.J., Masson-Delmotte, V., Morrison, A.K., Orsi, A.J., Raphael, M.N., Renwick, J.A., Schneider, D.P., Simpkins, G.R., Steig, E.J., Stenni, B., Swingedouw, D. and Vance, T.R. (2016) Assessing recent trends in high-latitude Southern Hemisphere surface climate. *Nature Climate Change* 6, 917-926.
40. Joussain, R., Colin, C., Liu, Z., Meynadier, L., Fournier, L., Fauquembergue, K., Zaragosi, S., Schmidt, F., Rojas, V. and Bassinot, F. (2016) Climatic control of sediment transport from the Himalayas to the proximal NE Bengal Fan during the last glacial-interglacial cycle. *Quaternary Science Reviews* 148, 1-16.
41. Kheirbeik, L., Hatté, C. and Balesdent, J. (2016) Labelled microbial culture as a calibration medium for $(13)\text{C}$ -isotope measurement of derivatized compounds: application to tert-butyldimethylsilyl amino acids. *Rapid Commun Mass Spectrom* 30, 1991-2001.
42. Kissel, C., Liu, Z., Li, J. and Wandres, C. (2016) Magnetic minerals in three Asian rivers draining into the South China Sea: Pearl, Red, and Mekong Rivers. *Geochemistry, Geophysics, Geosystems* 17, 1678-1693.
43. Konn C., Fourré E., Jean-Baptiste P., Donval J.P., Guyader V., Birot D., Alix A.S., Gaillot A., Perez F., Dapoigny A., Pelleter E., Resing J.-A., Charlou J.-L., Fouquet Y. and scientific parties (2016) Extensive hydrothermal activity revealed by multi-tracer survey in the Wallis and Futuna region (SW Pacific). *Deep Sea Research I*, 116, 127-144.
44. Labuhn I., Daux V. Genty D. (2016) A multi-proxy approach to drought reconstruction. *Quaternaire*, 27/3, 239-247.
45. Labuhn, I., Daux, V., Girardclos, O., Stievenard, M., Pierre, M. and Masson-Delmotte, V. (2016) French summer droughts since 1326 CE: a reconstruction based on tree ring cellulose $\delta^{18}\text{O}$. *Climate of the Past* 12, 1101-1117.
46. Landais A. (2016) Reconstruction du climat et de l'environnement des derniers 800 000 ans à partir des carottes de glace – variabilité orbitale et millénaire. *Quaternaire*, 27/3, 197-212.
47. Landais, A., Masson-Delmotte, V., Capron, E., Langebroek, P.M., Bakker, P., Stone, E.J., Merz, N., Raible, C.C., Fischer, H., Orsi, A., Prié, F., Vinther, B. and Dahl-Jensen, D. (2016) How warm was Greenland during the last interglacial period? *Climate of the Past* 12, 1933-1948.
48. Lavergne, A., Daux, V., Villalba, R., Pierre, M., Stievenard, M., Vimeux, F. and Srur, A.M. (2016) Are the oxygen isotopic compositions of *Fitzroya cupressoides* and *Nothofagus pumilio* cellulose promising proxies for climate reconstructions in northern Patagonia? *Journal of Geophysical Research: Biogeosciences* 121, 767-776.
49. Lavergne, A., Daux, V., Villalba, R., Pierre, M., Stievenard, M., and Srur, A.M. (2016) Improvement of isotope-based climate reconstructions in Patagonia through a better understanding of climate influences on isotopic fractionation in tree rings. *Earth Planet. Sci. Lett.* 459, 372-380.
50. Lazareth, C.E., Soares-Pereira, C., Douville, E., Brahmi, C., Dissard, D., Le Cornec, F., Thil, F., Gonzalez-Roubaud, C., Caquineau, S. and Cabioch, G. (2016) Intra-skeletal calcite in a live-collected *Porites* sp.: Impact on environmental proxies and potential formation process. *Geochimica et Cosmochimica Acta* 176, 279-294.
51. Lazzerini, N., Lécuyer, C., Amiot, R., Angst, D., Buffetaut, E., Fourel, F., Daux, V., et al. (2016) Oxygen isotope fractionation between bird eggshell calcite and body water: application to fossil eggs from Lanzarote (Canary Islands). *The Science of Nature* 103:81.



52. Le Gall, M., Evrard, O., Foucher, A., Laceby, J.P., Salvador-Blanes, S., Thil, F., Dapoigny, A., Lefevre, I., Cerdan, O. and Ayrault, S. (2016) Quantifying sediment sources in a lowland agricultural catchment pond using (137)Cs activities and radiogenic (87)Sr/(86)Sr ratios. *Sci Total Environ* 566-567, 968-980.
53. Leicher, N., Zanchetta, G., Sulpizio, R., Giaccio, B., Wagner, B., Nomade, S., Francke, A. and Del Carlo, P. (2016) First tephrostratigraphic results of the DEEP site record from Lake Ohrid (Macedonia and Albania). *Biogeosciences* 13, 2151-2178.
54. Lippold, J., Gutjahr, M., Blaser, P., Christner, E., de Carvalho Ferreira, M.L., Mulitza, S., Christl, M., Wombacher, F., Böhm, E., Antz, B., Cartapanis, O., Vogel, H. and Jaccard, S.L. (2016) Deep water provenance and dynamics of the (de)glacial Atlantic meridional overturning circulation. *Earth and Planetary Science Letters* 445, 68-78.
55. • Lourdeau, A., Carbonera, M., Pereira Santos, M.C., Hoeltz, S., Fontugne, M., Hatté, C., et al. (2016) Pré-história na foz do rio Chapecó. *Estudos arqueológicos regionais*, 29(45), doi: <http://dx.doi.org/10.22562/2016.45.09>.
56. • Lynch-Stieglitz J. I. Takamitsu, E. Michel, 2016, Antarctic Density Stratification and the Strength of the Circumpolar Current during the Last Glacial Maximum, *Paleoceanography*, 31, 539-552, doi:10.1002/2015PA002915.
57. • Marchal, O., Waelbroeck, C. and Colin de Verdière, A. (2016) On the Movements of the North Atlantic Subpolar Front in the Preinstrumental Past. *Journal of Climate* 29, 1545-1571.
58. • Marra, F., Rohling, E.J., Florindo, F., Jicha, B., Nomade, S., Pereira, A. and Renne, P.R. (2016) Independent ⁴⁰Ar/³⁹Ar and ¹⁴C age constraints on the last five glacial terminations from the aggradational successions of the Tiber River, Rome (Italy). *Earth and Planetary Science Letters* 449, 105-117.
59. Martínez, D.E., Fourré, E., Londoño, O.M.Q., Jean-Baptiste, P., Galli, M.G., Dapoigny, A. and Grondona, S.I. (2016) Residence time distribution in a large unconfined–semiconfined aquifer in the Argentine Pampas using ³H/³He and CFC tracers. *Hydrogeology Journal* 24, 1107-1120.
60. Menier, D., Estournès, G., Mathew, M.J., Ramkumar, M., Briend, C., Siddiqui, N., Traini, C., Pian, S. and Labeyrie, L. (2016) Relict geomorphological and structural control on the coastal sediment partitioning, North of Bay of Biscay. *Zeitschrift für Geomorphologie* 60, 67-74.
61. Michel, V., Valladas, H., Shen, G., Wang, W., Zhao, J.X., Shen, C.C., Valensi, P. and Bae, C.J. (2016) The earliest modern Homo sapiens in China? *J Hum Evol* 101, 101-104.
62. • Mügler, C., Jean-Baptiste, P., Perez, F. and Charlou, J.L. (2016) Modeling of hydrogen production by serpentinization in ultramafic-hosted hydrothermal systems: Application to the Rainbow field. *Geofluids* 16, 476-489.
63. Naughton, F., Sanchez Goñi, M.F., Rodrigues, T., Salgueiro, E., Costas, S., Desprat, S., Duprat, J., Michel, E., Rossignol, L., Zaragosi, S., Voelker, A.H.L. and Abrantes, F. (2016) Climate variability across the last deglaciation in NW Iberia and its margin. *Quaternary International* 414, 9-22.
64. Nicoud, E., Aureli, D., Pagli, M., Villa, V., Chaussé, C., Agostini, S., Bahain, J.-J., Boschian, G., Degeai, J.-P., Fusco, F., Giaccio, B., Hernandez, M., Kuzucuoglu, C., Lahaye, C., Lemorini, C., Limondin-Lozouet, N., Mazza, P., Mercier, N., Nomade, S., Pereira, A., Robert, V., Rossi, M.A., Virmoux, C. and Zupancich, A. (2016) Preliminary data from Valle Giumentina Pleistocene site (Abruzzo, Central Italy): A new approach to a Clactonian and Acheulian sequence. *Quaternary International* 409, 182-194.
65. • Nomade, S., Genty, D., Sasco, R., Scao, V., Feruglio, V., Baffier, D., Guillou, H., Bourdier, C., Valladas, H., Reigner, E., Debard, E., Pastre, J.F. and Geneste, J.M. (2016) A 36,000-Year-Old Volcanic Eruption Depicted in the Chauvet-Pont d'Arc Cave (Ardeche, France)? *PLoS One* 11, e0146621.
66. Nomade, S., Scao, V., Guillou, H., Messenger, E., Mgeladze, A., Voinchet, P., Renne, P.R., Courtin-Nomade, A., Bardintzeff, J.M., Ferring, R. and Lordkipanidze, D. (2016) New ⁴⁰Ar/³⁹Ar, unspiked K/Ar and geochemical constraints on the Pleistocene magmatism of the Samtskhe-Javakheti highlands (Republic of Georgia). *Quaternary International* 395, 45-59.
67. Ollivier, V., Fontugne, M., Lyonnet, B. and Chataigner, C. (2016) Base level changes, river avulsions and Holocene human settlement dynamics in the Caspian Sea area (middle Kura valley, South Caucasus). *Quaternary International* 395, 79-94.
68. PAGES, Past Interglacial Workin Group (2016) Interglacials of the last 800,000 years. *Reviews of Geophysics* 54, 162-219.
69. Paul, A., Hatté, C., Pastor, L., Thiry, Y., Siclet, F. and Balesdent, J. (2016) Hydrogen dynamics in soil organic matter as determined by ¹³C and ²H labeling experiments. *Biogeosciences*, 13, 6587-6598.



70. • Pereira, A., Nomade, S., Shao, Q., Bahain, J.-J., Arzarello, M., Douville, E., Falguères, C., Frank, N., Garcia, T., Lembo, G., Muttillio, B., Scao, V. and Peretto, C. (2016) 40Ar/39Ar and ESR/U-series dates for Guado San Nicola, Middle Pleistocene key site at the Lower/Middle Palaeolithic transition in Italy. *Quaternary Geochronology* 36, 67-75.
71. Peretto, C., Arzarello, M., Bahain, J.-J., Boulbes, N., Dolo, J.-M., Douville, E., Falguères, C., Frank, N., Garcia, T., Lembo, G., Moigne, A.-M., Muttillio, B., Nomade, S., Pereira, A., Rufo, M.A., Sala, B., Shao, Q., Thun Hohenstein, U., Tessari, U., Turrini, M.C. and Vaccaro, C. (2016) The Middle Pleistocene site of Guado San Nicola (Monteroduni, Central Italy) on the Lower/Middle Palaeolithic transition. *Quaternary International* 411, 301-315.
72. Petrenko, V.V., Severinghaus, J.P., Schaefer, H., Smith, A.M., Kuhl, T., Baggenstos, D., Hua, Q., Brook, E.J., Rose, P., Kulin, R., Bauska, T., Harth, C., Buizert, C., Orsi, A., Emanuele, G., Lee, J.E., Brailsford, G., Keeling, R. and Weiss, R.F. (2016) Measurements of ^{14}C in ancient ice from Taylor Glacier, Antarctica constrain in situ cosmogenic $^{14}\text{CH}_4$ and ^{14}CO production rates. *Geochimica et Cosmochimica Acta* 177, 62-77.
73. Pleurdeau, D., Moncel, M.-H., Pinhasi, R., Yeshurun, R., Higham, T., Agapishvili, T., Bokeria, M., Muskhelishvili, A., Le Bourdonnec, F.-X., Nomade, S., Poupeau, G., Bocherens, H., Frouin, M., Genty, D., Pierre, M., Pons-Branchu, E., Lordkipanidze, D. and Tushabramishvili, N. (2016) Bondi Cave and the Middle-Upper Palaeolithic transition in western Georgia (south Caucasus). *Quaternary Science Reviews* 146, 77-98.
74. Poisson, A., B. Vrielynck, R. Wernli, A. Negri, M.A. Bassetti, Y. Büyükmeriç, S. Özer, H. Guillou, K.S. Kavak, H. Temiz, F. Orszag-Sperber (2016). Miocene transgression in the central and eastern parts of the Sivas Basin (Central Anatolia, Turkey) and the Cenozoic palaeogeographical evolution. *International Journal of Earth Sciences*. 105(1), 339-368
75. Povinec, P.P., Liong Wee Kwong, L., Kaizer, J., Molnar, M., Nies, H., Palcsu, L., Papp, L., Pham, M.K. and Jean-Baptiste, P. (2016) Impact of the Fukushima accident on tritium, radiocarbon and radiocesium levels in seawater of the western North Pacific Ocean: A comparison with pre-Fukushima situation. *J Environ Radioact* 166, 56-66.
76. • Prud'homme, C., Lécuyer, C., Antoine, P., Moine, O., Hatté, C., Fourel, F., Martineau, F. and Rousseau, D.-D. (2016) Palaeotemperature reconstruction during the Last Glacial from $\delta^{18}\text{O}$ of earthworm calcite granules from Nussloch loess sequence, Germany. *Earth and Planetary Science Letters* 442, 13-20.
77. • Quiles, A., Valladas, H., Bocherens, H., Delqué-Količ, E., Kaltnecker, E., van der Plicht, J., Delannoy, J.-J., Feruglio, V., Fritiz, C., Monney, J., Philippe, M., Tosello, G., Clottes, J. and Geneste, J.-M. (2016) A high-precision chronological model for the decorated Upper Paleolithic cave of Chauvet-Pont d'Arc, Ardèche, France. *Proceedings of the National Academy of Sciences of the United States of America* 113, 4670-4675.
78. Rabouille, C., Olu, K., Baudin, F., Khripounoff, A., Dennielou, B., Arnaud-Haond, S., Babonneau, N., Bayle, C., Beckler, J., Bessette, S., Bombled, B., Bourgeois, S., Brandily, C., Caprais, J.C., Cathalot, C., Charlier, K., Corvaisier, R., Croguennec, C., Cruaud, P., Decker, C., Droz, L., Gayet, N., Godfroy, A., Hourdez, S., Le Bruchec, J., Le Saout, J., Lesaout, M., Lesongeur, F., Martinez, P., Mejanelle, L., Michalopoulos, P., Mouchel, O., Noel, P., Pastor, L., Picot, M., Pignet, P., Pozzato, L., Pruski, A.M., Rabiller, M., Raimonet, M., Ragueneau, O., Reyss, J.L., Rodier, P., Ruesch, B., Ruffine, L., Savignac, F., Senyarch, C., Schnyder, J., Sen, A., Stetten, E., Sun, M.Y., Tallefert, M., Teixeira, S., Tisnerat-Laborde, N., Toffin, L., Tourolle, J., Toussaint, F., Vétion, G., Jouanneau, J.M. and Bez, M. (2016) The Congolobe project, a multidisciplinary study of Congo deep-sea fan lobe complex: Overview of methods, strategies, observations and sampling. *Deep Sea Research Part II: Topical Studies in Oceanography*.
79. • Rassmann, J., Lansard, B., Pozzato, L. and Rabouille, C. (2016) Carbonate chemistry in sediment porewaters of the Rhône River delta driven by early diagenesis (northwestern Mediterranean). *Biogeosciences* 13, 5379-5394.
80. Regattieri, E., Giaccio, B., Galli, P., Nomade, S., Peronace, E., Messina, P., Sposato, A., Boschi, C. and Gemelli, M. (2016) A multi-proxy record of MIS 11–12 deglaciation and glacial MIS 12 instability from the Sulmona basin (central Italy). *Quaternary Science Reviews* 132, 129-145.
81.  Ritter, F., Steen-Larsen, H.C., Werner, M., Masson-Delmotte, V., Orsi, A., Behrens, M., Birnbaum, G., Freitag, J., Risi, C. and Kipfstuhl, S. (2016) Isotopic exchange on the diurnal scale between near-surface snow and lower atmospheric water vapor at Kohnen station, East Antarctica. *The Cryosphere* 10, 1647-1663.
82. • Roberts, J., Gottschalk, J., Skinner, L.C., Peck, V.L., Kender, S., Elderfield, H., Waelbroeck, C., Vázquez Riveiros, N. and Hodell, D.A. (2016) Evolution of South Atlantic density and chemical stratification across the last deglaciation. *Proceedings of the National Academy of Sciences of the United States of America* 113, 514-519.
83. Robin, A.K., Mouralis, D., Akköprü, E., Gratuze, B., Kuzucuoğlu, C., Nomade, S., Pereira, A., Doğu, A.F., Erturaç, K. and Khalidi, L. (2016) Identification and characterization of two new obsidian sub-sources in the Nemrut volcano



(Eastern Anatolia, Turkey): The Sicaksu and Kayacik obsidian. *Journal of Archaeological Science: Reports* 9, 705-717.

84. Roy-Barman, M. and Pons-Branchu, E. (2016) Improved U–Th dating of carbonates with high initial ^{230}Th using stratigraphical and coevality constraints. *Quaternary Geochronology* 32, 29-39.
85. Ruan, J., Kherbouche, F., Genty, D., Blamart, D., Cheng, H., Dewilde, F., Hachi, S., Edwards, R.L., Régnier, E., Michelot, J.-L. (2016) Evidence of a prolonged drought ca. 4200 yrBP correlated with prehistoric settlement abandonment from the Gueldaman GLD1 Cave, Northern Algeria. *Climate of the Past*, 12, 1, pp 1-14.
86. Sagnotti, L., Giancarlo Scardia, Biagio Giaccio, Joseph C. Liddicoat, Sébastien Nomade, Paul R. Renne, Courtney J. Sprain (2016). How fast was the Matuyama-Brunhes geomagnetic reversal? A new sub-centennial record from the Sulmona Basin, central Italy". *Geophysical Journal International*. 204 798-812
87. Samaniego, P., Rivera, M., Mariño, J., Guillou, H., Liorzou, C., Zerathe, S., Delgado, R., Valderrama, P. and Scao, V. (2016) The eruptive chronology of the Ampato–Sabancaya volcanic complex (Southern Peru). *Journal of Volcanology and Geothermal Research* 323, 110-128.
88. Schreuder, L.T., Beets, C.J., Prins, M.A., Hatté, C. and Peterse, F. (2016) Late Pleistocene climate evolution in Southeastern Europe recorded by soil bacterial membrane lipids in Serbian loess. *Palaeogeography, Palaeoclimatology, Palaeoecology* 449, 141-148.
89. Selçuk, A.S., Erturaç, M.K. and Nomade, S. (2016) Geology of the Çaldıran Fault, Eastern Turkey: Age, slip rate and implications on the characteristic slip behaviour. *Tectonophysics* 680, 155-173.
90. Simon, Q., Thouveny, N., Bourlès, D., Valet, J.-P., Bassinot, F., Ménabréaz, L., Guillou, V., , Choy, S., and Beaufort, L. (2016) Authigenic $^{10}\text{Be}/^{9}\text{Be}$ ratio signatures of the cosmogenic nuclide production linked to geomagnetic dipole moment variation since the Brunhes/Matuyama boundary, *J. Geophys. Res. : Solid Earth*, 121, 7716-7741.
91. Stenni, B., Scarchilli, C., Masson-Delmotte, V., Schlosser, E., Ciardini, V., Dreossi, G., Grigioni, P., Bonazza, M., Cagnati, A., Karlicek, D., Risi, C., Udisti, R. and Valt, M. (2016) Three-year monitoring of stable isotopes of precipitation at Concordia Station, East Antarctica. *The Cryosphere* 10, 2415-2428.
92. Tamburrino, S., Insinga, D.D., Pelosi, N., Kissel, C., Laj, C., Capotondi, L. and Sprovieri, M. (2016) Tephrochronology of a ~70ka-long marine record in the Marsili Basin (southern Tyrrhenian Sea). *Journal of Volcanology and Geothermal Research* 327, 23-39.
93. Tany, C., Valet, J.-P., Carlu, J., Bassinot, F. and Zaragosi, S. (2016) Acquisition of detrital magnetization in four turbidites, *Geochem. Geophys. Geosyst.*, 17, 3207-3223. doi : 10.1002/2016GC006378
94. Thil, F., Blamart, D., Assailly, C., Lazareth, C.E., Leblanc, T., Butsher, J. and Douville, E. (2016) Development of laser ablation multi-collector inductively coupled plasma mass spectrometry for boron isotopic measurement in marine biocarbonates: new improvements and application to a modern *Porites* coral. *Rapid Commun Mass Spectrom* 30, 359-371.
95. Touzeau, A., Landais, A., Stenni, B., Uemura, R., Fukui, K., Fujita, S., Guilbaud, S., Ekaykin, A., Casado, M., Barkan, E., Luz, B., Magand, O., Teste, G., Le Meur, E., Baroni, M., Savarino, J., Bourgeois, I. and Risi, C. (2016) Acquisition of isotopic composition for surface snow in East Antarctica and the links to climatic parameters. *The Cryosphere* 10, 837-852.
96. Ujiie, Y., Asahi, H., Sagawa, T. and Bassinot, F. (2016) Evolution of the North Pacific Subtropical Gyre during the past 190 kyr through the interaction of the Kuroshio Current with the surface and intermediate waters, *Paleoceanography*, 31(11), 1498-1513, doi: 10.1002/2015PA002914
97. Vancampenhout, K., Schellekens, J., Slaets, J., Hatté, C. and Buurman, P. (2016) Fossil redox-conditions influence organic matter composition in loess paleosols. *Quaternary International* 418, 105-115.
98. Varela, D.E., Brzezinski, M.A., Beucher, C.P., Jones, J.L., Giesbrecht, K.E., Lansard, B. and Mucci, A. (2016) Heavy silicon isotopic composition of silicic acid and biogenic silica in Arctic waters over the Beaufort shelf and the Canada Basin. *Global Biogeochemical Cycles* 30, 804-824.
99. Vázquez Riveiros, N., Govin, A., Waelbroeck, C., Mackensen, A., Michel, E., Moreira, S., Bouinot, T., Caillon, N., Orgun, A. and Brandon, M. (2016) Mg/Ca thermometry in planktic foraminifera: Improving paleotemperature estimations for *G. bulloides* and *N. pachyderma* left. *Geochemistry, Geophysics, Geosystems* 17, 1249-1264.
100. Victorero, L., Blamart, D., Pons-Branchu, E., Mavrogordato, M.N. and Huvenne, V.A.I. (2016) Reconstruction of the formation history of the Darwin Mounds, N Rockall Trough: How the dynamics of a sandy contourite affected cold-water coral growth. *Marine Geology* 378, 186-195.



101. Villa, P., Soriano, S., Grun, R., Marra, F., Nomade, S., Pereira, A., Boschian, G., Pollarolo, L., Fang, F. and Bahain, J.J. (2016) The Acheulian and Early Middle Paleolithic in Latium (Italy): Stability and Innovation. *PLoS One* 11, e0160516.
102. Villa, V., Pereira, A., Chaussé, C., Nomade, S., Giaccio, B., Limondin-Lozouet, N., Fusco, F., Regattieri, E., Degeai, J.-P., Robert, V., Kuzucuoglu, C., Boschian, G., Agostini, S., Aureli, D., Pagli, M., Bahain, J.J. and Nicoud, E. (2016) A MIS 15-MIS 12 record of environmental changes and Lower Palaeolithic occupation from Valle Giumentina, central Italy. *Quaternary Science Reviews* 151, 160-184.
103. Yau, A.M., Bender, M.L., Blunier, T. and Jouzel, J. (2016) Setting a chronology for the basal ice at Dye-3 and GRIP: Implications for the long-term stability of the Greenland Ice Sheet. *Earth and Planetary Science Letters* 451, 1-9.
104. Zaïbi, C., Kamoun, F., Viehberg, F., Carbonel, P., Jedoui, Y., Abida, H. and Fontugny, M. (2016) Impact of relative sea level and extreme climate events on the Southern Skhira coastline (Gulf of Gabes, Tunisia) during Holocene times: Ostracodes and foraminifera associations' response. *Journal of African Earth Sciences* 118, 120-136.
105. Zhang, Y., Zhang, X., Chiessi, C.M., Mulitza, S., Zhang, X., Lohmann, G., Prange, M., Behling, H., Zabel, M., Govin, A., Sawakuchi, A.O., Cruz, F.W. and Wefer, G. (2016) Equatorial Pacific forcing of western Amazonian precipitation during Heinrich Stadial 1. *Sci Rep* 6, 35866.



Autres publications

(les articles "discussions" ci-dessous n'ont pas de pendant publié en 2016)

1. Ayache, M., Dutay, J.-C., Mouchet, A., Tisnérat-Laborde, N., Montagna, P., Tanhua, T., Siani, G. and Jean-Baptiste, P. (2016) High resolution regional modeling of natural and anthropogenic radiocarbon in the Mediterranean Sea. *Biogeosciences Discussions*, 1-31.
2. Bréant, C., Martinerie, P., Orsi, A., Arnaud, L. and Landais, A. (2016) Modelling the firn thickness evolution during the last deglaciation: constraints on sensitivity to temperature and impurities. *Climate of the Past Discussions*, 1-36.
3. Bügelmayr-Blaschek, M., D. M. Roche, H. Renssen and C. Waelbroeck (2016) Disentangling the effect of ocean temperatures and isotopic content on the oxygen-isotope signals in the North Atlantic Ocean during Heinrich Event 1 using a global climate model (2016), *Climate of the Past Discussion*, doi:10.5194/cp-2016-31.
4. Ekaykin, A.A., Vladimirova, D.O., Lipenkov, V.Y. and Masson-Delmotte, V. (2016) Climatic variability in Princess Elizabeth Land (East Antarctica) over the last 350 years. *Climate of the Past Discussions*, 1-21.
5. Govin, A., Vázquez Riveiros, N., Réaud, Y., Waelbroeck C. and Giraudeau J. (2016) Unprecedented coring performance with the upgraded Research Vessel *Marion Dufresne*. *PAGES News*, 24, 27.
6. Hansen, J., Sato, M., Kharecha, P., von Schuckmann, K., Beerling, D.J., Cao, J., Marcott, S., Masson-Delmotte, V., Prather, M.J., Rohling, E.J., Shakun, J. and Smith, P. (2016) Young People's Burden: Requirement of Negative CO₂ Emissions. *Earth System Dynamics Discussions*, 1-40.
7. Hatté, C. (2016) Le carbone sous toutes ses formes. *Biofutur* 379, 30.
8. Hatté, C. and Balesdent, J. (2016) Carbone des sols et changements globaux : des impacts réciproques. *Biofutur* 379, 28-30.
9. Mary, Y., Eynaud, F., Colin, C., Rossignol, L., Brocheray, S., Mojtahid, M., Garcia, J., Peral, M., Howa, H., Zaragosi, S. and Cremer, M. (2016) Changes in Holocene meridional circulation and poleward Atlantic flow: the Bay of Biscay as a nodal point. *Climate of the Past Discussions*, 1-30.
10. Moriarty, J.M., Harris, C.K., Rabouille, C., Fennel, K., Friedrichs, M.A.M. and Xu, K. (2016) The Roles of Resuspension, Diffusion and Biogeochemical Processes on Oxygen Dynamics Offshore of the Rhone River, France: A Numerical Modeling Study. *Biogeosciences Discussions*, 1-39.
11. Raisbeck, G.M., Cauquoin, A., Jouzel, J., Landais, A., Petit, J.R., Lipenkov, V.Y., Beer, J., Synal, H.A., Oerter, H., Johnsen, S.J., Steffensen, J.P., Svensson, A. and Yiou, F. (2016) An improved North-South synchronization of ice core records around the 41 K beryllium 10 peak. *Climate of the Past Discussions*, 1-22.
12. Tisnérat-Laborde, N. and Hatté, C. (2016) ECHOMICADAS, un nouvel outil pour analyser le carbone 14. *Biofutur* 379, 32.



THÈSES SOUTENUES EN 2016





- thèse donnant lieu à une fiche ci-après

LAVERGNE Aliénor

soutenue le 8 janvier 2016

Evaluation de l'archives naturelle cernes d'arbre comme traceur du climat passé au nord de la Patagonie

COULARIS Cindy

soutenue le 23 juin 2016

Dynamique et transfert du carbone dans le bassin versant de la Loire: traçage par les isotopes du carbone

CASADO Mathieu

soutenue le 6 septembre 2016

Water stable isotopic composition on the East Antarctic Plateau : measurements at low temperature of the vapour composition, utilisation as an atmospheric tracer and implication for paleoclimate studies

RUAN Jiaoyang

soutenue le 16 septembre 2016

Characterization of Holocene climate variability in the west of Europe and Mediterranean basin using high resolution stalagmite records

- **FERSI Wiem**

soutenue le 30 septembre 2016

Reconstitution de la variabilité de la mousson indienne et ses impacts environnementaux sur le Nord-Ouest de la Mer d'Arabie et ses bordures continentales depuis le Dernier Maximum Glaciaire

- **RASSMAN Jens**

soutenue le 28 novembre 2016

La chimie des carbonates à l'interface eau sédiment dans l'océan côtier sous l'influence de la diagenèse précoce et l'acidification des océans

- **KAYVANTASH Dariouche**

soutenue le 28 novembre 2016

Traçage physico-chimique des oxydes de fer dans le bassin de la Seine

- **HADDAM Naoufel**

soutenue le 12 décembre 2016

Rôle de l'Océan Austral dans les échanges de Carbone depuis la dernière Déglaciation : approche Géochimique et Micropaléontologique

- **CHEN Quan**

soutenue le 8 décembre 2016

Past south-east Asian Monsoon variability and oceanic circulation in the South China Sea







Cafés-science de 2016

sous l'impulsion de l'équipe 2016 d'organisation des Cafés Sciences:

Alison Pereira, Marion Péral, Laurine Drugat, Clément Outrequin





COP21 : les enjeux pour le GIEC

Valérie Masson-Delmotte

le 5 janvier 2016

Les saumures dans le cycle du carbone

Elisabeth Michel & Bruno Lansard

le 3 février 2016

Glaciologie

Amaëlle Landais, Anals Orsi, Frédéric Prié, Camille Bréant

le 2 mars 2016

Café Sciences "spécial EGU"

Catherine Kissel, Amaëlle Landais, Etienne Guilpart, Jens Rassmann

le 12 avril 2016

Café Sciences "spécial stagiaires"

avec les stagiaires d'IUT, de master 1 et 2

le 2 juin 2016

Le projet et la mission ACCLIMATE

Claire Waelbroeck et l'équipe ACCLIMATE

le 6 juillet 2016

La composition isotopique de l'eau sur le plateau Est-Antarctique

Mathieu Casado

le 30 août 2016

Archéométrie en grotte

Hélène Valladas, Dominique Genty, Sébastien Nomade

le 3 octobre 2016

Les projets d'acquisition d'instruments dans le cadre de PANOPLY

Aline Govin et Catherine Kissel; Anaïs Orsi et Sébastien Nomade; Sophie Ayrault et Eric Douville

le 22 novembre 2016





Fiches illustrant les activités 2016





***... sur la base des publications
2016***

Phase relationships between orbital forcing and the composition of air trapped in Antarctic ice cores

L. Bazin, A. Landais, E. Capron, V. Masson-Delmotte, C. Ritz et al.

Climate of the Past, 12, 729-748. 2016.

Orbital tuning is central for ice core chronologies beyond annual layer counting, available back to 60 ka (i.e. thousands of years before 1950) for Greenland ice cores. While several complementary orbital tuning tools have recently been developed using $\delta^{18}\text{O}_{\text{atm}}$, $\delta\text{O}_2/\text{N}_2$ and air content with different orbital targets, quantifying their uncertainties remains a challenge. Indeed, the exact processes linking variations of these parameters, measured in the air trapped in ice, to their orbital targets are not yet fully understood. Here, we provide new series of $\delta\text{O}_2/\text{N}_2$ and $\delta^{18}\text{O}_{\text{atm}}$ data encompassing Marine Isotopic Stage (MIS) 5 (between 100 and 160 ka) and the oldest part (340–800 ka) of the East Antarctic EPICA Dome C (EDC) ice core. For the first time, the measurements over MIS 5 allow an inter-comparison of $\delta\text{O}_2/\text{N}_2$ and $\delta^{18}\text{O}_{\text{atm}}$ records from three East Antarctic ice core sites (EDC, Vostok and Dome F). This comparison highlights some site-specific $\delta\text{O}_2/\text{N}_2$ variations. Such an observation, the evidence of a 100 ka periodicity in the $\delta\text{O}_2/\text{N}_2$ signal and the difficulty to identify extrema and mid-slopes in $\delta\text{O}_2/\text{N}_2$ increase the uncertainty associated with the use of $\delta\text{O}_2/\text{N}_2$ as an orbital tuning tool, now calculated to be 3–4 ka. When combining records of $\delta^{18}\text{O}_{\text{atm}}$ and $\delta\text{O}_2/\text{N}_2$ from Vostok and EDC, we find a loss of orbital signature for these two parameters during periods of minimum eccentricity (~ 400 ka, ~ 720 –800 ka). Our data set reveals a time-varying offset between $\delta\text{O}_2/\text{N}_2$ and $\delta^{18}\text{O}_{\text{atm}}$

records over the last 800 ka that we interpret as variations in the lagged response of $\delta^{18}\text{O}_{\text{atm}}$ to precession. The largest offsets are identified during Terminations II, MIS 8 and MIS 16, corresponding to periods of destabilization of the Northern polar ice sheets. We therefore suggest that the occurrence of Heinrich-like events influences the response of $\delta^{18}\text{O}_{\text{atm}}$ to precession.

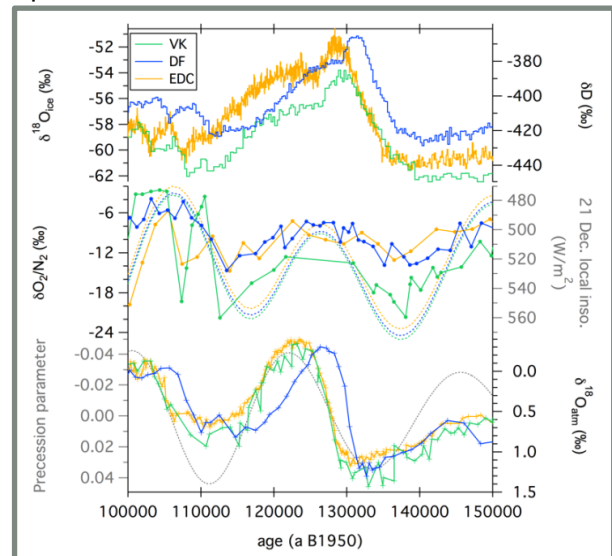


Fig. 1. : Inter-comparison of Vostok (green), Dome F (blue) and EDC (yellow) data covering MIS 5. Vostok and EDC data are presented on AICC2012 (Bazin et al., 2013, Veres et al., 2013) and Dome F on the DFO-2006 chronology (Kawamura et al., 2007). Top: water isotopic composition (Vostok $\delta^{18}\text{O}_{\text{ice}}$: Petit et al., 1999, Dome F $\delta^{18}\text{O}_{\text{ice}}$: Kawamura et al., 2007, EDC δD : Jouzel et al., 2007). Middle: $\delta\text{O}_2/\text{N}_2$ records and local summer solstice insolation at each site (Suwa and Bender 2008, Kawamura et al., 2007, this study). Bottom: $\delta^{18}\text{O}_{\text{atm}}$ and precession parameter shifted by 5 ka (Suwa and Bender 2008, Kawamura et al., 2007, Landais et al., 2013, this study).

Interglacials of the last 800,000 years

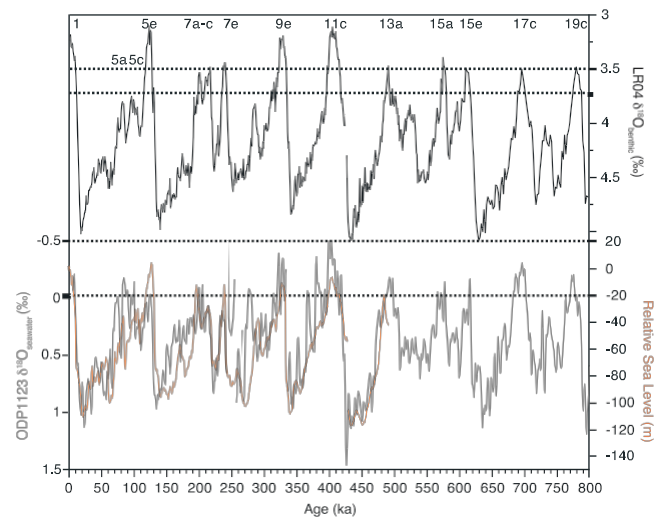
A. Berger, ..., A. Landais, ... V. Masson-Delmotte et al.

Reviews of Geophysics, 54, 162-164, 2016.

Interglacials, including the present (Holocene) period, are warm, low land ice extent (high sea level), end-members of glacial cycles. Based on a sea level definition, we identify eleven interglacials in the last 800,000 years. Data compilations suggest that despite spatial heterogeneity, Marine Isotope Stages (MIS) 5e (last interglacial) and 11c (~400 ka ago) were globally strong (warm), while MIS 13a (~500 ka ago) was cool at many locations. A step change in strength of interglacials at 450 ka is apparent only in atmospheric CO₂ and in Antarctic and deep ocean temperature. The onset of an interglacial (glacial termination) seems to require a reducing precession parameter (increasing Northern Hemisphere summer insolation), but this condition alone is insufficient. Terminations involve rapid nonlinear reactions of ice volume, CO₂, and temperature to external astronomical forcing. The precise timing of events may be modulated by millennial-scale climate change that can lead to a contrasting timing of maximum interglacial intensity in each hemisphere. The end of an interglacial (glacial inception) is a slower process involving a global sequence of changes. Interglacials have been typically 10-30 ka long. The combination of minimal reduction in northern summer insolation over the next few orbital cycles, owing to low eccentricity, and high atmospheric greenhouse gas concentrations implies that the next glacial

inception is many tens of millennia in the future.

Fig. 1. Definition of interglacials based on sea level. (top)



$\delta^{18}\text{O}$ of benthic foraminifera in the LR04 stack [Lisiecki and Raymo, 2005]; (bottom) probability maximum Red Sea relative sea level [Rohling et al., 2009] (orange line); and deconvolved $\delta^{18}\text{O}$ of seawater [Elderfield et al., 2012] (grey line). Marine Isotopic substages of interglacial status are indicated (as well as interstadials MIS 5a and 5c). Note that there is some confusion in the literature about the lettering of substages in MIS 9 and 15. Here we use the substage numbering recommended in a recent paper [Raisbeck et al., 2015], such that the oldest substages in MIS 9 and 15 are 9e and 15e. Dashed lines mark values discussed in the text that might be used in the definition of interglacials.



New data on a Pleistocene Archaeological sequence in South America: Toca do Sítio do Meio, Piauí, Brazil

E. Boëda, R. Rocca, A. da Costa, M. Fontugne, C. Hatté, et al.

PaleoAmerica, 2(4), 286-302, 2016.

Sítio do Meio, discovered in the 1990s, showed a sedimentary sequence clearly composed of two sets of deposits separated by a zone of large rockfall from the massive collapse of the shelter's overhang. The bottom set, slightly more than 60 cm thick, was trapped between the bedrock (upon which it rested) and the lower part of the roof fall (reaching more than 1 m in the excavation area), and yielded some charcoal without other archaeological material. New excavations, however, have revealed the presence of artifacts, additional charcoal, and an alignment of sandstone blocks providing clear boundaries for the artifact concentration. The typological and technological composition of the artifacts is classic, with tools made by shaping high-quality quartz pebbles and tools made on shaping chips or on chips obtained by bipolar percussion of quartz blocks. Quartzite was also used, but only in the manufacture of larger tools, of certain types. The toolkit is made of several convergent pieces, denticulates, rostres, scrapers, and end scrapers. Radiocarbon dating results indicate a Pleistocene age, corresponding to the end of the mid-Upper Pleistocene (MIS3). These dates confirm that Sítio do Meio is the seventh Pleistocene stratigraphic sequence known from a 20km-radius zone, coming from different sedimentary horizons, testifying to a human presence that extends from MIS3 until the middle Holocene, in this region of Piauí.

Particularly, we observed that this occupation still has periodic gaps, with phases of occupation occurring in either short or long periods. With the new data, we are able to consider the cultural specificities of each set in the context of climate data to better understand the diversity of occupation within a single territory, for example behavioral variation in the management of space, adaptive responses to environmental pressures, or both at the same time.

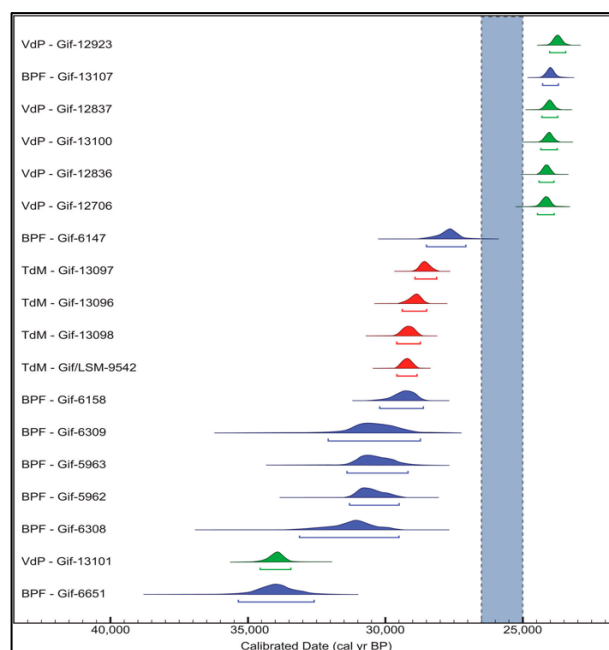


Fig. 1: Statistical representation of radiocarbon data from three sites: Boqueirão da Pedra Furada (BPF, blue), Vale da Pedra (VdP, green), and Toca do Sítio do Meio (TdM, red) (from data presented in Tables 1 and 2). The set of dates used for the dating of BPF comes from old excavations (Guidon and Parenti), except for 13107 Gif date, which comes from the new excavations since 2011.



An interactive tool for navigation within a database of water and carbon stable isotope records from natural archives.

T. Bolliet, P. Brockmann, V. Masson-Delmotte V., F. Bassinot F., V. Daux, D. Genty, A. Landais, M. Lavrieux, E. Michel, P. Ortega, C. Risi, D. Roche, F. Vimeux, C. Waelbroeck

Climate of the Past 12, 1693-1719, 2016 and <http://climateproxiesfinder.ipsl.fr>

Past climate is an important benchmark to assess the ability of climate models to simulate key processes and feedback. Model–data comparisons can help to constrain the uncertainties associated with transfer functions. We have put together a global database of proxy records of oxygen ($\delta^{18}\text{O}$), hydrogen (δD) and carbon ($\delta^{13}\text{C}$) stable isotopes from different archives: ocean and lake sediments, corals, ice cores, speleothems and tree-ring cellulose. Source records were obtained from the georeferenced PANGAEA and NOAA libraries, complemented by additional data obtained from a literature survey. About 3000 source records were screened for chronological information and temporal resolution of proxy records. Altogether, this database consists of hundreds of dated $\delta^{18}\text{O}$, $\delta^{13}\text{C}$ and δD records in a standardized simple text format, complemented with a metadata Excel catalog. This compilation effort highlights the need to homogenize and structure the format of datasets and chronological information as well as enhance the distribution of published datasets that are currently highly fragmented and scattered. In the last part, we illustrate the type of application allowed by our database by comparing several key periods highly investigated by the paleoclimate community. We focus on records spanning the past 200

years, the mid-Holocene (MH, 5.5–6.5 ka; calendar kiloyears before 1950), the Last Glacial Maximum (LGM, 19–23 ka), and those spanning the last interglacial period (LIG, 115–130 ka). Basic statistics have been applied to characterize anomalies between these different periods. Most changes from the MH to present day and from LIG to MH appear statistically insignificant. Significant global differences are reported from LGM to MH with regional discrepancies in signals from different archives and complex patterns.

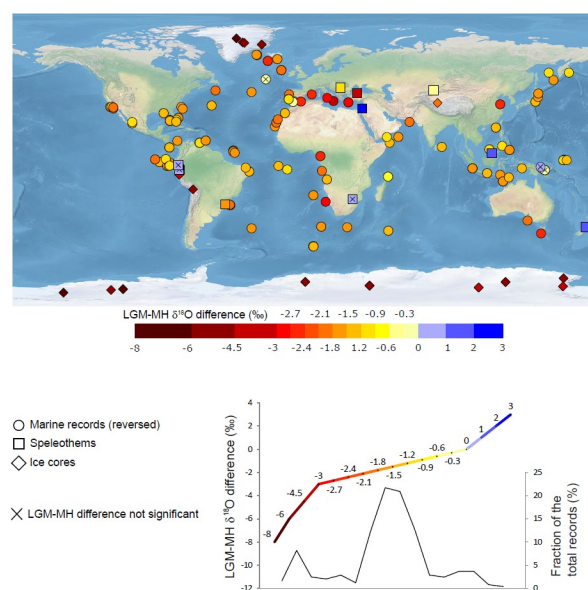


Fig. Top: location of $\delta^{18}\text{O}$ records spanning the LGM and MH. Bottom: color scale and fraction of records as a function of LGM-MH $\delta^{18}\text{O}$ anomaly.

Changes in the geometry and strength of the Atlantic Meridional Overturning Circulation during the last glacial (20–50 ka)

P. Burckel, C. Waelbroeck, Y. Luo, D. Roche, S. Pichat, S. Jaccard, J. Gherardi, A. Govin, J. Lippold, F. Thil

Climate of the Past, Vol. 12 : 2061-2075, 2016.

We reconstruct the geometry and strength of the Atlantic meridional overturning circulation during the Heinrich stadial 2 and three Greenland interstadials of the 20-50 ka period based on the comparison of new and published sedimentary $^{231}\text{Pa}/^{230}\text{Th}$ data with simulated sedimentary $^{231}\text{Pa}/^{230}\text{Th}$. We show that the deep Atlantic circulation during these interstadials was very different from that of the Holocene. Northern-sourced waters likely circulated above 2500 m depth, with a flow rate lower than that of the present-day North Atlantic deep water (NADW). Southern-sourced deep waters most probably flowed northwards below 4000 m depth into the North Atlantic basin and then southwards as a return flow between 2500 and 4000 m depth. The flow rate of this southern-sourced deep water was likely larger than that of the modern Antarctic bottom water (AABW). Our results further show that during Heinrich stadial 2, the deep Atlantic was probably directly affected by a southern-sourced water mass below 2500 m depth, while a slow, southward-flowing water mass originating from the North Atlantic likely influenced depths between 1500 and 2500 m down to the equator.

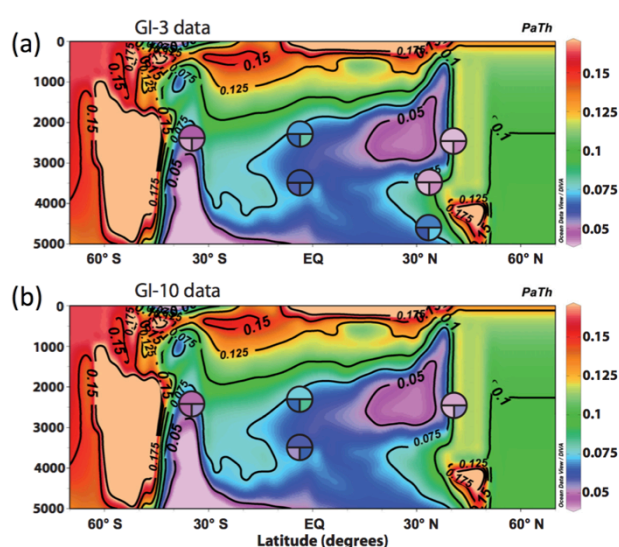


Fig. 1. Comparison of Pa/Th data for each of the time slices with the simulated Pa/Th values using the shallow overturning stream function. Time slices are Greenland Interstadial-3 (a) and GI-10 (b). The upper half of the circles represents the Pa/Th mean value, the lower left quarter, the mean value -1σ , and the lower right quarter represents the mean value $+1\sigma$.

Magnetic fabric in weakly deformed sediments from Northern Apennine orogenic belt (Italy)

C. Caricchi, F. Cifelli, C. Kissel, L. Sagnotti, and M. Mattei

Tectonics, 35, 238-256, 2016.

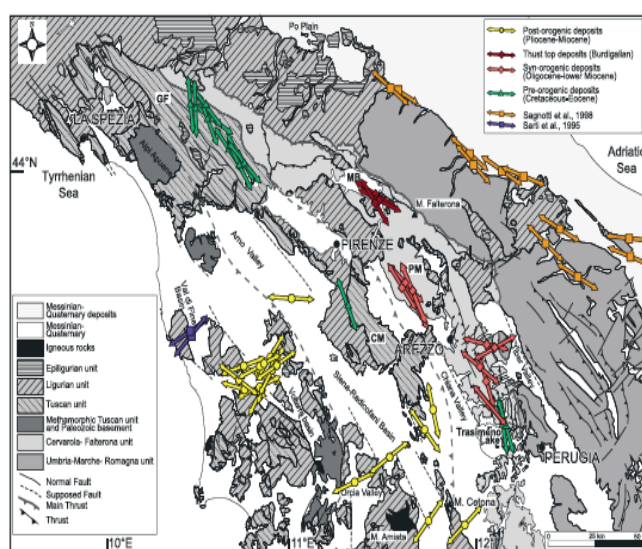
The anisotropy of magnetic susceptibility (AMS) gives access to the preferential alignment of elongated magnetic grains in sediments. This alignment arises from hydrodynamic forces at the time of deposition. When sediments are emerged and involved in an orogeny, they may be remobilized by the deformation and used as tracers for strain orientation.

We combined AMS data obtained about 15 years ago with new data from weakly deformed fine-grained sediments from the Northern Apennine orogenic system (Italy). Pre-, syn-, and post-orogenic sequences, differing in age, composition, depositional environment, degrees of deformation, and tectonic regimes were sampled.

We observe a magnetic foliation subparallel to the bedding plane and a magnetic lineation well defined in this plane. The orientation of the magnetic lineation is significantly different depending on whether the studied sites underwent extensional or compressional tectonic regimes. In the Northern Apennines, the magnetic lineation is mostly parallel to the main compressional structures suggesting a tectonic origin related to the compressional phases. In the extensional Tuscan Tyrrhenian margin, magnetic lineation is perpendicular to

the main extensional faults, which are the main deformation elements of the area.

The close relationship between the shape and orientation of magnetic fabric, and the tectonic rock history, confirms the valuable use of AMS to investigate the tectonic history of weakly



deformed sedimentary rocks.

Fig. 1. Orientation of the AMS lineation. In yellow, the extension, in green, red and orange, the pre- and syn-orogenic compressions following the curvature of the chain.

Experimental determination and theoretical framework of kinetic fractionation at the water vapour–ice interface at low temperature

M. Casado, A. Cauquoin, A. Landais, D. Israel, A. Orsi, ... F. Prié, J-F Doussin

Geochimica and Cosmochimica Acta, 174, 54-69, 2016.

Water isotopes are commonly used for climate reconstruction from ice cores. The different heavy isotopes of water such as H₂¹⁸O, H₂¹⁷O or HDO give information about local temperature but also temperature and humidity of water vapour sources. Quantification of these parameters relies on the good knowledge of equilibrium and kinetic isotopic fractionation at each step of the water cycle. One of the strongest limitations when interpreting water isotopes in remote Antarctic ice cores is the formulation of the isotopic fractionation at solid condensation (vapour to ice). This classical formulation also implies a good knowledge of coefficients for equilibrium fractionation and water vapour diffusion in air as well as supersaturation in clouds. The uncertainties associated with these different parameters make the formulation of isotopic fractionation at solid condensation only empirical.

Here, we make use (1) of recent development in the measurements of water isotopes in the water vapour through infra-red spectroscopy and (2) of the possibility to measure accurately ¹⁷O-excess of water to test the classical formulation and parameterization of isotopic fractionation at solid condensation. A first experiment involving very strong supersaturation evidences a strong kinetic effect on ¹⁷O-excess at solid condensation, similar to

d-excess. It also shows the limits of the classical formulation of water isotopic fractionation during solid condensation estimation at very low temperature. A second experiment performed in a cloud chamber under controlled conditions uses cavity ring down spectrometers (CRDS) to determine the spatial variability of water vapour isotopic composition due to diffusion (kinetic effect) during solid condensation. The spatial variability of water vapour isotopic composition can be relatively well reproduced by the resolution of diffusion toward a cold plate. This preliminary study opens new perspectives to revisit the classical formulation of water isotopic fractionation during solid condensation at very low temperature.

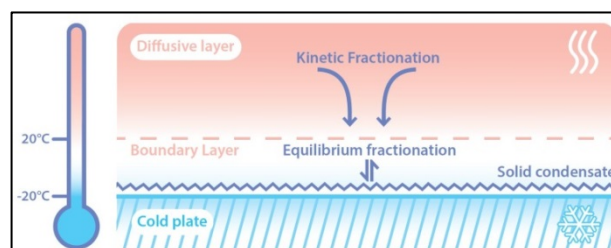


Fig. 1. Schematic representation of the solid condensation experiment and the associated concept of fractionation. At the solid vapour interface, it is classically assumed that equilibrium fractionation is occurring inside a boundary layer. More remotely, kinetic fractionation is at play.



Continuous measurements of isotopic composition of water vapour on the East Antarctic Plateau

M. Casado, A. Landais, V. Masson-Delmotte, C. Genthon, et al.

Atmospheric Chemistry and Physics, 16, 8521-8538, 2016.

Water stable isotopes in central Antarctic ice cores are critical to quantify past temperature changes. Accurate temperature reconstructions require to understand the processes controlling surface snow isotopic composition. Isotopic fractionation processes occurring in the atmosphere and controlling snowfall isotopic composition are well understood theoretically and implemented in atmospheric models. However, post-deposition processes are poorly documented and understood. To quantitatively interpret the isotopic composition of water archived in ice cores, it is thus essential to study the continuum between surface water vapour, precipitation, surface snow and buried snow. Here, we target the isotopic composition of water vapour at Concordia Station, where the oldest EPICA Dome C ice cores have been retrieved. While snowfall and surface snow sampling is routinely performed, accurate measurements of surface water vapour are challenging in such cold and dry conditions. New developments in infrared spectroscopy enable now the measurement of isotopic composition in water vapour traces. Two infrared spectrometers have been deployed at Concordia, allowing continuous, in situ measurements for one month in December-January 2014-2015. Comparison of the results from infrared spectroscopy with laboratory measurements of discrete samples trapped using cryogenic sampling validates the relevance

of the method to measure isotopic composition in dry conditions. We observe very large diurnal cycles in isotopic composition well correlated with temperature diurnal cycles. Identification of different behaviors of isotopic composition in the water vapour associated with turbulent or stratified regime indicates a strong impact of meteorological processes in local vapour/snow interaction. Even if the vapour isotopic composition seems to be, at least part of the time, at equilibrium with the local snow, the slope of δD against $\delta^{18}O$ prevents us from identifying a unique origin leading to this isotopic composition.

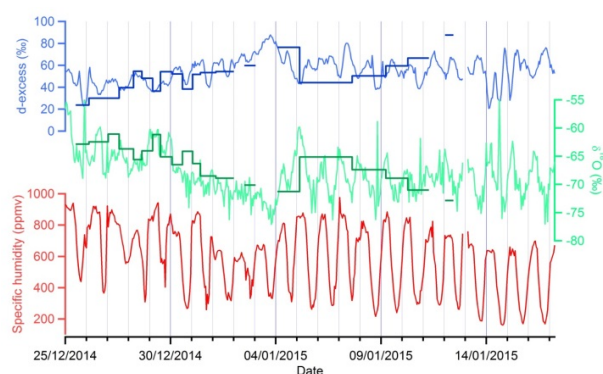


Fig. 1. hourly average $\delta^{18}O$ (‰) in green, raw d -excess (‰) in light blue (d -excess smoothed on a 3 hours span in thick blue), and hourly average of the specific humidity (ppmv) in red during the campaign 2014/2015. Measurements by the Picarro are displayed as the thin light lines and measurements performed in the laboratory from the cold trap samples are displayed as dark bars



Modeling the global bomb tritium transient signal with the AGCM LMDZ-iso: A method to evaluate aspects of the hydrological cycle.

A. Cauquoin, P. Jean-Baptiste, C. Risi, E. Fourré, A. Landais

Journal of Geophysical Research, 121, 12612-12129, 2016.

Improving the representation of the hydrological cycle in atmospheric general circulation models (AGCMs) is one of the main challenges in modeling the Earth's climate system. One way to evaluate model performance is to simulate the transport of water isotopes. Among those available, tritium is an extremely valuable tracer, because its content in the different reservoirs involved in the water cycle (stratosphere, troposphere, and ocean) varies by order of magnitude. Previous work incorporated natural tritium into Lab. LMDZ-iso, a version of the LMDZ general circulation model enhanced by water isotope diagnostics. Here, the anthropogenic tritium injected by each of the atmospheric nuclear bomb tests between 1945 and 1980 has been first estimated and further implemented in the model; it creates an opportunity to evaluate certain aspects of LMDZ over several decades by following the bomb tritium transient signal through the hydrological cycle. Simulations of tritium in water vapour and precipitation for the period 1950–2008, with both natural and anthropogenic components, are presented in this study. LMDZ-iso satisfactorily reproduces the shape of the temporal evolution of tritium. LMDZ-iso simulates too high a bomb tritium peak followed by too strong a decrease of tritium in precipitation. The too diffusive vertical advection in AGCMs crucially affects the residence time of tritium in the stratosphere. This insight into

model performance demonstrates that the implementation of tritium in an AGCM provides a new and valuable test of the modeled atmospheric transport, complementing water stable isotope modeling.

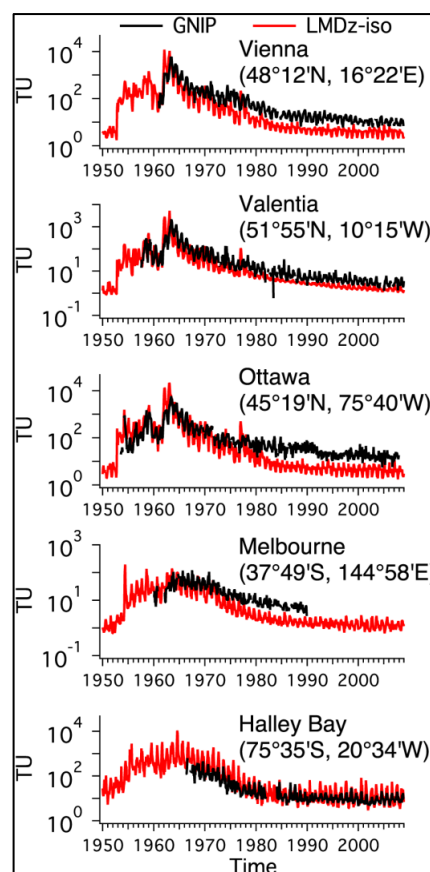


Fig. Monthly values of tritium in precipitation at Vienna, Valencia, Ottawa, Melbourne, and Halley Bay between 1950 and 2008. Black line : GNIP data, red line : our results from LMDZ-iso.

Additional correction for interstitial water changes in XRF core-scanning data from long sedimentary cores

Q. Chen, C. Kissel, A. Govin, Z. Liu, and X. Xie

Geochemistry, Geophysics, Geosystems, 17, 1925–1934, 2016.

Fast and nondestructive X-ray fluorescence (XRF) core scanning provides high-resolution element data that are widely used in paleoclimate studies. However, various matrix and specimen effects prevent the direct use of semi-quantitative raw XRF core-scanning intensities for robust paleoenvironmental interpretations.

Through a case study of a 50.8 m-long piston Core MD12-3432 retrieved from the northern South China Sea, we show that the absorption effect of interstitial water is the major source of deviations between XRF core-scanning intensities and measured element concentrations.

The existing two calibration methods, i.e., normalized median-scaled calibration (NMS) and multivariate log-ratio calibration (MLC), tested with this sequence after the application of water absorption correction, indicate that an improvement is still required to appropriately correct the influence of downcore changes in interstitial water content in the long sediment core, in particular for light elements.

Consequently, we proposed a new polynomial water content correction in both NMS and MLC calibration methods. Results calibrated with these two improved methods (e.g. NPS) indicate that the influence of downcore water content changes is now appropriately corrected.

This publication is part of Q. Chen' PhD thesis, defended with high honors on Dec. 8th, 2016.

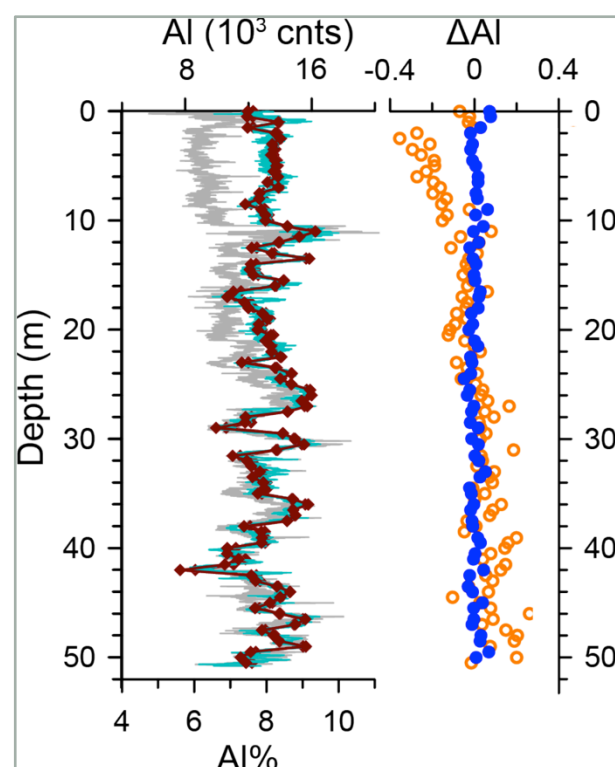


Fig. 1. Example of correction on Aluminium content. left: NMS corrected curve in grey, quantitative data in brown, NPS corrected data in turquoise. Right: difference between calibrated (NMS in orange and NPS in blue) and quantitative data.

Temporal and spatial variations of freshwater reservoir ages in the Loire river watershed

C. Coularis, N. Tisnérat-Laborde, L. Pastor, F. Siclet, M. Fontugne

Radiocarbon, 58, 549-563, 2016.

In order to map the freshwater reservoir effect (FRE) variability of the Loire River and its tributaries, spatial and temporal carbon isotope (^{13}C and ^{14}C) analyses of the dissolved inorganic Carbon (DIC) were conducted.

Sites were selected to represent the diversity of geological settings, soil type and land use. Results show a large spatial variability of ^{14}C FRE ranging between 135 and 2251 ± 30 years, objectively correlated to DIC contents and alkalinity. Deeper investigations of the relationship between ^{14}C activity of DIC and environmental variables show that the geological substrate is the dominant factor in the ^{14}C reservoir effect, and far more influential than the river flow discharge.

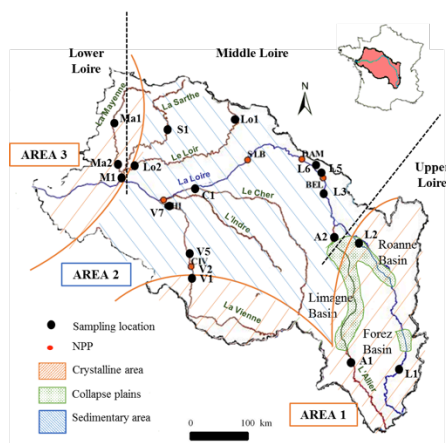


Fig.1: Loire River basin. Sampling sites and Nuclear Power Plants (NPP) are represented by black and red points, respectively. Three areas are identified: Area 1 and 3 are crystalline regions (striped orange zone) and area 2 is a region with carbonaceous sediments (striped blue zone). The dotted area represents the carbonated collapse plain between the Limagne plain, the Roanne basin and the Forez basin.

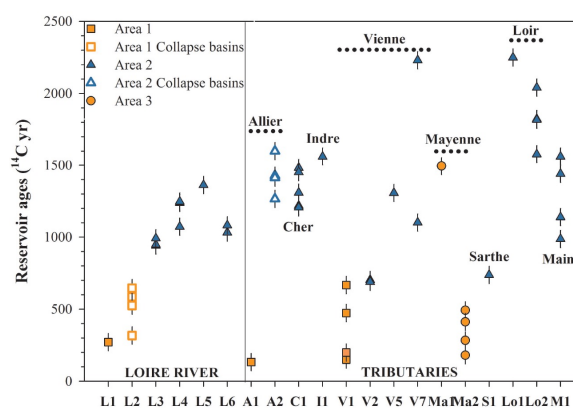


Fig.2: Reservoir ages evolution during the 4 campaigns from upstream to downstream for the Loire (L), Allier (A), Cher (C), Indre (I), Vienne (V), Mayenne (Ma), Sarthe (S), Loir (Lo) and Maine (M) Rivers. The orange markers correspond to sites included in Areas 1 and 3, the blue markers to the sites in Area 2. The error is expressed at 2σ .

Extreme storms during the last 6500 ys from lagoonal sedimentary archives in the Mar Menor (SE Spain)

L. Dezileau, A. Pérez-Ruzafa, P. Blanchemanche, J.-P. Degeai, O. Raji, P. Martinez, C. Marcos, U. von Grafenstein

Climate of thePast, 12, 1389–1400, 2016.

Storms and tsunamis, which may seriously endanger human society, are amongst the most devastating marine catastrophes that can occur in coastal areas. Many such events are known and have been reported for the Mediterranean. In a sediment core from the Mar Menor (SE Spain), we discovered eight coarse-grained layers which document marine incursions during periods of intense storm activity or tsunami events. Based on radiocarbon dating, these extreme events occurred around 5250, 4000, 3600, 3010, 2300, 1350, 650, and 80 years cal BP. No comparable events have been observed during the 20th and 21st centuries. The results indicate little likelihood of a tsunami origin for these coarse-grained layers, although historical tsunami events are recorded in this region. These periods of surge events seem to coincide with the coldest periods in Europe during the late Holocene, suggesting a control by a climatic mechanism for periods of increased storm activity. Spectral analyses performed on the sand percentage revealed 4 major periodicities of 1228 ± 327 , 732 ± 80 , 562 ± 58 and 319 ± 16 years. Amongst the well-known proxies that have revealed a millennial-scale climate variability during the Holocene, the ice-rafted debris (IRD) indices in the North Atlantic developed by Bond et al. (1997, 2001) present a cyclicity of 1470 ± 500 years, which

matches the 1228 ± 327 -year periodicity evidenced in the Mar Menor, considering the respective uncertainties in the periodicities. Thus, an in-phase storm activity in the western Mediterranean is found with the coldest periods in Europe and with the North Atlantic thermohaline circulation. However, further investigations, such as additional coring and high-resolution coastal imagery, are needed to better constrain the main cause of these multiple events.

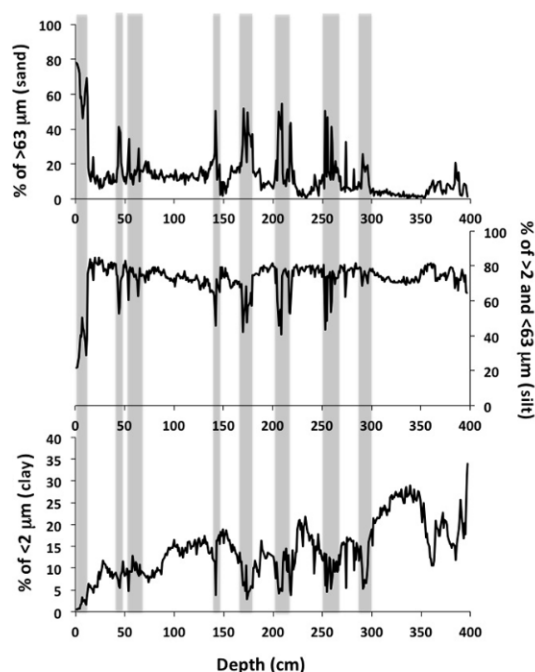


Fig. 1. Grain size population from the Mar Menor MM2 record with clay ($< 2 \mu\text{m}$), silt (> 2 and $< 63 \mu\text{m}$), and sand fraction ($> 63 \mu\text{m}$). Shaded areas mark the main variations of the sand fraction.

The Bengal fan: External controls on the Holocene Active Channel turbidite activity

L. Fournier, K. Fauquembergue, S. Zaragosi, C. Zorzi, B. Malaizé, F. Bassinot, R. Joussain, C. Colin, E. Moreno, F. Leparmentier

Geochemistry, Geophysics, Geosystems, 17, 3207–3223, 2016.

The eastern levee of the Active Channel in the Bengal fan has been investigated in order to better understand the history of turbidite activity in this channel during the Holocene in the context of Ganges-Brahmaputra ‘source-to-sink’ system. A robust ^{14}C -based chronostratigraphy provides high temporal resolution for reconstructing sediment accumulation history on the eastern levee of the Active Channel. Integration of this study with previous work in the area suggests that the Bengal fan has remained continually connected with the Ganges-Brahmaputra fluvial system through the Holocene, feeding through the main canyon, the Swatch of No Ground (SoNG). An intense turbidite activity occurred during a transgressive wet period from 14.5 to 9.2 ka cal. BP, followed by an abrupt shift in sedimentation at 9.2 ka cal. BP, probably due to the high sea level leading to a partial disconnection between massive river discharges and the deep turbidite system. During the last 9.2 ka cal. BP, turbidite activity is still present but irregular, likely modulated by a combination of various forcings such as monsoon variability and river migration. In total, three phases are distinguishable during this period: 9.2–5.5, 5.5–4, and 4 ka cal. BP to modern, according to the turbidite record. Unexpectedly, the Indo-Asian monsoon does

not appear to be the only predominant forcing on the establishment of the Bengal fan during the Holocene because of the combination of different forcings directly affecting transfers between the Ganges-Brahmaputra and the Bengal fan as well as river migrations, delta construction, and potentially anthropogenic impact.

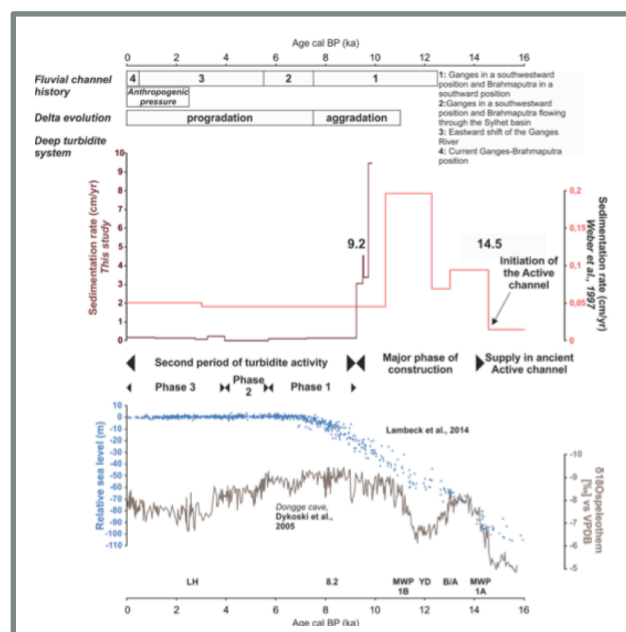


Figure 1 : Initiation and evolution of the Active channel during the last 18 ka cal. BP. Comparison between the Ganges-Brahmaputra river's history, the delta evolution, the deep turbidite system represented by the sedimentation rate obtained by Weber et al. (1997) and in this study, phase of activity of the Active Channel, relative sea level (Lambeck et al., 2014), and Indo-Asian monsoon (Dykoski et al., 2005). Sedimentation rate curve of Weber et al. (1997) has been calibrated.



Radiocarbon evidence for enhanced respired carbon storage in the Atlantic at the Last Glacial Maximum

E. Freeman, L.C. Skinner, C. Waelbroeck, D. Hodell

Nature Communications, 7:11998, 2016. doi: 10.1038/ncomms11998.

The influence of ocean circulation changes on atmospheric CO₂ hinges primarily on the ability to alter the ocean interior's respired nutrient inventory. Here we investigate the Atlantic overturning circulation at the Last Glacial Maximum and its impact on respired carbon storage using radiocarbon and stable carbon isotope data from the Brazil and Iberian Margins. The data demonstrate the existence of a shallow well-ventilated northern-sourced cell overlying a poorly ventilated, predominantly southern-sourced cell at the Last Glacial Maximum. We also find that organic carbon remineralization rates in the deep Atlantic remained broadly similar to modern, but that ventilation ages in the southern-sourced overturning cell were significantly increased. Respired carbon storage in the deep Atlantic was therefore enhanced during the last glacial period, primarily due to an increase in the residence time of carbon in the deep ocean, rather than an increase in biological carbon export.

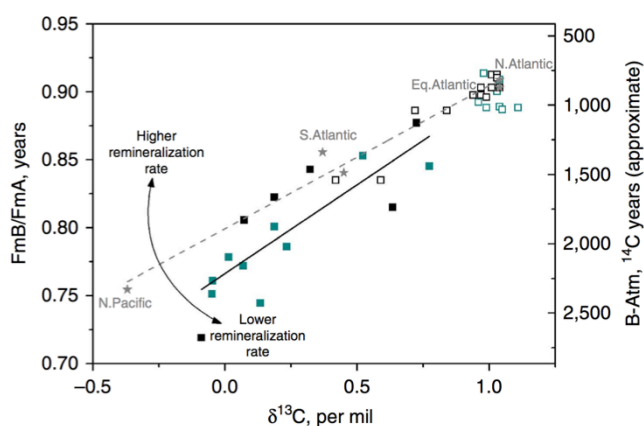


Fig. 1. Crossplot of ventilation age and stable carbon isotopic ratio. Ventilation ages are plotted as FmB/FmA , where $FmB/FmA = 1/4 \exp(B-Atm/-8033)$, and Fm $1/4$ fraction modern, because $B-Atm$ ages do not mix linearly due to the exponential decay of radiocarbon. Approximate $B-Atm$ values are shown as a guideline only. Modern whole ocean data (~ 2.5 km water depth; grey stars) is shown along with modern data for the entire water column 42 km (open squares) on the Iberian Margin (blue) and Brazil Margin (black). LGM data are shown (filled squares) for the Iberian Margin (blue) and the Brazil Margin (black; Modern data are from GEOSECS and GLODAP38). The modern gradient is 0.11 ± 0.01 and the LGM gradient is 0.13 ± 0.02 , equivalent to $1.1 \pm 0.1\%/kyr$ and $0.9 \pm 0.2\%/kyr$ in the modern and in the LGM, respectively. For a given rate of remineralization, an increase in residence time (that is, lower FmB/FmA) results in a greater amount of carbon storage.

Carbon isotope offsets between benthic foraminifer species of the genus *Cibicides* (*Cibicidoides*) in the glacial sub-Antarctic Atlantic

J. Gottschalk, N. Vázquez Riveiros, C. Waelbroeck, L. C. Skinner, E. Michel, J-C Duplessy, D. Hodell, and A. Mackensen

Paleoceanography, 31, 1583 – 1602, 2016. doi: 10.1002/2016PA003029

Epibenthic foraminifer $\delta^{13}\text{C}$ measurements are valuable for reconstructing past bottom water dissolved inorganic carbon $\delta^{13}\text{C}$ ($\delta^{13}\text{C}_{\text{DIC}}$), which are used to infer global ocean circulation patterns. Epibenthic $\delta^{13}\text{C}$ may also reflect the influence of ^{13}C -depleted phytodetritus, microhabitat changes, and/or variations in carbonate ion concentrations. Here we compare the $\delta^{13}\text{C}$ of two benthic foraminifer species, *Cibicides kullenbergi* and *Cibicides wuellerstorfi*, and their morphotypes, in three sub-Antarctic Atlantic sediment cores over several glacial-interglacial transitions. These species live above or directly below the sediment-water interface. While this might be consistent with the small inter-species $\delta^{13}\text{C}$ offset during late Pleistocene interglacial periods ($\Delta\delta^{13}\text{C} = -0.19 \pm 0.31\text{‰}$, $N=63$), it is less coherent with the significant inter-species offset found during glacial periods ($\Delta\delta^{13}\text{C} = -0.76 \pm 0.44\text{‰}$, $N=44$). We test possible scenarios by analyzing *Uvigerina* spp. $\delta^{13}\text{C}$ and benthic foraminifer abundances: (1) *C. kullenbergi* $\delta^{13}\text{C}$ is biased to light values due to microhabitat shifts or phytodetritus effects and (2) *C. wuellerstorfi* $\delta^{13}\text{C}$ is biased to heavy values, for instance by recording the sporadic occurrence of less depleted deepwater $\delta^{13}\text{C}_{\text{DIC}}$. Neither of these scenarios can be ruled out unequivocally. However, our findings emphasize

that supposedly epibenthic foraminifer $\delta^{13}\text{C}$ in the sub-Antarctic Atlantic may reflect several factors rather than being solely a function of bottom water $\delta^{13}\text{C}_{\text{DIC}}$. This could have a direct bearing on the interpretation of extremely light South Atlantic $\delta^{13}\text{C}$ values at the Last Glacial Maximum.

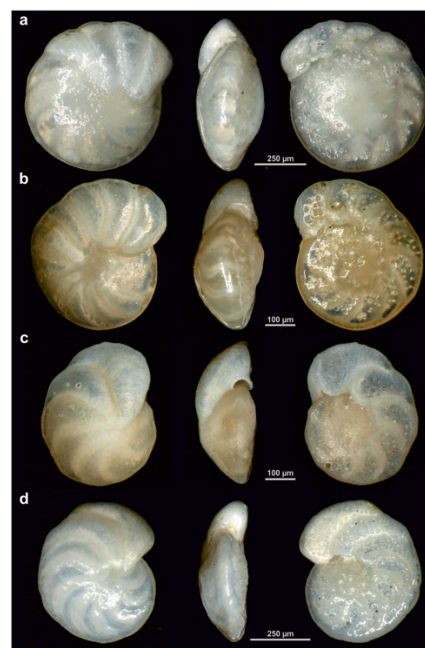


Fig. 1. (left) Umbilical, (middle) lateral, and (right) spiral view of type specimens of (a) *C. kullenbergi* sensu stricto; (b) *C. kullenbergi* sensu lato; (c) *C. wuellerstorfi* sensu lato, referred to as *C. cf. wuellerstorfi* in this study; and (d) *C. wuellerstorfi* sensu stricto, photographed with the digital microscope ShuttlePix by Nikon®. These strongly resemble type specimens of *C. wuellerstorfi* and *C. kullenbergi* (called *C. mundulus*) and their morphotypes shown in Rae et al. [2011].

Unprecedented coring performance with the upgraded Research Vessel *Marion Dufresne*

A. Govin, N. Vázquez Riveiros, Y. Réaud, C. Waelbroeck and J. Giraudeau

PAGES News, 24, 27, 2016.

The MD203 ACCLIMATE expedition was the first coring cruise onboard the Research Vessel *Marion Dufresne* since her midlife refit in 2015 (Rousseau et al. 2016). Taking place in March 2016 in the South Atlantic Roaring Forties and Howling Fifties, this cruise provided a full-scale exercise to test, in rough sea conditions, the latest generation of sediment coring equipment. To illustrate the unprecedented quality of long sediment sequences taken with the improved giant CALYPSO piston corer, we compared two deep-water cores collected ~13 km apart on the South African margin (Fig. 1): (1) core MD02-2587 taken in 2002 with the former coring facilities and (2) core MD16-3510 recovered with the new coring facilities.

The similarity of downcore sediment reflectance changes measured on board confirmed that both cores record the same climatic and environmental events (Fig. 1A-C). However, the 2002 core is stretched by up to 30% compared to the 2016 core, meaning that, for a similar core length, the 2016 core goes further back in time. Also, the 2002 core exhibited signs of coring deformation marked by bent dark layers, which, in contrast, are straight in the 2016 core (Fig. 1B). The absence of sediment stretching and deformation in the 2016 core thus highlighted the unprecedented quality of this ~45-meter-long core taken at ~4400 m of water-depth with a recovery rate higher than 94%!

The upgraded R/V *Marion Dufresne* is the sole research vessel able to collect up to 75-meter-long continuous sequences of undisturbed sediments at water depths as deep as 4500 m. The improved sediment coring facilities now yield cores of outstanding quality, which will provide indispensable high-resolution records to unravel past ocean and climate dynamics.

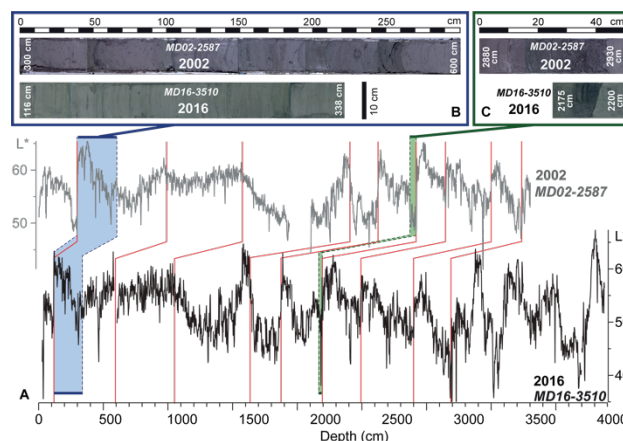


Fig. 1. Comparison of cores MD02-2587 (35°17.7'S, 29°22.2'E, 4468 m) and MD16-3510 (35°21.38'S, 29°14.78'E, 4435 m) collected in 2002 and 2016, respectively, at the same South African margin site. (A) Downcore reflectance (L^*) changes in both cores on their respective depth-scales. Red lines highlight conspicuous color changes synchronous in both cores. The 2002 core is stretched compared to the 2016 core. (B) Core photographs of the same time period (blue area) covered by 300 and 222 cm of sediments in the 2002 and 2016 cores, respectively. Dark layers are straight in the 2016 core, while bent in the 2012 core. (C) Core photographs of the same turbiditic event (green area). The characteristic downward coarsening of turbiditic sediments is stretched in the 2002 core. These features illustrate the absence of sediment stretching and deformation in the 2016 core, in opposition to the 2002 core



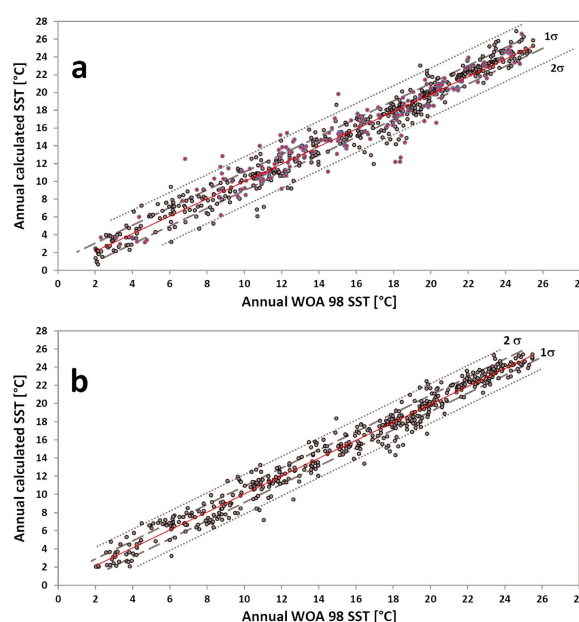
Improving past sea surface temperature reconstructions from the Southern Hemisphere oceans using planktonic foraminiferal census data

N.A. Haddam, E. Michel, G. Siani, G. Cortese, H.C Bostock, ..., G. Isgüder

Paleoceanography, 31, 822–837, 2016.

We present an improved database of planktonic foraminiferal census counts from the Southern Hemisphere oceans (SHO) from 15°S to 64°S. The SHO database combines three existing databases. Using this SHO database, we investigated dissolution biases that might affect faunal census counts. We suggest a depth ΔCO_3^{2-} threshold, under which core-top assemblages can be affected by dissolution and are less reliable for paleo-sea surface temperature (SST) reconstructions. We removed all core tops beyond these thresholds from the SHO database. This database has 598 core tops and is able to reconstruct past SST variations from 2° to 25.5°C, with a root mean square error of 1.00°C, for annual temperatures. To inspect how dissolution affects SST reconstruction quality, we tested the database with two “leave-one-out” tests, with and without the deep core tops. We used this database to reconstruct summer SST (SSST) over the last 20 ka, using the Modern Analog Technique method, on the Southeast Pacific core MD07-3100. This was compared to the SSST reconstructed using the three databases used to compile the SHO database, thus showing that the reconstruction using the SHO database is more reliable, as its dissimilarity values are the lowest. The most

important aspect here is the importance of a bias-free, geographic-rich database. We leave this data set open-ended to future additions; the new core tops must be carefully selected, with their chronological frameworks, and evidence of dissolution assessed.



Leave-one-out validation tests of our database for annual temperature reconstruction. (a) The database with deep core tops and (b) the database without dissolved, deep core tops (indicated in red dots). The dotted lines represent the 1σ and 2σ error (1.04°C and 2.76°C in (a), 0.89°C and 2.07°C in (b)).

Stable oxygen isotope evidence for mobility in mediaeval and post-mediaeval Trondheim, Norway

S. S. Hamre and V. Daux

Journal of Archaeological Science: reports, 8, 416-425, 2016.

Immigration and mobility in the mediaeval and post-mediaeval periods in Norway has, up until now, mainly been discussed on the basis of historical sources. This paper presents the results of stable oxygen isotope ($\delta^{18}\text{O}$) analyses of the 1st and 3rd molars from 95 individuals from mediaeval and post-mediaeval Trondheim, as well as new information about the $\delta^{18}\text{O}$ composition in the precipitation and drinking water in Trondheim. Through these analyses, the authors have attempted to shed light on the age of migrating individuals and directions of the migrations, investigate temporal changes with regard to migration, as well as making suggestions regarding the proportion of immigrants to locals in the population. The results show that the majority of the immigrants have come from areas to the north or east of Trondheim, and some have travelled, at least, 800-1000 kilometres to have come to Trondheim. It has also been shown that a large proportion of the mediaeval individuals moved during childhood (Fig. 1 & 2). Both with regard to child mobility and migration in general, the evidence suggests that the migratory activity decreased from the mediaeval to the post-mediaeval period.

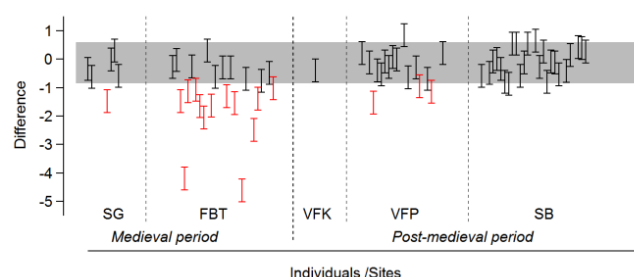


Fig. 1. Difference between the $\delta^{18}\text{O}_\text{C}$ of the M1 adjusted for weaning and the $\delta^{18}\text{O}_\text{C}$ of the M3 of the individuals excavated at Trondheim. The shaded area corresponds to ± 0.6 ‰ accepted range of variation that is to individuals who have likely not migrated during childhood. The red bars correspond to the individuals who may have migrated during childhood. SG: Søndregate; FBT: Folkebibliotekstomten; VFK: Vår frue kirke; VFP: Vestfrontplassen; SB: Servicebygget

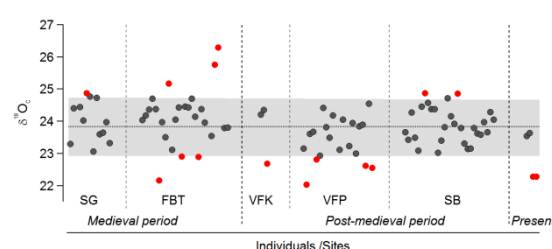


Fig. 2: Oxygen isotopic composition of the M3 teeth of the individuals excavated at Trondheim. The shaded area corresponds to an intra-population variability of 0.9 ‰. The red dots correspond to the individuals who may have migrated to Trondheim after the age of 14 years old.

Quantification of vertical solid matter transfers in soils during pedogenesis by a multi-tracer approach

M. Jagercikova, S. Cornu, D. Bourlès, O. Evrard, C. Hatté, J. Balesdent

Journal of Soils Sediments, 17, 408-422, 2016.

Vertical transfer of solid matter in soils (bioturbation and translocation) is responsible for changes in soil properties over time through the redistribution of most of the soil constituents with depth. Such transfers are, however, still poorly quantified.

In this study, we examine matter transfer in four eutric Luvisols through an isotopic approach based on ^{137}Cs , $^{210}\text{Pb}(\text{xs})$, and meteoric ^{10}Be . These isotopes differ with respect to chemical behavior, input histories, and half-lives, which allows us to explore a large time range. Their vertical distributions were modeled by a diffusionadvection equation with depth-dependent parameters. We estimated a set of advection and diffusion coefficients able to simulate all isotope depth distributions and validated the resulting model by comparing the depth distribution of organic carbon (including ^{13}C and ^{14}C isotopes) and of the 0–2- μm particles with the data.

We showed that (i) the model satisfactorily reproduces the organic carbon, ^{13}C , and ^{14}C depth distributions, indicating that organic carbon content and age can be explained by transport without invoking depth-dependent decay rates; (ii) translocation partly explains the 0–2- μm particle accumulation in the Bt

horizon; and (iii) estimates of diffusion coefficients that quantify the soil mixing rate by bioturbation are significantly higher for the studied plots than those obtained by ecological studies.

This study presents a model capable of satisfactorily reproducing the isotopic profiles of several tracers and simulating the distribution of organic carbon and the translocation of 0–2- μm particles.

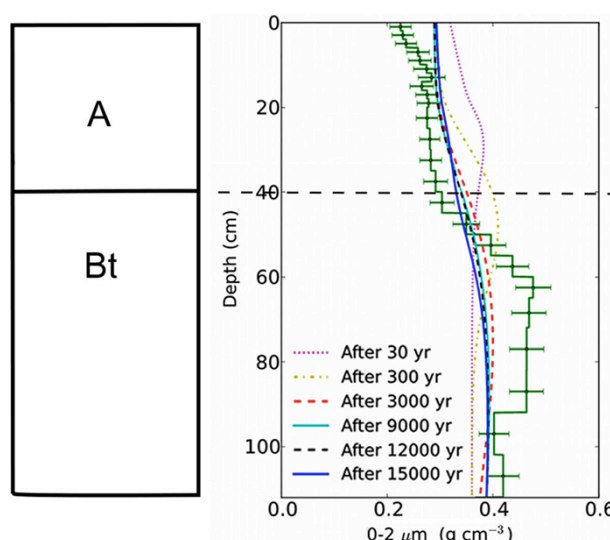


Fig. 1 Temporal evolution over 15,000 years of the 0–2- μm fraction vertical distribution at Mons grassland based on the transfer coefficients determined by this modelling. Tillage is simulated from year 14,700 to year 14,939

Early Neanderthal constructions deep in Bruniquel Cave in southwestern France

J. Jaubert, S. Verheyden, D. Genty, M. Soulier, Hai Cheng, D. Blamart et al.

Nature, Vol. 534, pp. 111-115, 2016.

Very little is known about Neanderthal cultures, particularly early ones. Other than lithic implements and exceptional bone tools, very few artefacts have been preserved. While those that do remain include red and black pigments and burial sites, these indications of modernity are extremely sparse and few have been precisely dated, thus greatly limiting our knowledge of these predecessors of modern humans. Here we report the dating of annular constructions made of broken stalagmites found deep in Bruniquel Cave in southwest France. The regular geometry of the stalagmite circles, the arrangement of broken stalagmites and several traces of fire demonstrate the anthropogenic origin of these constructions. Uranium-series dating of stalagmite regrowths on the structures and on burnt bone, combined with the dating of stalagmite tips in the structures, give a reliable and replicated age of 176.5 thousand years (± 2.1 thousand years), making these edifices among the oldest known well-dated constructions made by humans. Their presence at 336 metres from the entrance of the cave indicates that humans from this period had already mastered the underground environment, which can be considered a major step in human modernity. The attribution of the Bruniquel constructions to early Neanderthals is unprecedented in two ways. First, it reveals the appropriation of a deep karst space (including lighting) by a pre-modern human species. Second, it concerns elaborate constructions that have never been reported before, made with hundreds of partially

calibrated, broken stalagmites (speleofacts) that appear to have been deliberately moved and placed in their current locations, along with the presence of several intentionally heated zones. Our results therefore suggest that the Neanderthal group responsible for these constructions had a level of social organization that was more complex than previously thought for this hominid species.

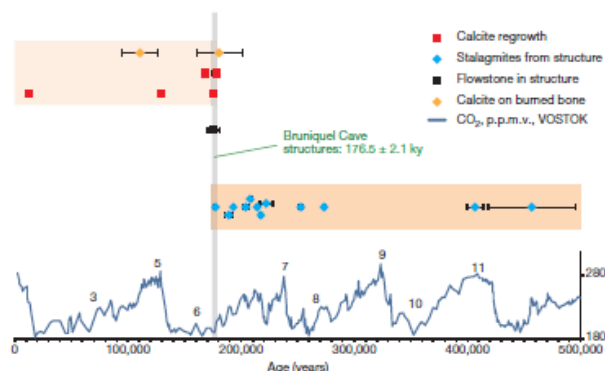


Fig 1 - Uranium-series ages (with 2σ error bars) obtained from the structures. Yellow, ages of the calcite covering the burnt bone in the accumulation structure E; red, ages obtained from the stalagmites covering the structure (regrowths) and representing a minimum age for the structure; blue, ages obtained from the stalagmites used by humans to build the structure (speleofacts) and representing a maximum age for the structures; black, age obtained from the flowstone partially covering the inside area of the main structure. The age of the structures is situated between 175.2 ± 0.8 thousand years (ky) and 177.1 ± 1.5 ky. The calcite covering the burnt bone is dated to 180.9 ± 20.3 ka, indicating a minimum age of the bone and adding evidence of earlier human presence in the cave. The general climatic context is given by the CO₂ concentration variation (expressed in p.p.m.v., low right y axis) extracted from the Vostok ice core record³⁰ (black numbers indicate major marine isotope stages).

Vertical distribution of helium and $^{40}\text{Ar}/^{36}\text{Ar}$ in porewaters of the Eastern Paris Basin (Bure/Haute Marne): constraints on transport processes through the sedimentary sequence

P. Jean-Baptiste, B. Lavielle, E. Fourré, T. Smith, M. Pagel

Geological Society Special Publications 443, 2016. Doi: 10.1144/SP443.25

As part of its ongoing project on repositories for high-activity, long-lived radioactive waste, a 2000 m deep borehole was drilled by the French Nuclear Waste Agency (ANDRA) in the layered structure of alternating aquifers and aquitards of the Eastern Paris Basin. Among the information retrieved from this borehole, the vertical distribution of chloride in porewaters showed that, in addition to vertical diffusion, lateral advection in the aquifers plays a major part in transporting chlorine away from the study area. Helium concentrations were also measured in porewaters along the borehole. Because the helium input function is different from that of chlorine, it represents an excellent alternative tracer to further constrain transport characteristics. We applied an advection–diffusion model to the helium profiles with the appropriate source term for ^4He based on U–Th measured concentrations of uranium and thorium. $^{40}\text{Ar}/^{36}\text{Ar}$ data, which were available along the whole sequence, were also simulated. The modelled and measured ^4He profiles were in good agreement, indicating that the transport parameters used for

the chlorine simulations were robust. $^{40}\text{Ar}/^{36}\text{Ar}$ simulations also gave coherent results and confirmed that most of the radiogenic ^{40}Ar remained trapped in the rocks (primarily in clays and feldspars).

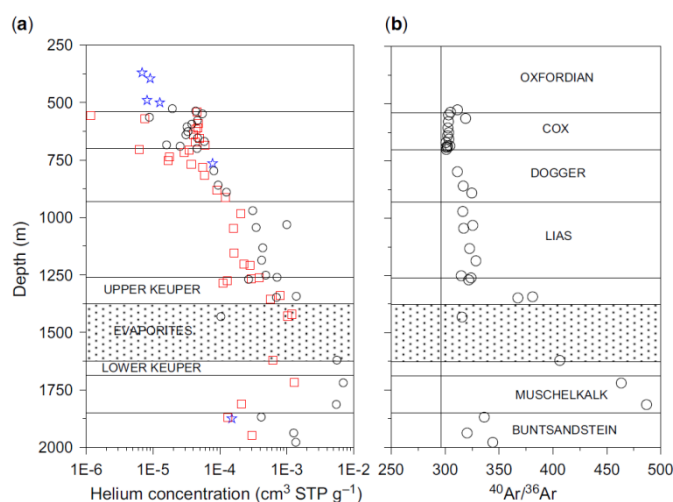


Fig.1. Depth profiles of (a) helium and (b) $^{40}\text{Ar}/^{36}\text{Ar}$ in porewaters. Open circles refer to the University of Bordeaux dataset (Smith 2010; Battani et al. 2011) and red squares to the University of Bern dataset (Waber & Vinsot 2010). Blue stars represent helium concentrations in aquifer free water samples reported by Fourré et al. (2011). COX, Callovo-Oxfordian



Labelled microbial culture as a calibration medium for ^{13}C -isotope measurement of derivatized compounds: application to tert-butyldimethylsilyl amino acids

L. Kheirbeik, C. Hatté, J. Balesdent

Rapid Comm. in Mass Spectrometry, 30, 1991-2001, 2016.

Compound-specific stable carbon isotope analysis by GC/C/IRMS is widely used in studies of environmental or biological functioning. In the case of derivatized molecules, a calibration might be required due to added non-analyte carbon and in some cases non-stoichiometric recovery by the mass spectrometer.

Two biological materials of known isotopic composition were produced by microbial cell cultures on either ^{13}C -labelled glucose or non-labelled glucose as sole source of carbon. Subsequent hydrolyzed amino acids were derivatized as tert-butyldimethylsilyl (tBDMSi) derivatives and analyzed by GC/C/IRMS. The ^{13}C -enrichment measurements were used as a direct calibration to calculate the original $^{13}\text{C}/^{12}\text{C}$ ratios of individual amino acids. We tested this calibration on both known and unknown samples.

For the main proteinogenic amino acids we could determine the number of non-analyte added carbon atoms and assess the non-stoichiometrical recovery of tBDMSi carbon atoms, due to their incomplete oxidation in the combustion step of GC/C/IRMS. The calibration enabled the determination of the natural abundances ($\delta^{13}\text{C}$ values) of amino acids with an average accuracy of $\pm 1.1\%$. We illustrate the application of the calibration to determine

the $^{13}\text{C}/^{12}\text{C}$ ratios of amino acids, and the associated uncertainty, in biological and plant materials.

The analysis of a labelled microbial cell culture offers a straightforward, rapid and reliable estimate of non-analyte carbon contribution to stable isotope composition. We recommend this method as a calibration or a control in artificial or natural ^{13}C -tracing experiments.

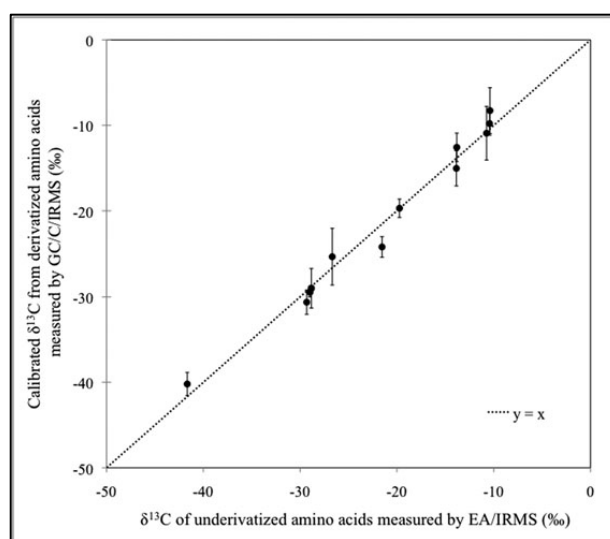


Fig. 1 Calibration curve for $\delta^{13}\text{C}$ values of underivatized commercial amino acids measured off-line (EA/IRMS) versus the derivatized ones measured by GC/C/IRMS and calibrated by the dilution factor. Every point represents the mean of triplicate measurements in GC and EA. Error bars represent propagated errors; Error bar on EA/IRMS $\delta^{13}\text{C}$ value is smaller than symbol.

Magnetic signature of three main Asian rivers drained into the South China Sea

C. Kissel, Z. Liu, J. Li, C. Wandres

Geochemistry, Geophysics, Geosystems, 17, 1678–1693, 2016.

LIA Franco-Chinois MONOCL (Monsoon, Ocean and Climate)

The use of marine sedimentary magnetic properties as tracers for changes in terrestrial precipitation rate and in oceanic water masses transport and exchanges, implies to identify and to characterize the different sources of the detrital fraction. This is of particular importance in a semi closed marginal sea such as the South China Sea that is fed by rivers among the most active ones in the world in terms of detrital discharge, and with the highest denudation rates mainly generated during the heavy rain seasons related to the monsoon climatic regime.

The magnetic composition of sediments collected from the main three Asian rivers draining into the South China Sea has been analyzed in detail. Large differences in the magnetic assemblages are observed in each catchment. The main stream of the Pearl River is rich in magnetite. Only the northern branch, which does not dominantly contribute to the sediment discharge is characterized by a higher content in hematite. The Mekong sediments are extremely rich in hematite. The Red River is intermediate with a mixture of both.

Compared to the previously studied clay mineralogical composition, it appears that the

magnetic mineralogy illustrates the geology of the catchment rather than the climatic conditions under which the rocks evolved in the floodplains. It therefore offers a complementary and valuable tool to study the modern and past provenance of sediments deposited in the South China Sea.

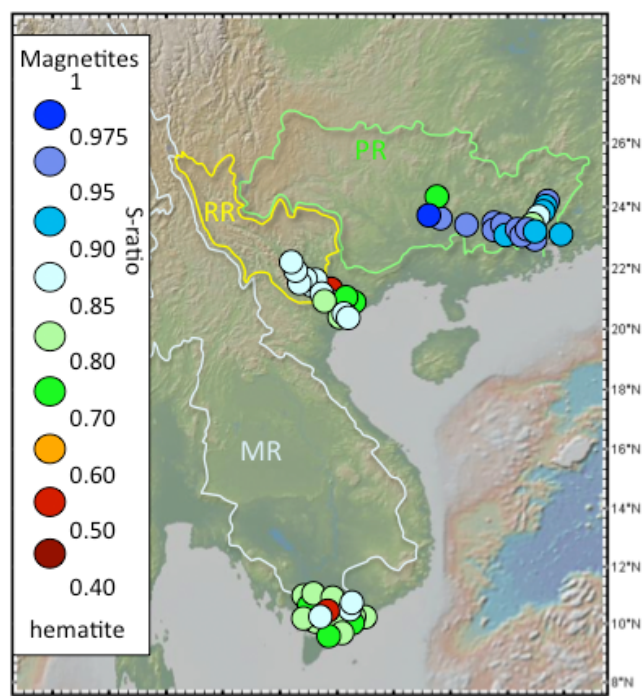


Fig. 1. Distribution of the magnetic coercivities in the sediments from Pearl (PR), Red (RR) and Mekong (MR) River (the limits of the catchment of each river are indicated)



French summer droughts since 1326 CE: a reconstruction based on tree ring cellulose $\delta^{18}\text{O}$

I. Labuhn, V. Daux, O. Girardclos, M. Stievenard, M. Pierre, V. Masson-Delmotte

Climate of the Past, 12, 1101–1117, 2016.

This article presents a reconstruction of summer droughts in France based on annually resolved, absolutely dated chronologies of oxygen isotope ratios ($\delta^{18}\text{O}$) in tree ring cellulose from *Quercus* spp. Samples were taken from living trees and timber wood from historic buildings at two sites: Fontainebleau (48°23' N, 2°40' E; 1326–2000 CE) and Angoulême (45°44' N, 0°18' E; 1360–2004 CE). Cellulose $\delta^{18}\text{O}$ from these sites proved to be a good proxy of summer climate, as the trees were sensitive to temperature and moisture availability. However, offsets in average $\delta^{18}\text{O}$ values between tree cohorts necessitated a correction before joining them to the final chronologies. Using the corrected $\delta^{18}\text{O}$ chronologies, we developed models based on linear regression to reconstruct drought, expressed by the standardized precipitation evapotranspiration index (SPEI). The significant correlations between the SPEI and cellulose $\delta^{18}\text{O}$ ($r=0.70$), as well as the verification of the models by independent data support the validity of these reconstructions. At both sites, recent decades are characterized by increasing drought. Fontainebleau displays dominantly wetter conditions during earlier centuries, whereas the current drought intensity is not unprecedented in the Angoulême record. While the $\delta^{18}\text{O}$ chronologies at the two studied

sites are highly correlated during the 19th and 20th centuries, there is a significant decrease in the correlation coefficient between 1600 and 1800 CE, which indicates either a weaker climate sensitivity of the tree ring proxies during this period, or a more heterogeneous climate in the north and the south of France. Future studies of tree ring isotope networks might reveal if the seasonality and spatial patterns of past droughts can explain this decoupling.

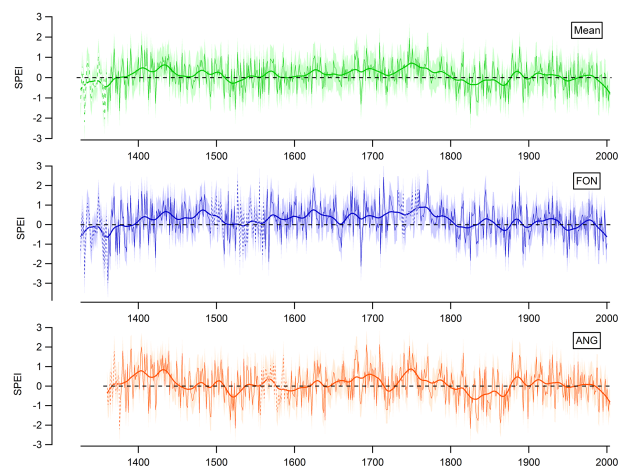


Fig. 1. Reconstructions of the drought index SPEI (June–August) based on tree ring cellulose $\delta^{18}\text{O}$ for Fontainebleau (FON), Angoulême (ANG), and a composite reconstruction for the two sites (mean). The thick lines are the fitted 30-year cubic smoothing splines. The shaded areas mark the confidence intervals of the reconstructions, and the dotted lines mark the parts of the chronologies where the number of trees is < 4 .

A multi-proxy approach to drought reconstruction

I. Labuhn, V. Daux, D. Genty

Quaternaire, 27 (3), 239-247, 2016.

In palaeoclimate reconstructions, the combination of proxy records measured in different climate archives is challenging because of the uncertainties associated with each proxy, but it can also help reduce some of these uncertainties. Here, we present a novel approach to combine speleothem and tree ring proxies for a drought reconstruction of the last 640 years: a fluid inclusion $\delta^{18}\text{O}$ record from a stalagmite from Villars Cave (southwest France) and a tree ring cellulose $\delta^{18}\text{O}$ record of *Quercus* spp. from the nearby Angoulême area. The $\delta^{18}\text{O}$ of the fluid inclusions is taken as an estimate of the $\delta^{18}\text{O}$ of the trees' source water. Then, the cellulose and source water $\delta^{18}\text{O}$ are used to calculate the leaf water isotopic enrichment, as well as relative humidity, which is the dominant controlling factor of this enrichment. The reconstructed long-term trends in relative humidity differ from a previously published reconstruction of moisture variability based on the tree ring record alone. Further measurements will be necessary to support either reconstruction. Nevertheless, this investigation demonstrates the great potential for combining isotope proxies from speleothems and tree rings to reconstruct both the low- and high-frequency variability of drought.

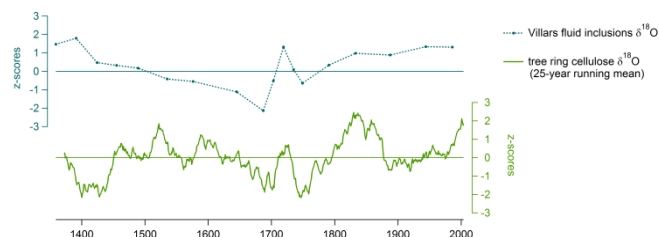


Fig. 1. Comparison of the speleothem fluid inclusion and tree ring cellulose $\delta^{18}\text{O}$ time series (z-scores). The cellulose $\delta^{18}\text{O}$ chronology has been smoothed by a 25-year running mean.

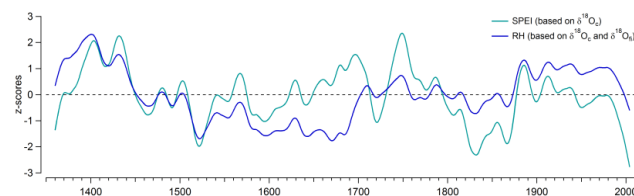


Fig. 2. The drought index (SPEI) and relative humidity (RH). The SPEI was reconstructed using tree ring cellulose $\delta^{18}\text{O}$, and RH was reconstructed using the calculation of leaf water enrichment from cellulose $\delta^{18}\text{O}$ and speleothem fluid inclusion $\delta^{18}\text{O}$ (as an estimate of the source water isotopic composition). Both curves were smoothed using a 30-year spline and transformed to z-scores. Positive values indicate wet conditions, negative values indicate dry conditions.

Reconstruction du climat et de l'environnement des derniers 800 000 ans à partir des carottes de glace – variabilité orbitale et millénaire.

A. Landais

Quaternaire, 27, 197-212, 2016.

Au cours des 40 dernières années, la recherche sur les carottes de glace a produit des résultats de référence pour l'évolution de la température polaire et de la composition atmosphérique au cours des 800 000 dernières années sur les échelles de temps orbitales et millénaires. Plus récemment, des progrès ont été faits dans la datation cohérente des carottes de glace en intégrant des marqueurs stratigraphiques et une méthode d'analyse bayésienne. Ces progrès permettent de compiler facilement les différents enregistrements issus des carottes de glace. Les avancées récentes dans l'analyse et la datation des carottes de glace ont permis de mieux documenter le déphasage entre augmentation de température et augmentation de concentration de dioxyde de carbone dans l'atmosphère. Lors des deux dernières déglaciations, il est maintenant établi que les augmentations initiales de concentration atmosphérique en dioxyde de carbone et température antarctique sont synchrones à ± 200 ans. Les mesures à haute résolution dans les carottes de glace et les efforts de datation relative entre Groenland et Antarctique permettent d'étudier les processus à l'œuvre lors de la variabilité millénaire de la dernière période glaciaire. En plus du phénomène de bascule bipolaire, il a été mis en évidence récemment une

variabilité climatique régionale en Antarctique lors de ces événements millénaires. Enfin, les carottes de glace apportent aussi des informations pertinentes pour l'étude du système couplé climat – calotte de glace dans un contexte de température plus élevée. Les reconstructions récentes du dernier interglaciaire à partir des carottes de glace groenlandaises indiquent en effet une température d'environ 8°C plus élevée qu'à l'actuel au Groenland.

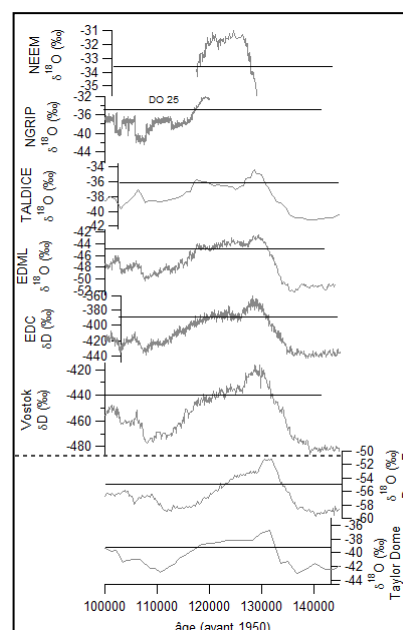


Fig. 1. Le dernier interglaciaire enregistré dans les carottes de glace. Les enregistrements de Taylor Dome et Dome F sont sur leur échelle d'âge d'origine. Les autres sont sur l'échelle d'âge AICC2012. Les traits horizontaux noirs indiquent le niveau actuel de $\delta^{18}\text{O}$ ou δD pour les différents sites. Le trait horizontal tireté sépare les carottes datées sur AICC2012.

How warm was Greenland during the last interglacial period?

A Landais, V. Masson-Delmotte, E. Capron, P. M. Langebroek, et al.

Climate of the Past, 12, 1933-1948, 2016.

The last interglacial period (LIG, ~129-116 thousand years ago) provides the most recent case study for multi-millennial polar warming above pre-industrial level. Past changes in Greenland ice sheet thickness and surface temperature during this period were recently derived from the NEEM ice core records, North-West Greenland. The NEEM paradox has emerged from an estimated large local warming above pre-industrial level ($7.5 \pm 1.8^\circ\text{C}$ at the deposition site 126 ka ago) based on water isotopes, together with limited local ice thinning, suggesting more resilience of the real Greenland ice sheet than shown in some ice sheet models. Here, we provide an independent assessment of the average LIG Greenland surface warming using ice core air isotopic composition ($\delta^{15}\text{N}$) and relationships between accumulation rate and temperature. The LIG surface temperature at the upstream NEEM deposition site without ice sheet altitude correction is estimated to be warmer by $+8.5 \pm 2.5^\circ\text{C}$ compared to the pre-industrial period. This temperature estimate is consistent with the $7.5 \pm 1.8^\circ\text{C}$ warming initially determined from NEEM water isotopes but on the upper end of the pre-industrial to LIG temperature difference of $+5.2 \pm 2.3^\circ\text{C}$ obtained at the NorthGRIP site by the same method. Climate simulations performed with present day ice sheet topography lead in general to a warming

smaller than reconstructed, but sensitivity tests show that larger amplitudes (up to 5°C) are produced in response to prescribed changes in sea ice extent and ice sheet.

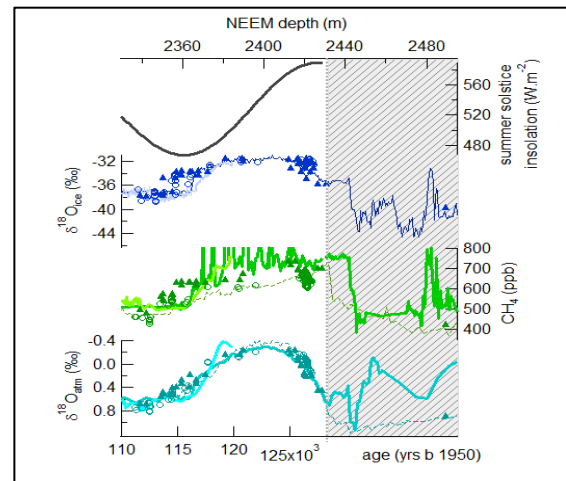


Fig. 1. From top to bottom: summer solstice insolation at 77°N (black); $\delta^{18}\text{O}_{\text{ice}}$ from NGRIP (light blue line), GRIP (open circles) and GISP2 (triangles) on the AICC2012 timescale (bottom axis) and NEEM $d^{18}\text{O}_{\text{ice}}$ (dark blue line) on its depth scale (top axis); CH_4 records from NGRIP (light green line), GRIP (open circles), GISP2 (triangles) and EDC (dashed line) on the AICC2012 timescale and NEEM (dark green line) on its depth axis; $\delta^{18}\text{O}_{\text{atm}}$ records from NGRIP (light blue), GRIP (open circles), GISP2 (triangles) and EDC (dashed line) on the AICC2012 timescale and NEEM $d^{18}\text{O}_{\text{atm}}$ (turquoise) on its depth axis. The shaded grey rectangle highlights the deepest part of the NEEM records, where no gas synchronization with Antarctic ice core records from the penultimate glaciation is feasible.

Are the oxygen isotopic composition of *Fitzroya cupressoides* and *Nothofagus pumilio* cellulose promising proxies for climate reconstructions in northern Patagonia?

A. Lavergne, V. Daux, R. Villalba, M. Pierre, M. Stievenard, F. Vimeux, A. Srur

Journal of Geophysical Research: Biogeosciences, 121, 767-776, 2016.

Tree ring $\delta^{18}\text{O}$ chronologies from two native species (*Fitzroya cupressoides* and *Nothofagus pumilio*) in northern Patagonia were developed to assess their potential for paleoclimate reconstructions. The five annually resolved cellulose chronologies of oxygen isotopic compositions ($\text{d}^{18}\text{O}_{\text{cell}}$; two for *F. cupressoides* and three for *N. pumilio*) are located on the Andes along the steep west-to-east precipitation gradient. Over the common 60 years long interval, the five site- $\text{d}^{18}\text{O}_{\text{cell}}$ chronologies exhibit a strong common signal as indicated by the significant mean intercorrelation ($r = 0.61$, $p < 0.05$) and the high percentage (65%) of total variance explained by the first empirical orthogonal function. Although correlation analyses reveal that the two mean species- $\delta^{18}\text{O}_{\text{cell}}$ chronologies are mainly modulated by December–May temperature, the *N. pumilio* chronology shows a greater sensitivity to record temperature variations ($r = 0.57$, $p < 0.05$; Fig. 1). The $\text{d}^{18}\text{O}_{\text{cell}}$ of *N. pumilio* contains a regional temperature signal representative of a large area in southern South America under the influence of the Southern Annular Mode (Fig. 2). This study indicates that $\delta^{18}\text{O}_{\text{cell}}$ in *N. pumilio* is a promising proxy to reconstruct past variations

in temperature in South America south of 38°S .

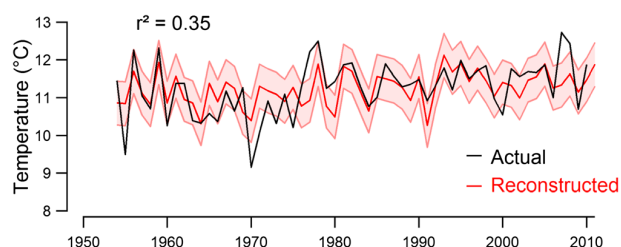


Fig. 1: Actual and reconstructed December–May mean temperatures with the *N. pumilio* $\text{d}^{18}\text{O}_{\text{cell}}$ mean chronology for the period 1954–2011. The pink color band around the reconstruction indicates the root-mean-square error ($\text{RMSE} = \pm 0.58^\circ\text{C}$). The explained variance (r^2) is indicated.

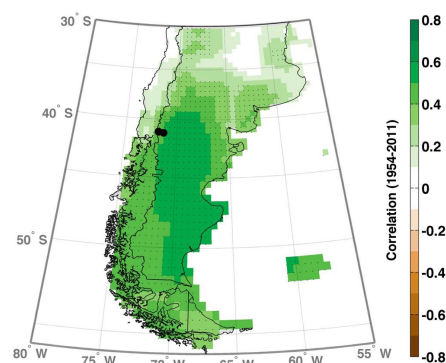


Fig. 2: Correlation field across South America between December and May temperature (CRUTS 3.2 data set [Harris et al., 2014]) and the *N. pumilio* $\delta^{18}\text{O}_{\text{cell}}$ chronology for the period 1954–2011. The stippling points indicate grid points with significant correlations ($p < 0.05$). The black points situate the sampling sites.



Improvement of isotope-based climate reconstructions in Patagonia through a better understanding of climate influences on isotopic fractionation in tree rings

A. Lavergne, V. Daux V., R. Villalba, M. Pierre, M. Stievenard, A. Srur

Earth Planet. Sci. Lett. 459, 372-380, 2016.

This study is the first presenting annually resolved chronologies of both $\delta^{18}\text{O}$ and $\delta^{13}\text{C}$ in *Nothofagus pumilio* and *Fitzroya cupressoides* trees from Northern Patagonia. Interannual variability in $\delta^{18}\text{O}$ and $\delta^{13}\text{C}$ was assessed over the period 1952-2011. Based on these chronologies, we determined the primary climatic controls on stable isotopes and tree physiological responses to changes in atmospheric CO_2 concentrations (c_a), temperature and humidity. Changes in specific intrinsic water use efficiency (iWUE) were inferred from variations in $\delta^{13}\text{C}$ whereas the effects of CO_2 increase on stomatal conductance were explored using $\delta^{18}\text{O}$. Over the 60-year period, iWUE increased significantly (by ca. 25%) in coincidence with the rise of c_a . The two species appear to have different strategies of leaf gas-exchange. Whereas iWUE variations were likely driven by both stomatal conductance and photosynthetic assimilation rates in *Fc*, they were largely related to stomatal conductance in *Np*. After removing the low-frequency trends related to increasing c_a , significant relationships between $\delta^{13}\text{C}$ and summer temperatures were recorded for both species.

However, $\delta^{13}\text{C}$ variations in *Fc* were more strongly influenced by summer temperatures than in *Np*. Our results advocate for an indirect effect of summer temperatures on stable

isotope ratios, which are mostly influenced by sunlight radiation in *Fc* and relative humidity/soil moisture in *Np*. $\delta^{13}\text{C}$ variations in *Fc* were spatially correlated to a large area south of 35°S in southern South America. These promising results encourage the use of $\delta^{13}\text{C}$ variations in *Fc* for reconstructing past variations in temperature and large-scale circulation indexes such as the Southern Annular Mode.

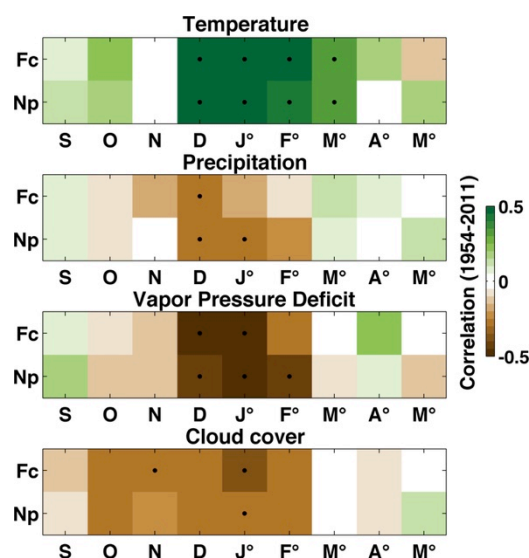


Fig. Correlation between $\delta^{13}\text{C}$ chronologies from *F. cupressoides* and *N. pumilio* and monthly meteorological parameters. 9-month window corresponding to the growing season from September to May

Intra-skeletal calcite in a live-collected *Porites*: Impact on environmental proxies and potential formation process

C.E. Lazareth, C. Soares-Pereira, E. Douville, C. Brahmi, D. Dissard, F. LeCornec, F. Thil, C. Gonzalez-Roubaud, S. Caquineau, G. Cabioch

Geochimica & Cosmochimica Acta 176, 279–294, 2016.

Geochemical proxies measured in the carbonate skeleton of tropical coral *Porites* have commonly been used to reconstruct SST and pH. Nevertheless, both reconstructed SST and pH depend on the preservation state of the skeleton, here made of aragonite; i.e., diagenetic processes and its related effects should be limited. In this study, we report on the impact of the presence of calcite on the skeleton geochemistry of a live-collected *Porites*. The skeleton preservation state was analysed using X-ray diffraction and SEM. Sr/Ca, Mg/Ca, U/Ca, Ba/Ca, Li/Mg, and B/Ca ratios were measured at a monthly and yearly resolution using ICP-QMS and MC-ICP-MS. The coral colony presents various levels of calcite presence reaching 32% for the annual band the most impacted. This intra-skeletal calcite replaces partly or completely numerous centers of calcification. All investigated geochemical tracers are impacted by the presence of calcite. The reconstructed SST decreases by about 0.1°C per calcite-percent as inferred from the Sr/Ca ratio. Such impact reaches up to 0.26°C for SST deduced from the Li/Mg ratio. Seawater pH reconstruction inferred from boron isotopes drop by about 0.011 pH-unit per calcite-percent. Such sensitivity to calcite presence is particularly dramatic for fine paleo-pH reconstructions.

Here we suggest that after being brought to shallow waters following a cyclone, the studied coral was seasonally subjected to rainfall-related water freshening that could have mimicked a vadose environment like can be encountered on raised fossil coral reefs. Nevertheless, the process of calcite precipitation remains to be determined.

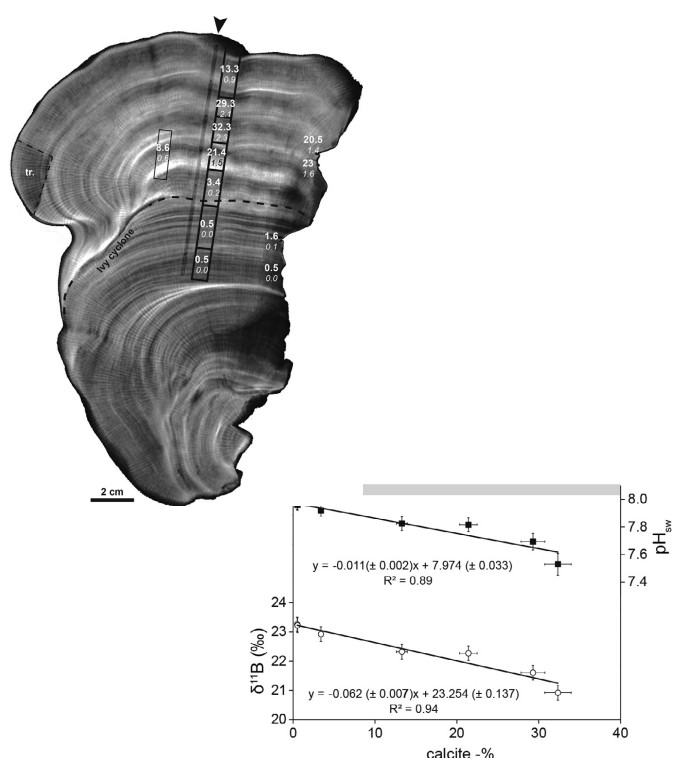


Fig.1: X-ray picture of the studied *Porites* colony. Influence of intra-skeletal calcite on the $\delta^{11}\text{B}$ signature and on reconstructed seawater pH.



Oxygen isotope fractionation between bird eggshell calcite and body water: application to fossil eggs from Lanzarote (Canary Islands)

N. Lazzerini , C. Lécuyer, R. Amiot, D. Angst, E. Buffetaut, F. Fourel , V. Daux et al.

The Science of Nature 103:81.

Oxygen and carbon isotope compositions of fossil bird eggshell calcite ($\delta^{18}\text{O}_{\text{calc}}$ and $\delta^{13}\text{C}_{\text{calc}}$) are regularly used to reconstruct paleoenvironmental conditions. The $\delta^{18}\text{O}_{\text{calc}}$ values mainly reflect the oxygen isotope composition of the waters ingested by birds ($\delta^{18}\text{O}_{\text{w}}$), which in turn are controlled by local climatic parameters (air temperature, local humidity), whereas the $\delta^{13}\text{C}_{\text{calc}}$ value provides information on birds foraging environment as well as local relative humidity. However, the interpretation of $\delta^{18}\text{O}_{\text{calc}}$ values of fossil eggshells is limited to qualitative variations in local climatic conditions as oxygen isotope fractionations between calcite, body fluids and drinking water have not been determined yet. For this purpose, eggshells, albumen and drinking water of extant birds have been sampled and analyzed for their oxygen and carbon isotope compositions. Enrichments in ^{18}O relative to ^{16}O between body fluids and drinking water of $+2.2 \pm 0.4 \text{‰}$ for semi-aquatic birds and of $+4.1 \pm 0.5 \text{‰}$ for terrestrial birds are observed. Using our dataset and published values, two empirical equations relating the $\delta^{18}\text{O}_{\text{calc}}$ value of eggshell calcite to the $\delta^{18}\text{O}_{\text{w}}$ value of ingested water have been established for terrestrial and semi-aquatic birds. These equations have been applied to two cases of fossil eggshells from Lanzarote, Canary Islands,

in order to infer the ecologies of the Pleistocene marine bird *Puffinus* sp. and of the enigmatic giant birds from the Pliocene of Valle Grande. Both $\delta^{18}\text{O}_{\text{calc}}$ and $\delta^{13}\text{C}_{\text{calc}}$ of *Puffinus* eggshells point to a semi-aquatic marine bird ingesting mostly seawater with a $\delta^{18}\text{O}_{\text{w}}$ value $-0.6 \pm 0.3 \text{‰}$. In the case of the Pliocene giant bird, low $\delta^{13}\text{C}_{\text{calc}}$ values of eggshells point to a terrestrial lifestyle and the $\delta^{18}\text{O}_{\text{calc}}$ values allowed us to calculate an ingested local freshwater $\delta^{18}\text{O}_{\text{w}}$ value of $-2.8 \pm 0.3 \text{‰}$. This set of equations can help to quantitatively estimate the origin of waters ingested by extinct birds as well as to infer either local environmental (marine or freshwater) or climatic (local air temperatures, precipitations) conditions.

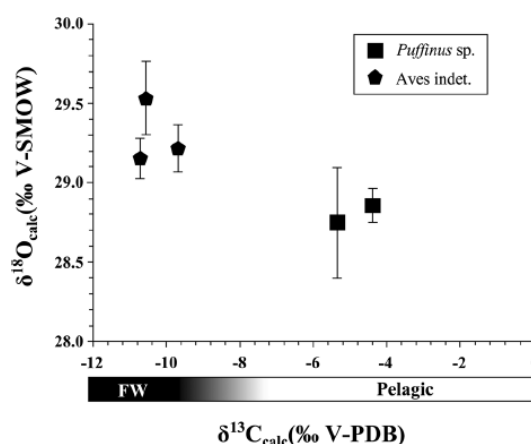


Fig. $\delta^{18}\text{O}$ of fossil bird eggshells from *Puffinus* sp. and an indeterminate giant bird.



Pré-história na foz do rio Chapecó

A. Lourdeau, M. Carbonera, M.C. Pereira Santos, S. Hoeltz., M. Fontugne, C. Hatté et al.

Estudos arqueológicos regionais, 29(45), doi: <http://dx.doi.org/10.22562/2016.45.09>.

O alto rio Uruguai é uma área importante para compreender o povoamento pré-histórico da bacia do rio da Prata. Nela foram localizados sítios de caçadores-coletores, referentes ao passado mais antigo da região, e de grupos ceramistas relacionados às unidades arqueológicas Tupiguarani e Taquara-Itararé. Este artigo apresenta os primeiros resultados das pesquisas realizadas no sítios ACH-LP-07 situado próximo à foz do rio Chapecó, à margem direita do rio Uruguai, no oeste de Santa Catarina. O rio apresentou várias ocupações de populações de caçadores-coletores no início do Holoceno, caracterizadas por uma variabilidade nas produções de pedra lascada, onde se destaca a produção de lâminas por uma debitage específica. No último milênio, o local também foi povoado por grupos ceramistas Guaraní. O sítio tem trazido diferentes contribuições a respeito dessas antigas sociedades, especialmente as modalidades de ocupação e de sucessão dos

grupos humanos no alto rio Uruguai

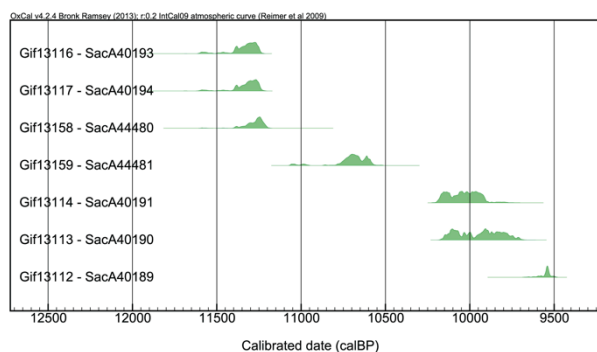


Fig. 1. ACH-LP-07, Setor 1. Distribuição cronológica das datas radiocarbônicas calibradas (a data Gif13115/SacA40192, considerada intrusiva, não está no gráfico)

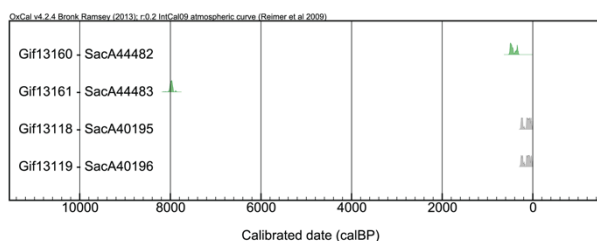


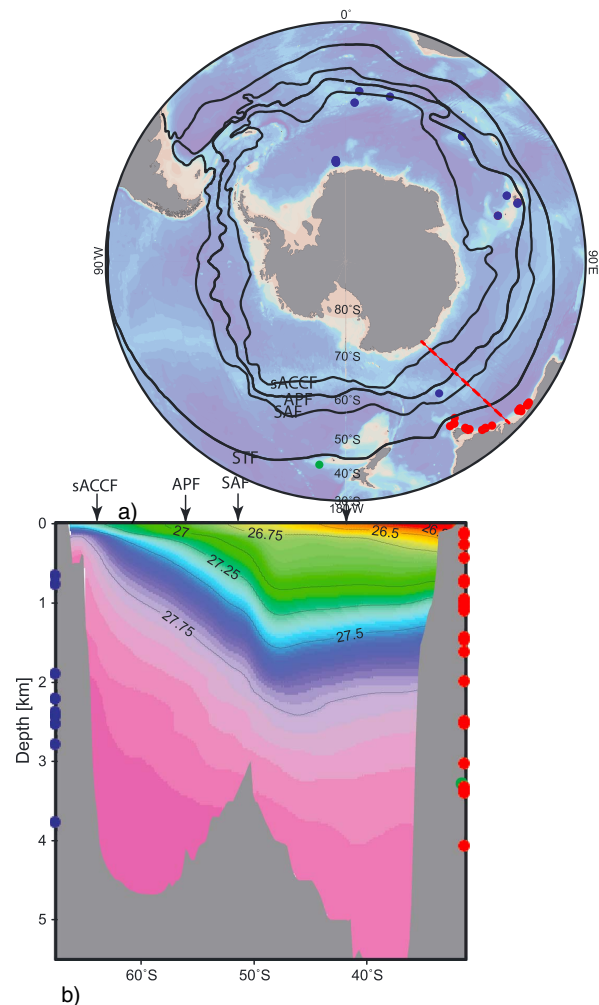
Fig. 2. ACH-LP-07, Setor 2. Distribuição cronológica das datas radiocarbônicas calibradas (as datas em cinza referem-se a áreas de combustão contemporâneas)

Antarctic density stratification and the strength of the circumpolar current during the Last Glacial Maximum

J. Lynch-Stieglitz, T. Ito, E. Michel

Paleoceanography, 31, 539-552, 2016.

The interaction between ocean circulation and biological processes in the Southern Ocean is thought to be a major control on atmospheric carbon dioxide content over glacial cycles. A better understanding of stratification and circulation in the Southern Ocean during the Last Glacial Maximum (LGM) provides information that will help us to assess these scenarios. First, we evaluate the link between Southern Ocean stratification and circulation states in a suite of climate model simulations. While simulated Antarctic Circumpolar Current (ACC) transport varies widely (80–350 Sverdrup (Sv)), it co-varies with horizontal and vertical stratification and the formation of the southern deep water. We then test the LGM simulations against available data from paleoceanographic proxies, which can be used to assess the density stratification and ACC transport south of Australia. The paleoceanographic data suggest a moderate increase in the Southern Ocean stratification and the ACC strength during the LGM. Even with the relatively large uncertainty in the proxy-based estimates, extreme scenarios exhibited by some climate models with ACC transports of greater than 250 Sv and highly saline Antarctic Bottom Water are highly unlikely.



a) Locations of data used in ACC density reconstruction. The solid black lines are the positions of the Antarctic Fronts [Orsi et al., 1995]. b) Present-day density structure south of Australia (σ_θ) with depth of sediment cores north (red) and south (blue) of the ACC marked; the dashed red line in Figure 1a shows the section shown in Figure 1b.

On the Movements of the North Atlantic Subpolar Front in the Preinstrumental Past

O. Marchal, C. Waelbroeck, A. Colin de Verdière

Journal of Climate 29 : 1545-1571, 2016.

Three sediment records of sea surface temperature (SST) are analyzed that originate from distant locations in the North Atlantic, have centennial-to-multicentennial resolution, are based on the same reconstruction method and chronological assumptions, and span the past 15 000 yr. Using recursive least squares techniques, an estimate of the time-dependent North Atlantic SST field over the last 15 kyr is sought that is consistent with both the SST records and a surface ocean circulation model, given estimates of their respective error (co)variances. Under the authors' assumptions about data and model errors, it is found that the 10°C mixed layer isotherm, which approximately traces the modern Subpolar Front, would have moved by ~15° of latitude southward (northward) in the eastern North Atlantic at the onset (termination) of the Younger Dryas cold interval (YD), a result significant at the level of two standard deviations in the isotherm position. In contrast, meridional movements of the isotherm in the Newfoundland basin are estimated to be small and not significant. Thus, the isotherm would have pivoted twice around a region southeast of the Grand Banks, with a southwest–

northeast orientation during the warm intervals of the Bølling–Allerød and the Holocene and a more zonal orientation and southerly position during the cold interval of the YD. This study provides an assessment of the significance of similar previous inferences and illustrates the potential of recursive least squares in paleoceanography.

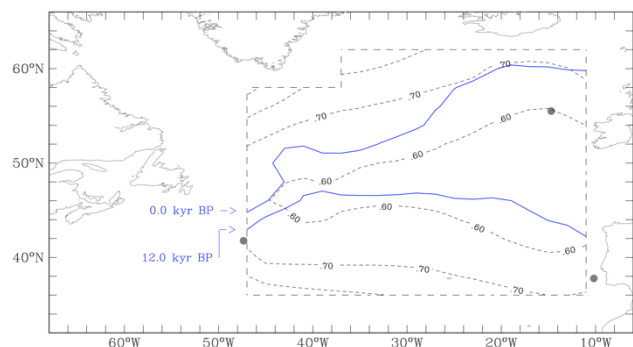


Fig. 1. Position of the 10°C mixed layer isotherm at 0 and 12 000 yr BP (blue lines), and distribution of mixed layer temperature error at 12 000 yr BP (short dashed black lines) in the smoothing solution. The mixed layer temperature errors are shown with a contour interval of 0.1°C and increase meridionally from the middle latitude of the domain (bounded with long dashed black lines). The gray circles show the location of sediment cores SU81–18, CH69–K09, and NA87–22.

Independent $^{40}\text{Ar}/^{39}\text{Ar}$ and ^{14}C age constraints on the last five glacial terminations from the aggradational successions of the Tiber River, Rome (Italy)

F. Marra, E.J. Rohling, F. Florindo, B. Jicha, S. Nomade, A. Pereira, P.R. Renne

Earth and Planetary Science Letters 449, 105–117, 2016.

We use 13 new $^{40}\text{Ar}/^{39}\text{Ar}$ and 4 new ^{14}C datings of volcanic deposits and organic material found within near-coastal aggradational successions deposited by the Tiber River near Rome, Italy, to integrate a larger dataset previously achieved in order to offer independent age constraints to the sea-level fluctuations associated with Late Quaternary glacial cycles during the last 450 ka. We find good agreements for the timings of change, and in several cases for both the amplitudes and timings of change during glacial terminations T-1, T-2, T-3, and T-5. There is one striking exception, namely for glacial termination T-4 that led into interglacial Marine Isotope Stage (MIS) 9. T-4 in our results is dated a full 18 ka earlier than in the Red Sea and deep-sea benthic $\delta^{18}\text{O}$ records (which are in good agreement with each other in spite of their independent chronological constraints). The observed discrepancy is beyond the scale of the combined age uncertainties. One possible explanation is that the documented aggradation represents an early phase, triggered by a smaller event in the sea-level record, but the thickness of the aggradational sediment sequence then suggests that the amplitude of this earlier sea-level rise is

underestimated in the Red Sea and benthic $\delta^{18}\text{O}$ records. Also, this would imply that the aggradational succession of the main T-4 deglaciation has not yet been located in the study region, which is hard to reconcile with our extensive fieldwork and borehole coverage, unless unlikely non-deposition or complete erosion.

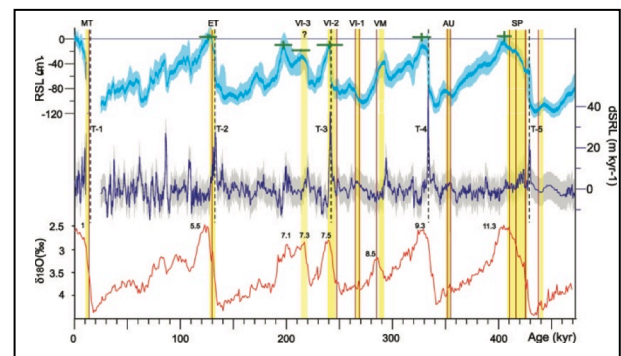


Fig. 1. Phases of aggradation in the coastal area of Rome (yellow vertical bars) compared with the independently dated curves of relative sea-level and rate of sea-level change (Grant et al., 2014) (blue shade and purple) and with the astronomically tuned deep-sea benthic $\delta^{18}\text{O}$ curve. The line lines are tephras intercalated in the Tiber river terraces and dated by $^{40}\text{Ar}/^{39}\text{Ar}$ and ^{14}C .

Modeling of hydrogen production by serpentinization in ultramafic-hosted hydrothermal systems: application to the Rainbow field

C. Mügler, P. Jean-Baptiste, F. Perez, J. L. Charlou

Geofluids 16(3), 476-489.

The production of hydrogen by serpentinization in ultramafic-hosted hydrothermal systems is simulated by coupling thermodynamic and dynamic modeling in the framework of a thermo-hydraulic single-pass model where a high-temperature hydrothermal fluid moves preferentially through a main canal of high permeability. The alteration of ultramafic rocks is modeled with a first-order kinetic formulation, wherein the serpentinization rate coefficient, K_r , takes the form: $K_r = A \exp(-\alpha(T-T_0)^2)$. In this formulation, α determines the temperature range of the reaction and T_0 is the temperature at which the serpentinization rate reaches its maximum. This model is applied to the Rainbow hydrothermal system, which is situated on the Mid-Atlantic Ridge, and characterized by a high temperature, a high mass flux, and a very high hydrogen concentration. The results show that a first-order kinetic law gives a useful representation of the kinetics of serpentinization. The estimated value for the parameter A in the temperature-dependent formulation of the serpentinization rate coefficient lies in the range $(1-5) \times 10^{-11} \text{ s}^{-1}$.

This effective parameter is several orders of magnitude lower than the values obtained from small grain-size experiments, but in agreement with other published modeling studies of natural systems. Numerical simulations show that the venting site is able to produce the observed high concentration of hydrogen during the whole continuous lifetime of the Rainbow site.

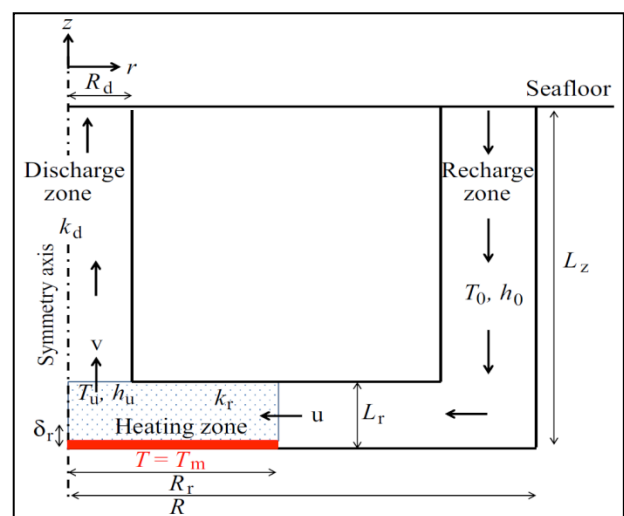


Fig. 1. Configuration of the single-pass geometry used to model the Rainbow vent site.



A 36,000-Year-Old Volcanic Eruption Depicted in the Chauvet-Pont d'Arc Cave (Ardèche, France)?

S. Nomade, D. Genty, R. Sasco, V. Scao, V. Féruglio, D. Baffier, H. Guillou, C. Bourdier, H. Valladas, E. Reigner, E. Debard, J.-F. Pastre, J.-M. Geneste.

PLoS ONE 11(1): e0146621. doi:10.1371/journal.pone.0146621

Volcanic eruptions are among the most impressive geological events on the surface of the earth. It is interesting to notice, however, that the oldest testimony of such an event in human history dates back to about 10000 years

Among the paintings and engravings found in the Chauvet-Pont d'Arc cave (Ardèche, France), several peculiar spray-shape signs have been previously described in the Megaloceros Gallery. Here we document the occurrence of strombolian volcanic activity located 35 km northwest of the cave, and visible from the hills above the cave entrance. The volcanic eruptions were dated, using $^{40}\text{Ar}/^{39}\text{Ar}$, between 29 ± 10 ka and 35 ± 8 ka (2σ), which overlaps with the ^{14}C AMS and thermoluminescence ages of the first Aurignacian occupations of the cave in the Megaloceros Gallery. Our work provides the first evidence of an intense volcanic activity between 40 and 30 ka in the Bas-Vivarais region, and it is very likely that Humans living in the Ardèche river area witnessed one or several eruptions. We propose that the spray-shape signs found in the Chauvet-Pont d'Arc cave could be the oldest known depiction of a volcanic eruption, predating by more than 34 ka the description by Pliny the Younger of the Vesuvius eruption (AD 79) and by 28 ka the Çatalhöyük mural discovered.

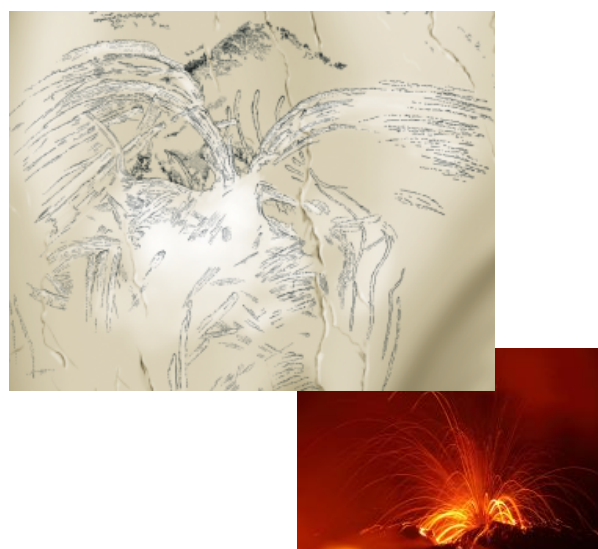


Fig. 1. Top left: Example of a spray-shape sign from Chauvet-Pont d'Arc cave (megaceros panel). Low right: Picture of a strombolian eruption

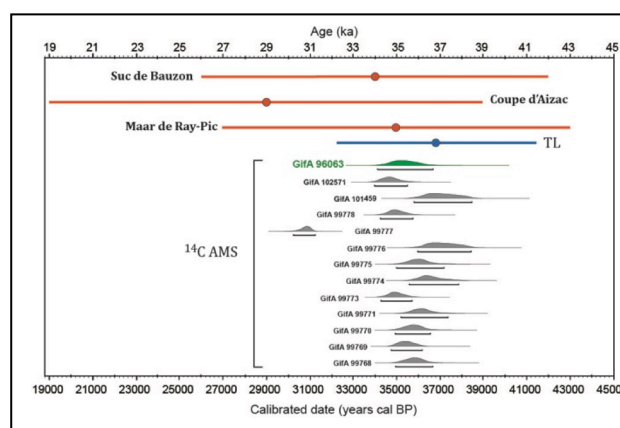


Fig. 2. Volcanic centers $^{40}\text{Ar}/^{39}\text{Ar}$ ages and spray-shape sign TL and ^{14}C AMS dates. In red: $^{40}\text{Ar}/^{39}\text{Ar}$ ages of the three volcanic centers studied; blue: TL age on reddened limestone in the Megaloceros Gallery. ^{14}C AMS dates correspond to the first occupation of the Megaloceros Gallery in the Chauvet-Pont d'Arc cave. The ^{14}C AMS in green corresponds to the date obtained for the sample taken from the rump of the Megaloceros.

$^{40}\text{Ar}/^{39}\text{Ar}$ and ESR/U-series dates for Guado San Nicola, Middle Pleistocene key site at the Lower/Middle Palaeolithic transition in Italy

A. Pereira, S. Nomade, QF. Shao, J.-J. Bahain, M. Arzarello, E. Douville, C. Falguères, N. Frank, T. Garcia, G. Lembo, B. Muttillo, V. Scao, C. Peretto

Quaternary Geochronology 36, 67–75, 2016

The Middle Pleistocene archaeological site of Guado San Nicola was discovered in 2005 in a fossil fluvial terrace of the Volturno River, close to the village of Monteroduni, Molise, Italy. Palaeontological remains and lithic artefacts, including both handaxes and Levallois, discoid and opportunistic debitage, were recovered in fluvial and slope sediments rich in volcanoclastic materials. This site includes four distinct human occupation levels. In two of them both “shaping-façonnage” and “knapping-débitage” technologies are highlighted, placing this site at the Lower/Middle Palaeolithic transition. In the present study, geochronological analyses by $^{40}\text{Ar}/^{39}\text{Ar}$ on single-crystal and ESR/U-series on teeth were performed to precise the chronological framework of the occupations. The $^{40}\text{Ar}/^{39}\text{Ar}$ data obtained securely bracket the human occupation levels at the transition between the interglacial and glacial marine isotopic stages MIS 11 (i.e. 400 ± 9 ka) and MIS 10 (i.e. 345 ± 9 ka). The weighted mean age obtained from ESR/U-series dating of six teeth

(i.e. 364 ± 36 ka) is in very good agreement with the $^{40}\text{Ar}/^{39}\text{Ar}$ results. The radio-isotopic constraints we presented place the Guado San Nicola site as one of the earliest testimonies of Levallois debitage in Western Europe and confirm the potential and accuracy of paleodosimetric methods to date Middle Pleistocene sites.

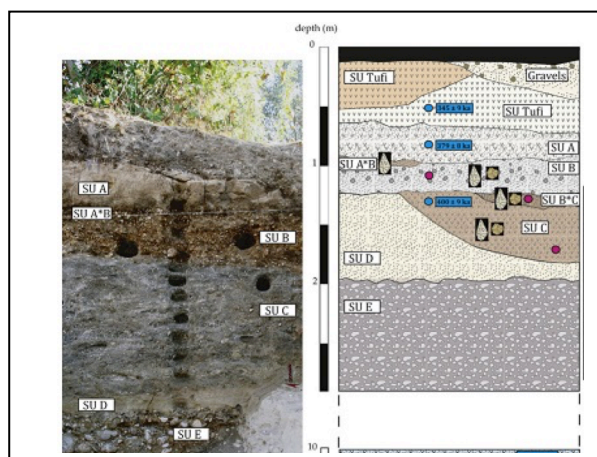


Fig. 1. Photo and schematic stratigraphy of Guado San Nicola showing the sampling positions for the $^{40}\text{Ar}/^{39}\text{Ar}$ and ESR/U-series methods and the archaeological deposits as well as ages obtained.

Palaeotemperature reconstruction during the Last Glacial from $\delta^{18}\text{O}$ of earthworm calcite granules from Nussloch loess sequence, Germany

C. Prud'homme, C. Lécuyer, P. Antoine, O. Moine, C. Hatté, et al.

Earth and Planetary Science Letters, 442, 13-20, 2016.

The Nussloch loess–palaeosol sequence (Rhine Valley, Germany) is considered to be one of the most complete records of the last glacial period in Western Europe due to its very high sedimentation rate and its good chronological control. This sequence is therefore a good framework in which to develop new proxies for palaeoenvironmental reconstructions. In this study, we explore, for the first time, the potential of earthworm calcite granules as a new bio-indicator and climatic proxy of absolute air and soil temperature in the context of Last Glacial loess. These granules are composed of rhomboedric calcite crystals, organized in a radial crystalline structure. As these granules are individually generated by earthworms at a relative fast rate, they are expected to record intra-annual variations in the available sources of oxygen: percolating waters of meteoric origin. We extracted thirty earthworm calcite granules from 11 of 5 cm layers thick from tundra gley and brown soil horizons previously, dated at 45 to 23ka. Oxygen isotope ratios were measured on each individual granule. The $\delta^{18}\text{O}$ of calcite granules and interlinked transfer functions between water cycle, air and soil temperatures allowed us to estimate air temperatures ranging from 10 to $12 \pm 4^\circ\text{C}$, which most likely reflect the

warm periods of the year when earthworms were the most active.

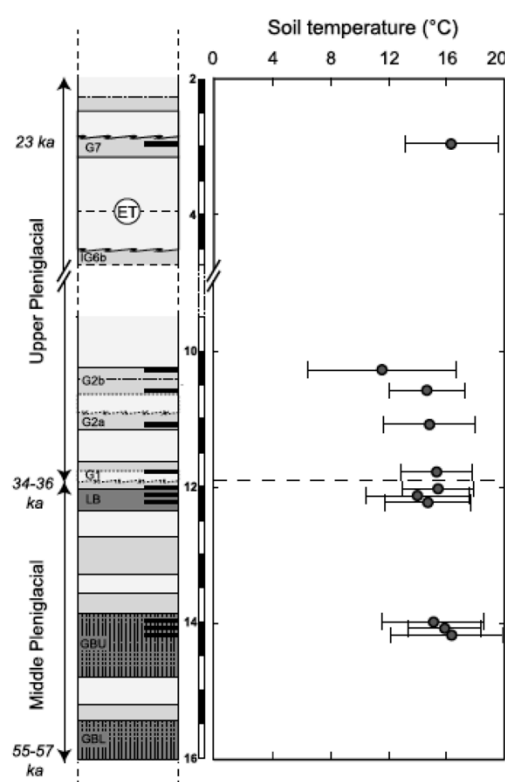


Fig. Soil temperatures inferred from the $\delta^{18}\text{O}$ values of earthworm calcite granules for profile P8 at Nussloch, Germany. The upper part of the section represents the temperatures corresponding to the five selected tundra gleys horizons while the lower part represents the temperatures corresponding to the six selected boreal brown soils. The bars illustrate the standard deviations (1σ) associated with the mean oxygen isotope ratios.

A high-precision chronological model for the decorated Upper Paleolithic cave of Chauvet-Pont d'Arc, Ardèche, France

A. Quiles, H. Valladas, H. Bocherens, E. Delque Količ et al.

Proceedings of the National Academy of Sciences, 113 (17), 4670-4675, 2016.

Radiocarbon dates for the ancient drawings in the Chauvet-Pont d'Arc Cave revealed ages much older than expected. These early ages and nature of this Paleolithic art make this United Nations Educational, Scientific and Cultural Organization (UNESCO) site indisputably unique. A large multidisciplinary dating program has recently mapped the anthropological evolution associated with the cave. More than 350 dates (by ^{14}C , U-Th, TL and ^{36}Cl) were obtained over the last 15 years. They include 259 radiocarbon dates, mainly related to the rock art and human activity in the cave. We present heremore than 80 previously unpublished dates. All of the dates were integrated into a high-precision Bayesian model based on archaeological evidence to securely reconstruct the complete history of the Chauvet-Pont d'Arc Cave on an absolute timescale. It shows that there were two distinct periods of human activity in the cave, one from 37 to 33,500 yr ago, and the other from 31 to 28,000 yr ago. Cave bears also took refuge in the cave until 33,000 yr ago.



Fig. 1 : Panneau des chevaux (Salle Hillaire) . Trois figures ont été datées par le carbone 14 entre 37 000 et 33 000 yr.

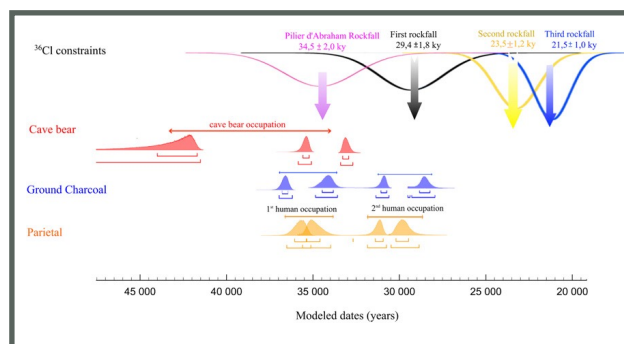


Fig. 2. High-precision Bayesian model obtained for the Chauvet-Pont d'Arc Cave. Modeled boundaries for the start and end of each occupation phase are represented in red for the Cave Bear model (postulating a continuous occupation), in blue for the Cave Floor Charcoal model, and in orange for the Parietal model. Two distinct human occupations are clearly identified, extending from 37,000 to 33,500 yr ago for the first one, and from 31,000 to 28,000 yr ago for the second one. Cave bear presence in the cave is attested until 33,000 yr ago.

Carbonate chemistry in sediment porewaters of the Rhône River delta driven by early diagenesis (northwestern Mediterranean)

J. Rassmann, B. Lansard, L. Pozzato, C. Rabouille

Biogeosciences, 13, 5379-5394, 2016.

The Rhône River is the largest source of terrestrial organic and inorganic carbon for the Mediterranean Sea. A large fraction of this terrestrial carbon is either buried or mineralized in the sediments close to the river mouth. This mineralization follows aerobic and anaerobic pathways, with a range of impacts on calcium carbonate precipitation and dissolution in the sediment near the sediment-water interface. This study focuses on the production of dissolved inorganic carbon (DIC) and total alkalinity (TA) by early diagenesis, consequential pH variations and the effect on calcium carbonate precipitation or dissolution. The sediment porewater chemistry was investigated along a transect from the Rhône River outlet to the continental shelf. TA and concentrations of DIC, SO_4^{2-} and Ca^{2+} were analyzed on bottom waters and extracted sediment porewaters, whereas pH and oxygen concentrations were measured in situ using microelectrodes. The average oxygen penetration depth into the sediment was 1.7 ± 0.4 mm close to the river mouth and 8.2 ± 2.6 mm in the continental shelf sediments, indicating intense respiration rates. Diffusive oxygen fluxes through the sediment–water interface ranged between 3 and $13 \text{ mmol O}_2 \text{ m}^{-2} \text{ d}^{-1}$. In the first 30 cm of the sediment, TA and DIC porewater concentrations increased with depth up to 48 mmol L^{-1} near the river outlet and up to 7 mmol L^{-1} on the shelf as a result of aerobic and anaerobic mineralization processes. Due to aerobic processes, at all

stations pH decreased by 0.6 pH units in the oxic layer of the sediment accompanied by a decrease of the saturation state regarding calcium carbonate. In the anoxic layer of the sediments, sulfate reduction was the dominant mineralization process and was associated with an increase of porewater saturation state regarding calcium carbonate. Ultimately anoxic mineralization of organic matter caused calcium carbonate precipitation demonstrated by a large decrease in Ca^{2+} concentration with depth in the sediment. Carbonate precipitation decreased in the offshore direction, together with the carbon turnover and sulfate consumption in the sediments. The large production of porewater alkalinity characterizes these sediments as an alkalinity source to the water column, which may increase the CO_2 buffering capacity of these coastal waters. Estuarine sediments should therefore receive more attention in future estimations of global carbon fluxes.

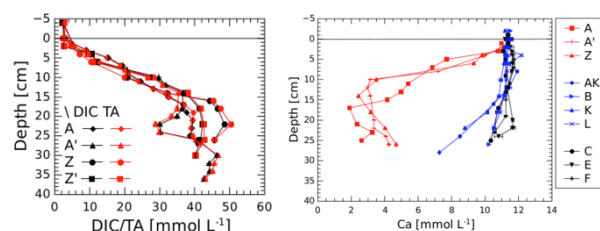


Fig. 1. Vertical profiles of DIC (black), TA (red) and calcium in sediment porewaters from the Rhône River prodelta.



Improved U-Th dating of carbonates with high initial ^{230}Th using stratigraphical and coevality constraints

M. Roy-Barman, E. Pons-Branchu

Quaternary Geochronology 32, 29-39, 2016.

With high precision measurements now achievable by MC-ICPMS, the uncertainty on the initial ^{230}Th content can be the major source of uncertainty for U-Th ages of carbonates. The initial ^{230}Th content is usually derived from the ^{232}Th content of the sample and the initial $^{230}\text{Th}/^{232}\text{Th}$ ratio calculated using isochron techniques or using stratigraphical constraints along the speleothem growth axis. These two methods are based on different hypotheses and have not been couple previously. Here, we present a new algorithm called STRUTages that combines stratigraphical and coevality constraints in order to obtain the best estimate on the initial $^{230}\text{Th}/^{232}\text{Th}$ ratio of each sample. STRUTages and isochron results are compared on a suite of speleothems and a coral core. Comparison of the U-Th and growth-band counted ages of the coral core demonstrates the validity of the STRUTages approach. An Octave (Matlab-compatible) script allowing the use of stratigraphical and coevality constraints is provided.

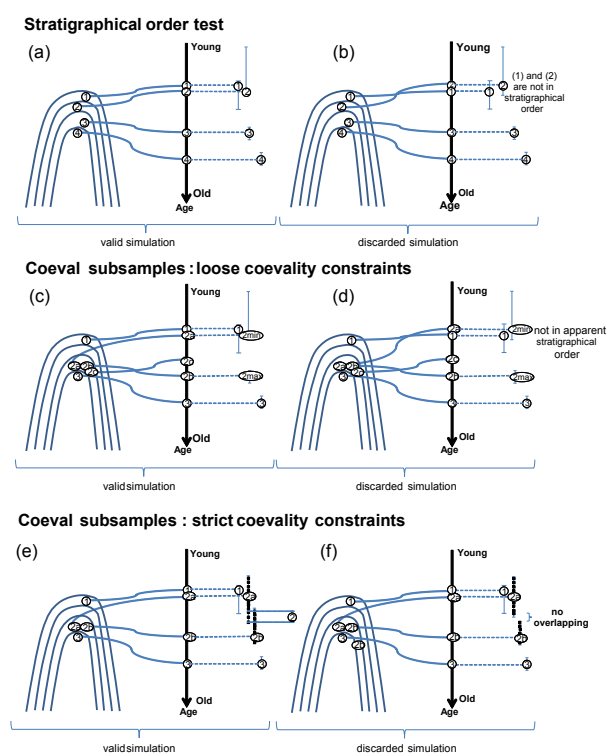


Fig. 1. Principle of the stratigraphical and coevality constraints as calculated in STRUTages. a: example of valid simulation for a stalagmite without coeval samples. b: example of discarded simulation for a stalagmite without coeval samples. Cases a and b correspond to the Hellstrom (2006) approach with no coeval samples. c: example of valid simulation with the loose coevality constraints applied to coeval samples. d: example of discarded simulation with the loose coevality constraints applied to coeval samples. e: example of valid simulation with the strict coevality constraints applied to coeval samples. f: example of discarded simulation with the strict coevality constraints applied to coeval samples.

Evolution of South Atlantic density and chemical stratification across the last deglaciation

J. Roberts, J. Gottschalk, L.C. Skinner, V.L. Peck, S. Kender, H. Elderfield, C. Waelbroeck, N. Vázquez Riveiros, D.A. Hodell

Proceedings of the National Academy of Sciences, 113, 514-519, 2016.

Deep-ocean density stratification has been proposed as a mechanism to promote the storage of CO₂ in the deep ocean during glacial times. A wealth of proxy data supports the presence of a “chemical divide” between intermediate and deep water in the glacial Atlantic Ocean, which indirectly points to an increase in deep-ocean density stratification. We use Mg/Ca-derived seawater temperature and salinity estimates determined from temperature-corrected $\delta^{18}\text{O}$ measurements on the benthic foraminifer

Uvigerina spp. from deep and intermediate water-depth marine sediment cores to reconstruct the changes in density of sub-Antarctic South Atlantic water masses over the last deglaciation (i.e., 22-2 ka before present). A major breakdown in the physical density stratification significantly lags the breakdown of the deep-intermediate chemical divide, as indicated by the chemical tracers of benthic foraminifer $\delta^{13}\text{C}$ and foraminifer/coral ^{14}C . Our results indicate that chemical destratification likely resulted in the first rise in atmospheric pCO₂, whereas the density destratification of the deep South Atlantic lags the second rise in atmospheric pCO₂ during the late deglacial period. Our findings emphasize that the physical and chemical destratification of the ocean are not as tightly coupled as generally assumed.

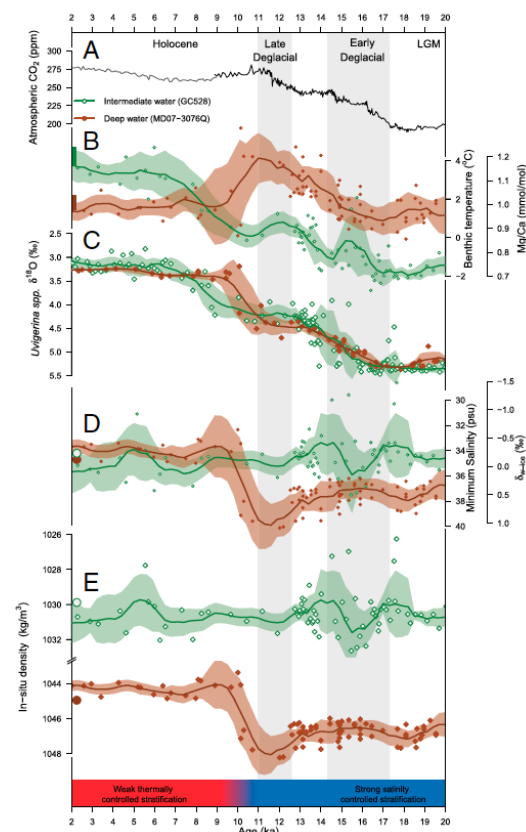


Fig. 1. Deglacial records from intermediate (GC528) and deep (MD07-3076Q) water. (A) Atmospheric CO₂ [West Antarctic Ice Sheet (WAIS) Divide (50), black; EPICA Dome C (EDC) (51), gray]. (B) Mg/Ca-derived benthic temperatures for the intermediate site (GC528; green, open symbols) and the deep site (MD07-3076Q; brown, closed symbols). Thick bars at the start of each timeseries show modern temperature range. (C) Foraminiferal $\delta^{18}\text{O}$ for the same sites as in B. (D) $\delta^{18}\text{O}$ offset from contemporaneous global mean $\delta^{18}\text{O}$ ($\delta\text{w-ice}$) for the same sites as in B. Large circles at the start of each timeseries show modern salinity at each core site. (E) In situ density of the intermediate site (GC528) and the deep site (MD07-3076Q). Modern in situ density shown by large circle at the start of each timeseries. The 1.5-ky spline and 1 σ confidence interval for each plot shown as solid line and polygon, respectively.

Late Pleistocene climate evolution in Southeastern Europe recorded by soil bacterial membrane lipids in Serbian loess

L. Schreuder, C. Beets, M. Prins, C. Hatté, F. Peterse

Palaeogeography, Palaeoclimatology, Palaeoecology, 449, 141-148, 2016.

Loess–paleosol sequences in the Vojvodina region in the southeastern Carpathian Basin have been intensively studied to obtain a high-resolution stratigraphical framework for the Upper Pleistocene in this part of Europe. In these studies, millennial-scale sedimentation variations in the Upper Pleniglacial have been coupled to the Greenland Ice dust record, indicating that the rapid climate variability characterizing the North Atlantic and Greenland areas, is reflected in the loess deposits at the southern edge of the European loess belt. Rapid variations were recently also reported for the stable isotopic composition of organic matter in the Surduk loess–paleosol sequence, located in the Vojvodina region, and were interpreted as episodes of increased C₄-vegetation over the last glacial period. Based on potential coinciding changes in oceanic and atmospheric circulation patterns, these episodes were attributed to plant moisture stress rather than by fluctuations in temperature, although exclusive proof has not yet been provided. Here we report a high-resolution record of continental air temperature and precipitation over the past 40,000 years based on soil bacterial lipid signatures preserved in the Surduk loess–paleosol sequence. Our temperature record shows a gradual warming trend, suggesting that moisture availability indeed seems to be the main factor driving the excursions to C₄-vegetation around Surduk. We

also find that continental air temperature changes in this region may be seasonally biased, and were driven by regional influences rather than by Northern Hemisphere climate forcings, likely as a result of the inland isolation of the Carpathian Basin by surrounding mountains. Support for a regional climate driver comes from comparison of our lipid based temperature and precipitation records with similar records from the near-by Crvenka loess–paleosol sequence, which resemble the climatic trends recorded at Surduk.

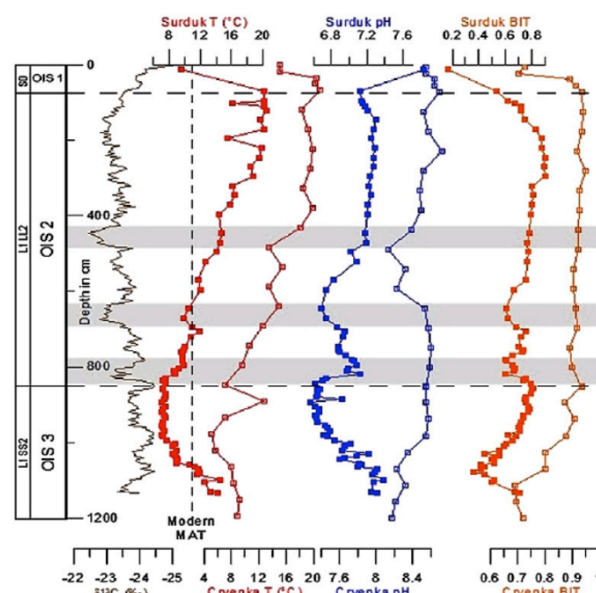


Fig. 1: Variations in reconstructed air temperature, pH and BIT at the Surduk loess–paleosol sequences (closed symbol) with the same records from the Crvenka loess–paleosol sequences (open symbol). Gray areas indicate excursions in the $\delta^{13}\text{C}$ record towards C₄-plant-dominated vegetation



Authigenic $^{10}\text{Be}/^9\text{Be}$ ratio signatures of the cosmogenic nuclide production linked to geomagnetic dipole moment variation since the Brunhes/Matuyama boundary

Q. Simon, N. Thouveny, D. L. Bourlès, JP Valet, F. Bassinot, L. Ménébréaz, V. Guillou, S. Choy, L. Beaufort

J. Geophys. Res. Solid Earth, 121, 7716-7741, 2016.

Geomagnetic dipole moment variations associated with polarity reversals and excursions are expressed by large changes of the cosmogenic nuclide beryllium-10 (^{10}Be) production rates. Authigenic $^{10}\text{Be}/^9\text{Be}$ ratios (proxy of atmospheric ^{10}Be production) from oceanic cores therefore complete the classical information derived from relative paleointensity (RPI) records. This study presents new authigenic $^{10}\text{Be}/^9\text{Be}$ ratio results obtained from cores MD05-2920 and MD05-2930 collected in the west equatorial Pacific Ocean. Be ratios from cores MD05-2920, MD05-2930 and MD90-0961 have been stacked and averaged. Variations of the authigenic $^{10}\text{Be}/^9\text{Be}$ ratio are analyzed and compared with the geomagnetic dipole low series reported from global RPI stacks. The largest ^{10}Be overproduction episodes are related to dipole field collapses (below a

threshold of $2 \times 10^{22} \text{ Am}^2$) associated with the Brunhes/Matuyama reversal, the Laschamp (41 ka) excursion, and the Iceland Basin event (190 ka). Other significant ^{10}Be production peaks are correlated to geomagnetic excursions reported in literature. The record was then calibrated by using absolute dipole moment values drawn from the Geomagia and Pint paleointensity value databases. The ^{10}Be -derived geomagnetic dipole moment record, independent from sedimentary paleomagnetic data, covers the Brunhes-Matuyama transition and the whole Brunhes Chron. It provides new and complementary data on the amplitude and timing of millennial-scale geomagnetic dipole moment variations and particularly on dipole moment collapses triggering polarity instabilities

Tephrochronology of a ~70 ka long marine record in the Marsili Basin (southern Tyrrhenian Sea)

S. Tamburrino, D.D. Insing, N. Pelosi, C. Kissel, C. Laj, L. Capotondi, M. Sprovieri

Journal of Volcanology and Geothermal Research 327, 23–39, 2016.

A sequence of tephra layers has been studied in a 13.9 m-long deep-sea core (MD01-2474G) from the southern Tyrrhenian Sea, covering the last 70 ka. Based on a precise chronological framework, proximal-distal correlations could be performed and allowed to identify in this proximal core, the Y-1 (~ 16 ka), Y-6 (~ 42.5 ka) and Y-7 (~ 54.8 ka) main marker tephras previously recognized farther away.

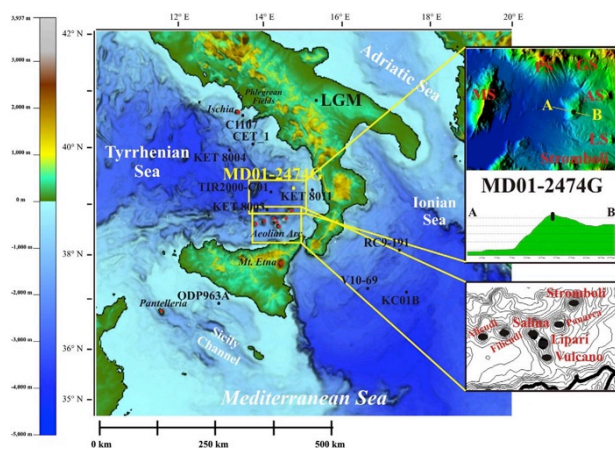
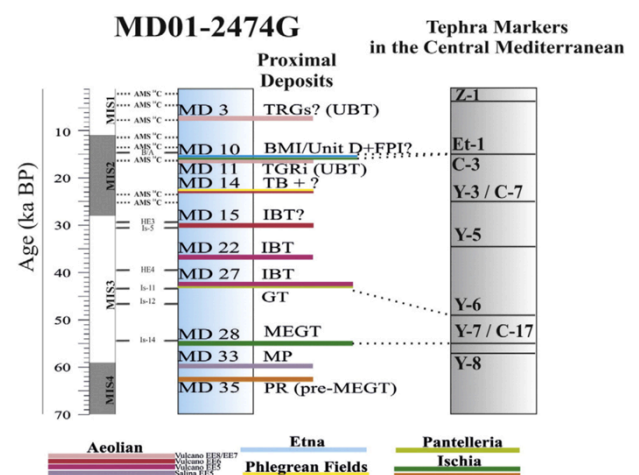


Fig. 1. Location of the core with respect to the location of the main volcanic centers giving rise to tephra layers found at sea.

In addition, detailed compositional data on fresh micro-pumice or glass shards were performed. They allowed to correlate these tephra with the coeval volcanic activity of Aeolian Arc (Vulcano and Salina), Mt. Etna,



Phlegrean Fields, Pantelleria and Ischia. At the end, the tephra sequence of core MD01-2474G contains a number of deposits documenting recurrent activity on Vulcano Island at ca. 6.9 ka, ca. 16.7 ka, ca. 23.2 ka, ca. 29.6 ka, ca. 36.9 ka and ca. 42.5 ka BP.

The results improve the southern Tyrrhenian Sea tephrostratigraphic framework and provide new insights into chemistry and dispersal area of Aeolian Arc pyroclastic deposits in this sector of the Central Mediterranean.

Fig. 2. MD01-2474G tephra record from MIS4 to MIS1 and correlation with some of the main marker tephras of the Central Mediterranean.



Acquisition of detrital magnetization in four turbidites

C. Tanty, J.-P. Valet, J. Carlut, F. Bassinot, S. Zaragosi

Geochemistry Geophysics Geosystems, 17, 3207–3223, 2016.

Turbiditic events are mostly avoided in paleomagnetic studies and therefore their remanence and magnetic properties are poorly described. Turbidites are exempt of bioturbation and potentially provide pertinent information about depositional remanence. We studied four quaternary turbidites of different origins in marine sediment cores. Upward fining of both magnetic and sedimentary fractions indicates that coarser grains reached the bottom first. We observe a progressive shallowing of the magnetic inclinations between the upper and bottom layers of the turbidites that increases with the size of the events and obeys a simple linear scaling law. Measurements of magnetic anisotropy suggest that hydrodynamic conditions prevailing during deposition seem to be dominant for the alignment of the magnetic grains. We suggest that small spherical grains are randomly oriented with zero resultant magnetization in presence of strong turbulent conditions, while the alignment of elongated grains is constrained by the competition between gravity and magnetic forces. A possible scenario is that under

turbulent conditions they tend to rest at the bottom with their long axes parallel to the sediment surface and therefore with shallow inclinations, whereas weakly turbulent conditions like during the smallest (26 cm thick) event do not disturb the magnetic alignment and therefore do not generate inclination shallowing.

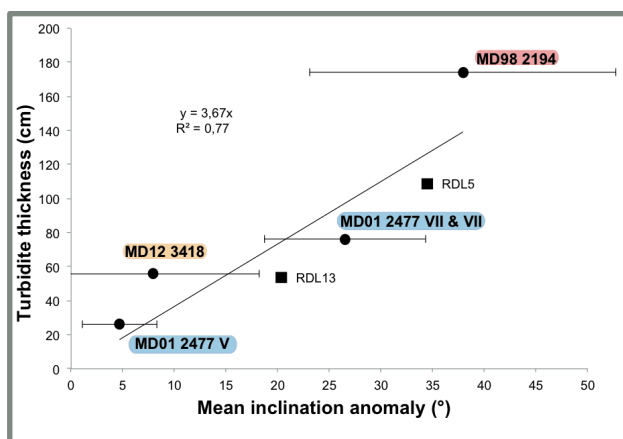


Fig. 1: Linear fit of the deviation of the mean inclination from the GAD value at each site as a function of turbidite thickness for the four turbidites of this study and two turbidites (RDL5 and RDL13) from St.-Onge et al. (2004).

Development of LA-MC-ICPMS for boron isotopic measurement in biocarbonates

F. Thil, D. Blamart, C. Assailly, C.E. Lazareth, T. Leblanc, J. Butsher, E. Douville

Rapid Commun. Mass Spectrom., 30, 359–371, 2016.

Laser Ablation coupled to Multi-Collector Inductively Coupled Plasma Mass Spectrometry (LA-MCICPMS) is a powerful tool for the high-precision measurement of the isotopic ratios of many elements in geological samples, with the isotope ratio ($^{11}\text{B}/^{10}\text{B}$) of boron being used as an indicator of the pH of oceanic waters. Most geological samples or standards are polished and ablation occurs on flat surfaces. However, the shape and the irregularities of marine biocarbonates (e.g., corals, foraminifera) can make precise isotopic measurements of boron difficult. Even after polishing, the porosity properties and the presence of holes or micro-fractures affect the signal and the isotopic ratio when ablating the material, especially in raster mode. The effect of porosity and of the crater itself on the ^{11}B signal and the isotopic ratio acquired by LA-MCICPMS in both raster and spot mode was studied. Characterization of the craters was then performed with an optical profilometer to determine their shapes and depths (Fig. 1). Surface state effects were examined by analyzing the isotopic fractionation of boron in silicate (NIST-SRM 612 and 610 standards) and in carbonate (corals). Surface irregularities led to a considerable loss of signal when the crater depth exceeded 20 μm . The stability and precision were degraded when ablation occurred in a deep cavity. The effect of laser

focusing and of blank correction was also highlighted and our observations indicate that the accuracy of the boron isotopic ratio does not depend on the shape of the surface. After validation of the analytical protocol for boron isotopes, a raster application on a *Porites* coral, which grew for 18 months in an aquarium after field sampling, was carried out. This original LA-MC-ICPMS study revealed a well-marked boron isotope ratio temporal variability, probably related to growth rate and density changes, irrespective of the pH of the surrounding seawater.

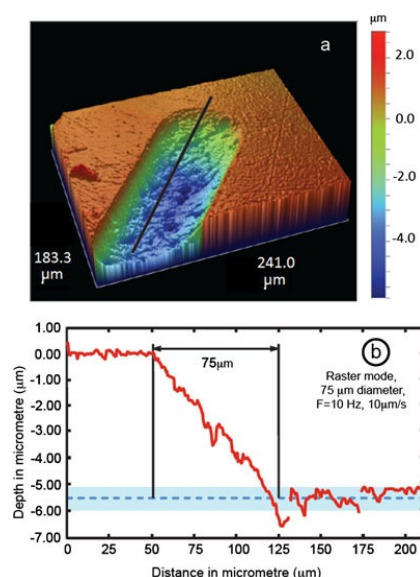


Fig.1: Crater characterization in raster mode, on a carbonate. (a) Laser ablation in raster mode. 3D surface image obtained by optical profilometer (b) and axial section.



Acquisition of isotopic composition for surface snow in East Antarctica and the links to climatic parameters

A. Touzeau, A. Landais, B. Stenni, R. Uemura et al.

The Cryosphere, 10, 837-852, 2016.

Used alone, the isotopic compositions of O and H in ice give insights into the variations of the local temperature, whereas taken together they can provide information on the climatic conditions at the point of origin of the moisture. Recent analyses of snow from shallow pits indicate that the climatic signal can become erased in very low accumulation regions, due to local processes of snow reworking. The signal-to-noise ratio decreases and the climatic signal can then only be retrieved using stacks of several snow pits. The signal is not completely lost at this stage, otherwise it would be impossible to extract valuable climate information from ice cores. To better understand how the climatic signal is passed from the precipitation to the snow, we present here results from varied snow samples from East Antarctica. We look at the relationship between isotopes and temperature, using results from 3 traverses across Antarctica. We take advantage of these measures to see how 2nd-order parameters (d-excess, ^{17}O -excess) are related to $\delta^{18}\text{O}$. d-excess increases in the interior of the continent, due to the distillation process, whereas ^{17}O -excess decreases in remote areas, due to kinetic fractionation at low temperature. In both cases, these changes are associated with the loss of original information regarding the source. Then, we look at the same relationships in precipitation

samples collected over 1 year at Dome C and Vostok, as well as in surface snow at Dome C. The slope of the $\delta^{18}\text{O}$ vs. temperature relationship decreases in these samples compared to those from the traverses, and thus caution is advocated when using spatial slopes for past climate reconstruction. The 2nd-order parameters behave in the same way in the precipitation as in the surface snow from traverses, indicating that similar processes are active and that their interpretation is complicated by local temperature effects in East Antarctica. We then check if the same relationships between $\delta^{18}\text{O}$ and 2nd-order parameters are found in the snow from four snow pits. While the d-excess remains opposed to $\delta^{18}\text{O}$ in most snow pits, the ^{17}O -excess is no longer positively correlated to $\delta^{18}\text{O}$ and even shows anti-correlation to $\delta^{18}\text{O}$ at Vostok. This may be due to a stratospheric influence at this site and/or to post-deposition processes.

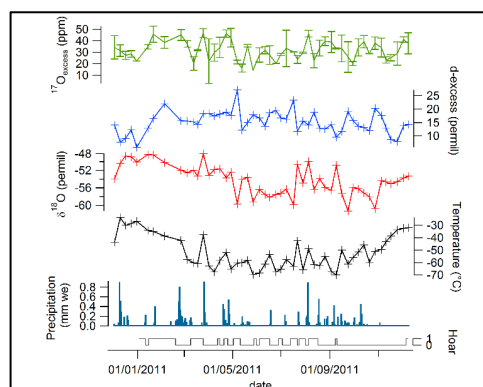


Fig1: Isotopic composition of surface snow

Fossil redox-conditions influence organic matter composition in loess paleosols

K. Vancampenhout, J. Schellekens, J. Slaets, C. Hatté, P. Buurman

Quaternary International, 418, 105-115, 2016.

The soil memory recorded in paleosols of loess-paleosol sequences is an important contributor to our understanding of past climatic conditions. Molecular proxies based on the organic matter preserved in paleosols form an essential part of this record, but the long-term preservation of SOM is poorly understood, especially for sediment traps and slope profiles. This paper addresses the composition of organic material from the Early Weichselian A-horizons of the Rocourt paleosol, a major paleostratigraphic marker for the Eemian and Early Weichselian in Western Europe. NaOH-extractable organic matter from an exceptionally thick Rocourt profile in the Kesselt Quarry (Belgian Loess Belt) was analyzed by pyrolysis-Gas Chromatography/Mass Spectrometry (pyrolysis-GC/MS) and the results evaluated against paleopedological data. The molecular composition of the organic matter at Kesselt was compared with reference samples from two nearby quarries (including the type locality at Veldwezelt-Hezerwater), and to a sample from the contemporary Nussloch sequence in Germany. The SOM composition found at the four sites indicated a large content of microbial matter and was dominated by carbohydrates and N compounds, many of which were not

reported before from SOM pyrolysates. Differences in the molecular composition between samples, both within profiles and between sites, coincided with differences in landscape position (slope-shoulder-plateau) and fossil redox conditions (surface gleys). Samples from drier and more upland situations contained more burnt material, while samples from slope profiles and surface gleys contained even more microbial material, in particular chitin. Results therefore suggest that the admixture of microbial SOM is considerable in loess-paleosols and that differences in edaphic conditions (in particular slope position and soil moisture) and occurrence of wildfires are important for the long-term preservation of SOM. These should therefore be considered when interpreting biogeochemical proxies.

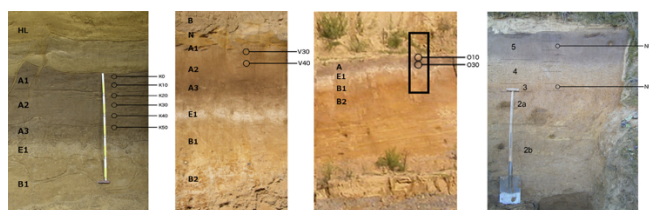


Fig. 1. Profiles at Kesselt (K; left) Veldwezelt-Hezerwater (V; middle-left), Kesselt-Op de Schans II (O; middle-right) and Nussloch (N; right). Sampling locations for pyrolysis-GC/MS are indicated by open circles

Mg/Ca thermometry in planktic foraminifera: improving paleotemperature estimations for *G. bulloides* and *N. pachyderma* left

N. Vázquez Riveiros, A. Govin, C. Waelbroeck, A. Mackensen, E. Michel, S. Moreira, T. Bouinot, N. Caillon, A. Orgun, M. Brandon

Geochemistry, Geophysics, Geosystems, 17, 1249-1264, 2016.

Planktic foraminiferal Mg/Ca ratios have become a fundamental seawater temperature proxy in past climate reconstructions, due to the temperature dependence of Mg uptake into foraminiferal calcite. However, empirical calibrations for single species from methodologically consistent data are still lacking. Here we present species-specific calibrations of Mg/Ca versus calcification temperature for two commonly used species of planktic foraminifera: *Globigerina bulloides* and *Neogloboquadrina pachyderma* left, based on a series of Southern Ocean and North Atlantic core tops. Combining these new data with previously published data, we derive an integrated *G. bulloides* Mg/Ca-temperature calibration for mid and high latitudes of both hemispheres between 2 and 18°C, where $\text{Mg/Ca} = 1.006 \pm 0.032 * e^{0.065 \pm 0.003 * T_{\text{iso}}} (R^2 = 0.82)$. *G. bulloides* is found to calcify deeper in the Southern Ocean (~ 200 m) than in the North Atlantic (top 50 m). We also propose a Mg/Ca temperature calibration to describe the temperature response in *N. pachyderma* left that calcified away from the influence of sea ice in the Southern Ocean, valid between ~ -1 and 9°C, of the form $\text{Mg/Ca} = 0.580 \pm 0.016 * e^{0.084 \pm 0.006 * T_{\text{iso}}} (R^2 = 0.70)$. These calibrations

account for uncertainties on Mg/Ca measurements and calcification temperature that were carefully estimated and propagated using Monte Carlo iterations. The 1 σ propagated error in Mg/Ca-derived temperatures is 1.1°C for *G. bulloides* and 0.9°C for *N. pachyderma* left for the presented data sets. Geographical extension of genotypes must be assessed when choosing to develop regional or global calibrations.

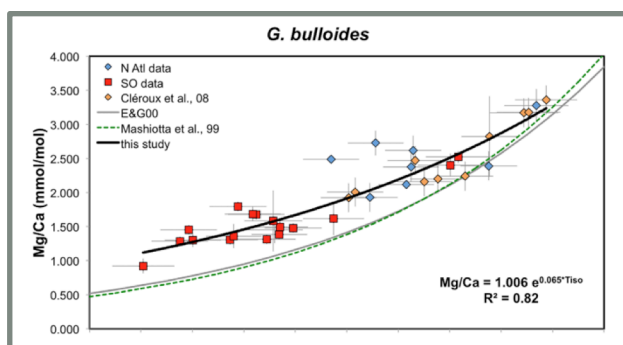


Fig. 1. Mg/Ca (mmol/mol) versus isotopic temperature (8C) for *G. bulloides*. All symbols are site averages; red squares are new Southern Ocean data; blue diamonds are new North Atlantic data presented in this study [Bouinot, 2011]; orange diamonds are the data set of Cléroux et al. [2008] with T_{iso} recalculated as explained in section 2.4. Black thick line indicates the regression including all sites (equation(4)). The regression curves of Mashiotta et al. [1999] (*G. bulloides*, green-dashed line) and Elderfield and Ganssen [2000] (multispecies, grey line) are also shown for comparison.





Projets des thèses soutenues et des postdoctorats de 2016



Multi-archive coherent and precise chronological framework for the Last Interglacial and MIS 3

Lucie Bazin, A. Govin (CliMag group) and collaborators from IPSL

Post-doctoral position (2 years). Framework Labex L-IPSL

On November 1st, 2016, Lucie Bazin joined the CliMag group as a post-doctoral researcher for a two years position funded by the labex L-IPSL. The project is at the interface between the different paleoclimate communities represented within IPSL.

While numerous proxies are now systematically measured over paleoclimate archives, the inconsistency of the dating methods and the uncertainty of chronologies are often the limiting factors for their proper interpretations. This is especially true for the millennial climate variability characterizing the last glacial period (MIS 3) and the timing of the last interglacial (LIG) climate optimum. These periods are very important for better understanding the sequence of events and the interactions between the different climate components. Indeed, the MIS 3 and LIG are now target periods for the CMIP6/PMIP4 modelling exercises, and the subjects of recent transient simulations. Consequently, in order to benefit from future model-data comparisons, the paleodata community needs to propose precise and coherent proxy reconstructions to better assess/ constrain model simulations. The project aims at building a coherent and precise multi-archive chronological frameworks covering the LIG and the MIS 3 periods. Such a framework will permit to discuss past climate changes as recorded by selected proxies measured from different archives located at different latitudes with a proper assessment of the chronological uncertainties and hypotheses of synchronization.

To obtain such a coherent chronological framework we will use the “Datice” dating tool, first used to date ice cores and now adapted for multi-archive dating. Datice permits to coherently date several cores/archives using absolute and relative age constraints and calculates the chronology uncertainty. In this project we mainly aim to combine temperature and isotope records from different archives (e.g. ice cores, marine cores, corals, lake sediments, speleothems and loess). We will make the best use of records from well-dated regions (e.g. volcanic regions) to obtain a precise chronology. These age constraints will then be transferred to the other sites through the synchronization of records as independently of the climate as possible, or with a proper assessment of the uncertainties associated with the tuning method.

Detrital signature of Late Quaternary paleo-environmental changes in the northern South China Sea

Quan Chen

PhD thesis, Université Paris-Saclay (co-tutelle C. Kissel, LSCE CliMag group and Z. Liu, Tongji University, Shanghai), Defended on Dec. 8th 2016, with high honors. Framework LIA-MONOCL

With the aim of reconstructing late Quaternary changes in land-sea interaction, East Asian monsoon, and oceanic circulation in the northern part of the South China Sea, a multi-proxy investigation has been conducted on the 50.8 m-long marine sediment core MD12-3432 (Fig. 1).

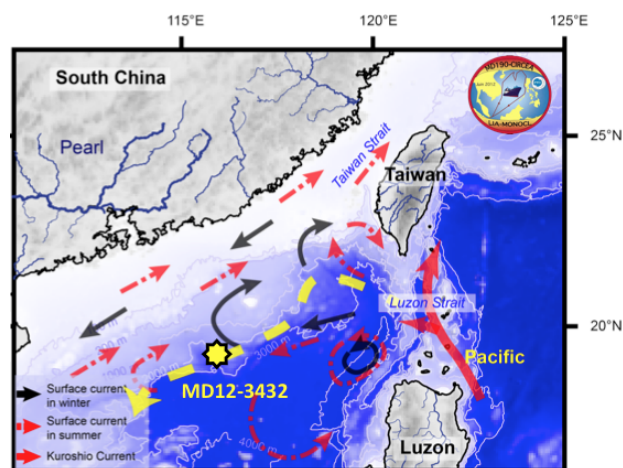


Fig. 1. Location of the studied core in the northern part of the South China Sea, on the continental slope, off the Pearl River mouth

Clay and magnetic mineralogy, major element composition, sedimentary and magnetic grain size, as well as the preferential alignment of magnetic grains in the sediment were analyzed at high resolution over the last 400 ka. Low-latitude

climate changes are recorded at different time scales (400, 100 and 23 ka) by the various terrigenous fractions that originate from Taiwan, Luzon and mainland Asia.

The long-term increase in pyrrhotite and illite+chlorite supply suggests that the Taiwan orogeny has intensified over the last 400 ka.

In addition, enhanced East Asian summer monsoon during interglacials is shown by increased K_2O/Al_2O_3 ratios related to precipitation and denudation rate in Taiwan, and by increased smectite/(illite+chlorite) ratios due to contemporaneous enhanced chemical weathering intensity in Luzon. Also, at that time scale, glacials low sea-levels reduce the land-site distance inducing the deposition of more kaolinite (Pearl River), coarser grains and remobilization of shelf sediments from Taiwan and Pearl River.

Smectite content increases during precession maxima due to increased precipitation over Luzon, while high hematite-rich magnetic inputs are observed during precession minima. These events occurring during arid periods may illustrate enhanced eolian inputs caused by changes in wind intensity and/or winds pathway due to the weak summer monsoon.



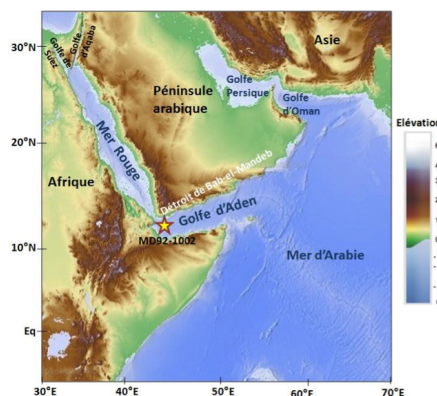
Reconstitution de la variabilité de la mousson indienne et ses impacts environnementaux sur le Nord-Ouest de la Mer d'Arabie et ses bordures continentales depuis le Dernier Maximum Glaciaire

Wiem Fersi

Thèse de Doctorat, Université Paris Saclay, soutenue le 30 septembre 2016.

La carotte MD92-1002 prélevée dans le Golfe d'Aden (12°01'32 N- 44°19'02E -1327 m de profondeur) fournit un enregistrement paléoenvironnemental et paléoclimatique unique permettant de discuter l'évolution des milieux continentaux et océaniques depuis 20 000 ans BP. Les grains de pollen révèlent des conditions régionales hyper-arides pendant la période glaciaire caractérisée par une végétation clairsemée d'origine Saharo-Sindienne. L'abondance des taxons steppiques associés aux microparticules de charbon suggère une activité éolienne élevée. Les marqueurs d'humidité augmentent dès 14 900 ans BP et atteignent leur maximum entre 9 000 et 7 500 ans BP, au moment où se développe une mangrove à Rhizophora dans le Golfe d'Aden reflétant des conditions tropicales avec une saison pluvieuse d'été. La chronologie des événements élaborée à partir des résultats polliniques et des enregistrements continentaux tels les témoins des lacs et marécages et les spéléothèmes de Socotra et d'Oman documente la progression vers le Nord et l'Ouest de la limite estivale de la Zone de Convergence Inter-Tropicale (ITCZ) au cours de la transition glaciaire-interglaciaire, au moment de la mise en place de la Période Humide Holocène (PHH). L'ITCZ est localisée au Sud de l'Éthiopie à 19 000 ans BP puis migre vers le Nord pour atteindre Socotra à 14 510 ans BP, Qunf à 10 400 ans BP et Hoti à 10 000 ans BP. Les mouvements de l'ITCZ vers l'Ouest sont documentés par le développement de la mangrove

à Rhizophora à partir de 12 600 ans BP. La carotte MD 92-1002 permet également de documenter la fin de la PHH qui débute très tôt comparativement à ce qui est observé en Afrique nord tropicale, en deux étapes successivement datées de 7500 et 4000 BP. Les assemblages de dinoflagellés montrent que la période glaciaire est caractérisée par de faibles upwellings et des eaux profondes bien ventilées. La productivité primaire marine dans le Golfe d'Aden augmente à partir de 14 500 ans BP et atteint un maximum pendant la transition glaciaire/interglaciaire, entre 12 600 et 10 800 ans BP. Il survient ~ 3 000 ans avant le pic d'intensité des upwellings de la marge d'Oman associé au maximum des vents de la mousson du S-O. Cette singularité pourrait s'expliquer par les conditions très particulières du Golfe d'Aden qui est situé à l'intersection de deux systèmes de vents orthogonaux pendant l'été boréal (des vents du S-O à l'Est du golfe et des vents orientés du N-O en provenance de la Mer Rouge).



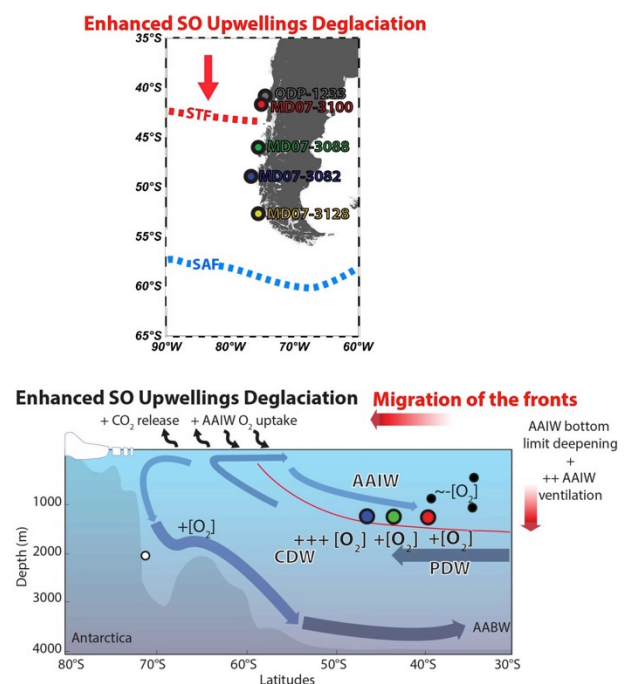
Role of the Southern Ocean in the millennial scale climatic events of the glacial - Holocene transition: geochemical and micropaleontological approach

Naoufel A. Haddam

PhD thesis- Université Paris-Saclay (co-direction E. Michel, LSCE Paleocean group and G. Siani GEOPS, Université Paris Sud,), Defended on Dec. 12th 2016, Gif-sur-Yvette.

The last 22 ka are marked by abrupt climatic events, non-synchronous between the southern and northern hemispheres. A see-saw mechanism of the polar temperatures, amplified by the deep ocean ability to store and release atmospheric CO₂, depending and the intensity of the thermohaline circulation and/or of the large upwellings along the southern Ocean divergence, has been proposed to explain these observations. However, the various Earth System Model simulations indicates two different possible mode of Southern Ocean behavior: zonal or opposite in the Atlantic and Pacific sectors, linked to either a pure ocean or a coupled atmospheric-ocean bi-polar see-saw mechanism. While the Atlantic sector behavior is well documented, the evolution of the Southern Ocean pacific sector is poorly documented. The main aim of this thesis was to assess the role of the Southern Ocean during these abrupt climatic events, studying 3 marine cores retrieved on a latitudinal gradient, along the Chilean margin, under the influence of oceanic fronts and westerly wind belt. The reconstruction of the sea surface temperatures (SST) allowed to reconstruct the evolution of the SST latitudinal gradient during the last 22 ka. We highlight southward migration of the subtropical front during abrupt events that is coeval with nutrient input increases in surface waters and enrichment of intermediate water CO₂. Our results indicate that a) stronger upwellings at

the southern divergence that delivers CO₂ to the atmosphere (as indicated by atmospheric CO₂ increases in Antarctic ice cores) leads to an increase in Antarctic intermediate waters formation that fill the 3 majors ocean basins (Atlantic, Indian and Pacific) b) these enhanced Southern Ocean upwellings are the results of rapid



coupled atmosphere-ocean reorganization and not of a pure ocean thermohaline mechanism.

Fig. Evolution of the oceanic fronts and the intermediate southern ocean circulation during upwelling events that released CO₂ from the deep ocean to the atmosphere.

Characterization of the ferruginous particles in the Seine River using environmental magnetism

Dariouche Kayvantash

PhD thesis– (co-tutelle C. Kissel, LSCE CliMag group and I. Cojan, Ecole des Mines, Fontainebleau).
Defended on Nov. 28th 2016. Framework Piren-Seine.

Iron (hydr)oxides, are ubiquitous in natural and anthropogenic environments, and are sensitive to environmental changes. They can hence be used as tracers for environmental sources and processes. The impact of recent human activities on the ferruginous compounds of the suspended particulate matter (SPM) of the Seine River (France) was investigated using environmental magnetism methods (mainly hysteresis properties).

SPM sampling was conducted along the Seine River and its main tributaries under different hydrological conditions (work conducted by L. Konecny in 2011-2012). In order to test the representativeness of sampling and methods, a non-managed meander in the upstream stretch of the Seine River has also been studied at Marnay-sur-Seine (cross and depth sections during low- and high-water stages). Finally samples were collected before and after treatment at the main wastewater plant.

The main magnetic carrier is magnetite, concentrated in the fine particulate fraction ($< 63\mu\text{m}$). Along the river, an increase in magnetic concentration and grain size is associated to urbanization and industrial activities which are sources of anthropogenic particles. Significant

variations can be observed between the upstream and downstream of confluences. Part of the decrease in concentration at the exit of the wastewater plant is related to dilution by iron-poor rejected waters. Time variations in magnetic concentration along the Seine can also be associated to hydrodynamic processes such as dilution, accretion, transport and re-suspension of the ferruginous particles.

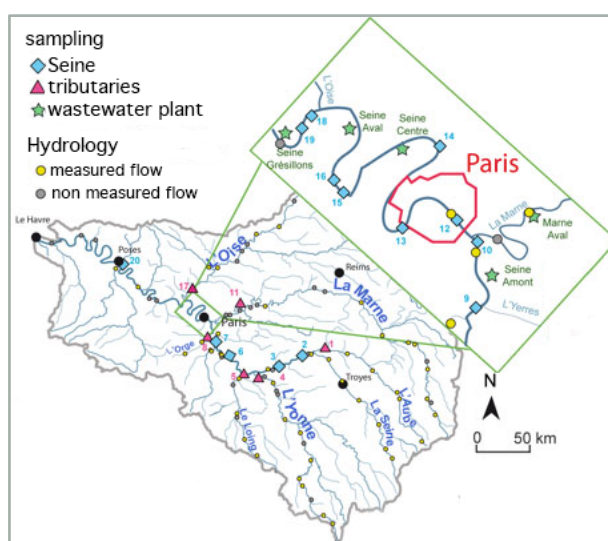


Fig. 1. Location of the studied sites along the main stream of the Seine river, in its tributaries, in the wastewater plants.

Le système des carbonates influencé par la diagenèse précoce dans les sédiments côtiers méditerranéens en lien avec l'acidification des océans

Jens Rassmann

PhD thesis - University Paris-Saclay – Supervisors : C. Rabouille and B. Lansard, LSCE) – defended on 28th Nov. 2016.

L'océan côtier occupe une position clé dans le cycle du carbone et est exposé à l'acidification des océans. Une grande partie de matière organique (MO) marine et continentale est minéralisée dans les sédiments estuariens par des voies aérobies ou anaérobies. Cette minéralisation produit du carbone inorganique dissous (DIC), mais aussi de l'alcalinité totale (TA) pour la partie anoxique, ce qui tamponne les variations de pH du système et augmente la capacité de l'eau de mer à absorber du CO_2 .

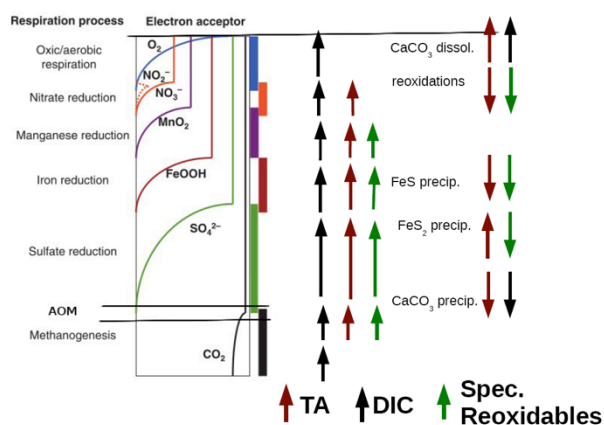


Fig. 1. Succession des réactions diagénétiques avec leur effet sur les flux de TA (rouge) et de DIC (noir) dans les eaux interstitielles. La respiration anaérobie produit des espèces chimiques réoxydables (sauf la dénitrification) qui sont représentées en vert.

Des mesures dans les sédiments du prodelta du Rhône ont montré que la minéralisation anoxique, surtout la sulfato-réduction, y est dominante et produit des forts taux de TA et de DIC. Proche de l'embouchure, c'est surtout la MO continentale qui est minéralisée et la fraction marine augmente vers le large.

Une expérience d'acidification de sédiments de la baie de Villefranche-sur-Mer a montré que l'acidification des océans cause la dissolution des carbonates ce qui tamponne le pH dans les sédiments.

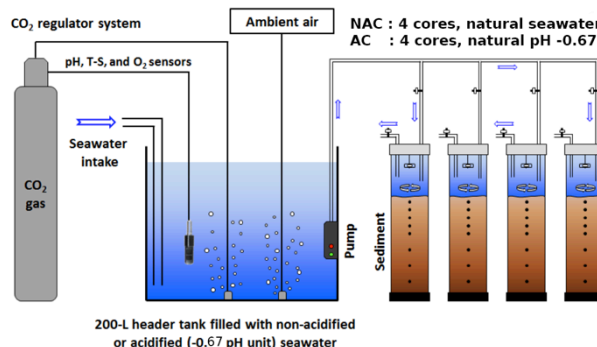


Fig. 2. Schéma de l'expérience ACIBIOS pour étudier la réponse biogéochimique des sédiments côtiers à l'acidification de l'océan. Des sédiments prélevés dans la baie de Villefranche-sur-Mer ont été acidifiés et mis en incubations pendant une période d'un mois.





Autres activités marquantes de 2016



Inter-comparaison des mesures d'O₂ dissous dans l'océan Arctique

B. Bombled, B. Lansard, J. Boutin et E. Michel

(<http://ilsremontentletemps.inflexion.info/?q=node/3>)

La mission STEP a été réalisée en Juillet 2016 à bord du N/O L'Atalante (IFREMER), dans le Storfjorden (Spitzberg) dans une zone de formation d'eaux denses de saumure. Le projet vise à comprendre les processus physiques de formation d'eaux profondes et leur impact sur le cycle des gaz à effet de serre et la circulation océanique.

Une inter-comparaison a été réalisée entre les mesures de concentrations en oxygène dissous (O₂) par la méthode chimique de titration, dite de Winkler (en $\mu\text{mol/l}$) sur les eaux prélevées par la rosette et celles obtenues, aux mêmes profondeurs, avec un capteur in situ d'O₂ à membrane (SBE43 en $\mu\text{mol/kg}$) fixé également sur la rosette. La conversion utilisée est : O₂ ($\mu\text{mol/kg}$) = O₂ ($\mu\text{mol/l}$)/densité eau de mer (ρ).

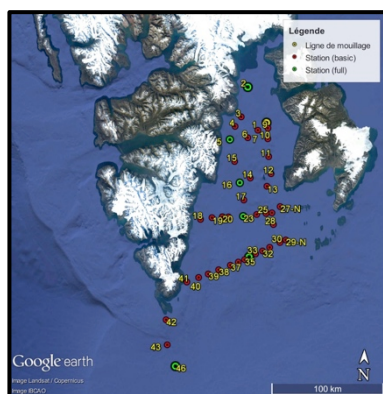


Fig. 1: localisation des sites de prélèvement

Au total, 69 dosages ont été effectués avec trois dosages par niveau (surface, mi- profondeur et fond) avec une excellente reproductibilité (0.3 $\mu\text{mol/l}$ en moyenne). Aucune dérive de la mesure d'O₂ sur la SBE43 n'a été notée au cours de la campagne. Les valeurs d'O₂ sont cohérentes avec un décalage allant de 1 à 2 $\mu\text{mol/kg}$ entre les mesures in-situ (SBE 43) et ex-situ (Winkler), en fonction des stations échantillonnées. Les plus

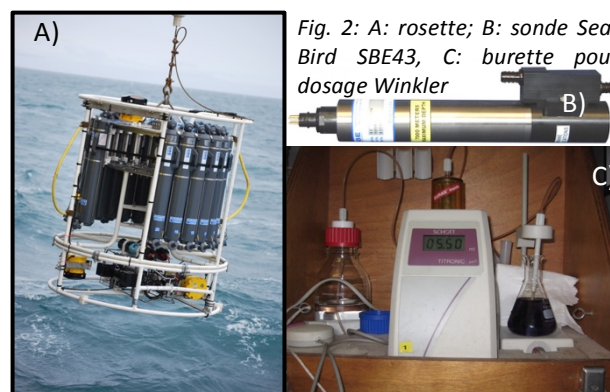


Fig. 2: A: rosette; B: sonde Sea-Bird SBE43, C: burette pour dosage Winkler

forts écarts d'O₂ sont observés en station 23 (Fig. 4) probablement lié à un pic de fluorescence vers 20 m de profondeur (DCM pour Deep Chlorophyll Maximum). Il peut également s'agir d'un problème d'échantillonnage ou de conservation des échantillons prélevés.

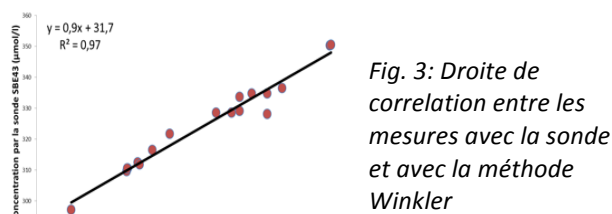


Fig. 3: Droite de corrélation entre les mesures avec la sonde et avec la méthode Winkler

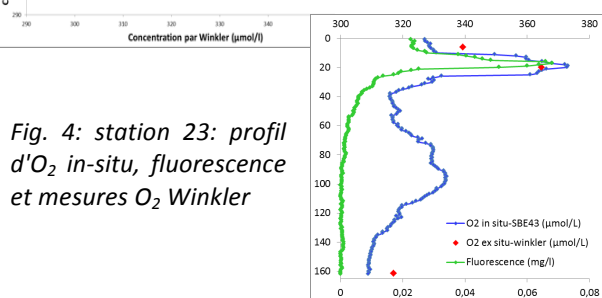


Fig. 4: station 23: profil d'O₂ in-situ, fluorescence et mesures O₂ Winkler

La très bonne cohérence observée ($R^2 = 0.97$) entre les mesures in- et ex-situ d'O₂ montre notre maîtrise des compétences pour la mesure des concentrations d'oxygène dissous dans la colonne d'eau et valide, une fois encore, nos méthodes de prélèvements et de dosage que nous utilisons lors des missions océanographiques du LSCE.



Mise en ligne du site web de la plateforme analytique PANOPLY

N. Caud et les membres de PANOPLY

Le site web de la plateforme PANOPLY a été mis en ligne en avril 2016 : <http://panoply-geops.lsce.ipsl.fr>

Il sert de portail à l'ensemble des analyses disponibles via la plateforme, une cinquantaine, classées selon plusieurs critères :

La thématique scientifique : Géochronologie ; Géochimie et transfert de l'eau et des contaminants dans l'environnement ; Paléoclimatologie et paléocéanographie ; Transferts sédimentaires, diagénèse et ressources.

Le type d'analyse : Minéralogique ; Élémentaire ; Isotopique ; Mesure de la radioactivité

Le type d'échantillon : Eau ; Glace ; Sédiments - sols ; Roches - minéraux ; Carbonates ; Bois-matière organique ; Gaz ; Autre...

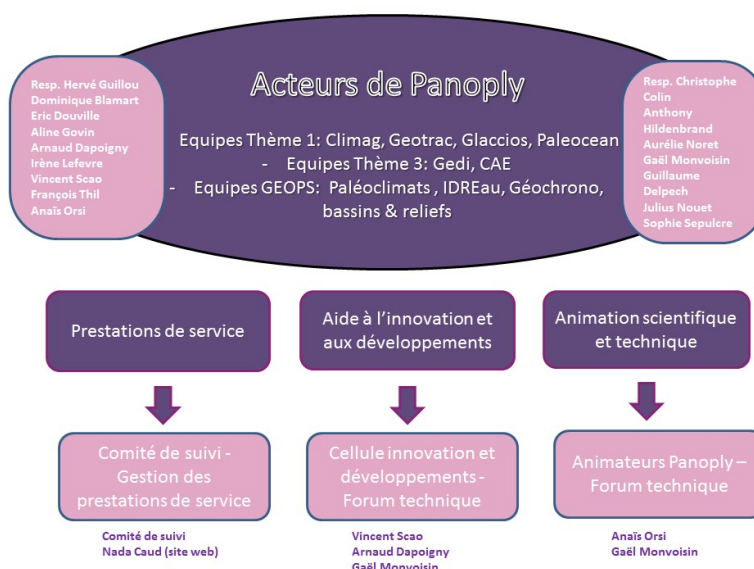
L'élément chimique

Les échanges portant sur des questions techniques, sont facilités par le **forum technique** pour lequel PANOPLY a ouvert un espace collaboratif dédié : https://extra.core-cloud.net/collaborations/PANOPLY/Forum_Technique/SitePages/Accueil.aspx



Inauguration de la plateforme analytique PANOPLY – 06 avril 2016

H. Guillou, C. Colin, N. Caud et les membres de PANOPLY



L'inauguration de la plateforme analytique PANOPLY s'est déroulée le 6 Avril 2016 en présence des tutelles et des organismes impliqués (CEA, CNRS, UPSud, UVSQ, IPSL, Université Paris-Saclay, Conseil Général Essonne, Région Ile-de-France, BNP Paribas).

Insérée dans le tissu technologique du plateau de Saclay, PANOPLY¹ met à la disposition de la communauté scientifique académique et industrielle un éventail de ressources analytiques et expérimentales de hautes performances dédié aux Sciences de la Terre, du Climat et de l'Environnement.

PANOPLY s'appuie sur les expertises reconnues nationalement et internationalement des équipes de recherches du LSCE et de GEOPS pour proposer via un guichet unique l'accès à des services analytiques de haute qualité (de la prestation de routine à la collaboration scientifique) portant

notamment sur le domaines de la géochronologies, de géochimie et la minéralogie.

Articulée autour du comité de suivi, PANOPLY propose en plus des prestations analytiques, des animations techniques et scientifiques visant à consolider le lien entre les aspects expérimentaux aux sens large et les thématiques de recherche menées au LSCE et à GEOPS.

PANOPLY héberge également une cellule « développements-innovations ». Elle recense les besoins en évolutions expérimentales et technologiques des équipes. En créant un tissu collaboratif rassemblant les compétences en ingénierie du LSCE et de GEOPS, elle accompagne le déroulement de ces projets.

¹ <http://panoply-geops.lsce.ipsl.fr>



The μ metal shielded room ready to be moved into ICE

LSCE CliMag group

The ultra-low noise level magnetic measurements are performed by the CliMag group within a three-layer (one soft iron and two μ metal) shielded room constructed in 1987 and extended in 1995 by the Soudupin Enterprise in the CFR/LSCE building located within the CNRS campus in Gif-sur-Yvette. Because this building is oriented about N030° and the paleomagnetic lab is located close to the main transformer of the building, generating high electromagnetic noise, the entrance of the shielded room was not direct. An entrance corridor was made to filter the magnetic field lines.

At the end of 2017, the shielded room will be dismantled and moved from the present building into the new ICE building where it will be reassembled. The ICE building is oriented North-South, roughly parallel to the earth magnetic field, and the paleomagnetic laboratory will be away from any magnetic disturbance (e.g. lift). Therefore, the entrance corridor will not be needed anymore.

The decision was made to modify the shielded room in order to gain inner space. This modification consists in taking apart the internal wall of the corridor, replacing it with a wooden beam, extending the external wall to the full length of the room, creating the missing part of the sealing and floor and embedding a sliding door.

In order not to combine at the same time two complicated operations that are the move of the shielded room and the modification of the

entrance, the latter has been made by Soudupin in 2016, one year before moving.

About four square meters have been gained yielding to a total of 28 m² for the modified shielded room which is now ready to be moved next year to the new ICE building.



Fig. 1. Left: after dismantling the entrance corridor (part of missing sealing and floor is visible). Right: new entrance from inside the shielded room with apparent wooden beam and “direct” entrance.

The polynya and brine dense water multi-disciplinary study: the STEP project and 2016 oceanographic cruise.

E. Michel (LSCE), F. Vivier (LOCEAN) and B. Lansard (LSCE) and the team of the STEP 2016 oceanographic cruise

Dense water formation from brine rejection during ice freezing plays an important role in deep ocean circulation and greenhouse gas (GHG) cycles. Brine rejection is known to contribute to the CO₂ solubility pump by the release of alkalinity and dissolved inorganic carbon. It has been proposed that brine rejection helped maintain a 30% reduction in atmospheric CO₂ content during glacial periods. Yet, processes linked to brine rejection and its impact on GHG cycles, through the solubility and bio-logical oceanic pumps, and on oceanic deep circulation are not fully understood. It is thus not possible to reliably evaluate its role in the near future in a context of rapidly decreasing Arctic sea ice cover. Also, improving the representation of polynyas and brine-enriched shelf waters (BSW) in numerical models is an essential requirement for a correct simulation of deep waters, both in the Arctic and Antarctic. From the test case of an Arctic polynya, the STeP (STor fjorden Polynya multidisciplinary study) project is designed to improve our knowledge on polynya dynamics and processes associated with brine-enriched deep water formation, as well as on the impact of brine on the oceanic circulation and Green house Gases (GHG) cycles through a multi-disciplinary physical-biogeochemical approach.

This program will strengthen an ongoing effort to build a team including physical, biochemical, paleo-oceanographers and modellers. This French consortium has teamed-up with Belgian, German and Norwegian colleagues to promote Storfjorden as an observatory region to investigate processes specific to polynyas, which may ultimately fit within the Svalbard Integrated Observing System (SiOS), a

European Infrastructure under construction (ESFRI). Storfjorden, Svalbard, is of particular interest with this respect as it hosts a relatively accessible latent heat polynya where dense water forms through brine rejection. Previous and ongoing studies have shown high inter-annual variability in the properties of the dense brine-enriched shelf water. Because of the availability of observations, Storfjorden is being used as a test case to assess the capability of state of the art coupled ocean-sea ice models to depict the process of dense water formation within polynya regions. This project relies on oceanographic cruises with mooring deployment/servicing, for the pluriannual survey of the variability of brine-enriched deep water formation, and its impact Green house Gases cycles.

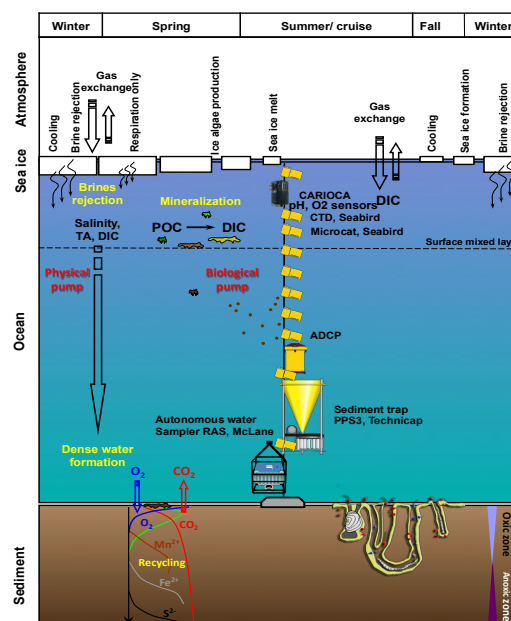


Fig. Annual cycle and mooring line description for a global physical and biogeochemical survey.



ECHoMICADAS, a new AMS research facility at Gif-sur-Yvette, France

N. Tisnérat-Laborde, C. Hatté, F. Thil, C. Gauthier, E. Kaltnecker, C. Noury et collaborateurs*

* GEOPS: Massault Marc, Michelot Jean-Luc, Noret Aurélie, Siani Giuseppe,
AASPE: Zazzo Antoine, Tombret Olivier, Vigne Jean-Denis,
ETH Laboratory of Ion Beam Physics : Synal Hans-Arno, Wacker Lukas.

A Compact Radiocarbon System, *ECHoMICADAS* (for Environment, Climate Human sciences Mini Carbon DATING System), has been installed at Gif-sur-Yvette at the LSCE, in July 2015. It was designed by ETH Ion Beam Physics, in collaboration with LSCE and two others laboratories GEOPS and AASPE (Paris area, France). *ECHoMICADAS* is equipped with i- the hybrid gas ion source that can accommodate samples as solid graphite and gaseous CO₂, ii- permanent magnets, and iii- a stripper gas with helium.



Fig.1: *ECHoMICADAS* at Gif-sur-Yvette, France.

The LSCE-GeoTrAc preparation laboratory can handle samples as organic material, bone, carbonate, dissolved inorganic and organic carbon, soil and sediment fractions, individual lipids.

In 2016, an operating time of 73% of *ECHoMICADAS* was reached although 14 weeks of downtime occurred due to power supply and pump controller problems. During this year, we mainly defined the performance of *ECHoMICADAS* in routine operation (Tab. 1), tested Automated

Graphitisation system and Gas Interface. A significant part of the ¹⁴C laboratory activities consisted in establishing handling protocol and measurement of microsamples (< 100µg de carbon). In 2016, we also started routine analyses.

Standards	Type cible	Référence F ¹⁴ C	F ¹⁴ C mesuré ± 1-σ (1σ)	N _{éch}
NIST OxA2	Graphite	1.3407 (0.0005)	1.3408 ± 0.0025 (0.2%)	72
	EA-GIS		1.3402 ± 0.008 (0.6%)	34
IAEA C7 (OxA)	Graphite	0.4953 (0.0012)	0.4953 ± 0.0015 (0.3%)	24
	EA-GIS		0.4998 ± 0.0112 (2%)	17
IAEA-C8 (OxA)	Graphite	0.1503 (0.0017)	0.1509 ± 0.0017 (1.1%)	23
			0.1517 ± 0.0183 (10%)	8
VIRI-E (Collagène)	Graphite	0.0075 (0.0017)	0.0083 ± 0.0015 (18%)	26
Blancs	Type cible	F ¹⁴ C mesuré ± 1-σ	(Eqv. age BP)	N _{éc}
Acide phtalique	Graphite	0.0022 ± 0.0007	49 250 ± 2 400	45
	EA-GIS	0.015 ± 0.006	33750 ± 3 200	52
IAEA-C1 (Carbonate)	Graphite	0.0014 ± 0.0004	53 000 ± 2 200	14
	GIS	0.0024 ± 0.0018	48 400 ± 6 300	8

Tab.1: F¹⁴C values obtained from four reference standards and two blanks measured in graphite or CO₂ gas.

The activity of the *ECHoMICADAS* Research Facility is summarized by the number of measured samples for the three partners during the year 2016.

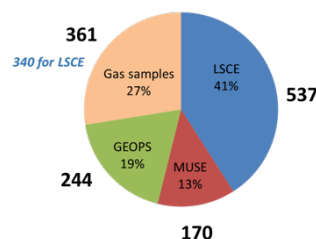


Fig.2: Number of samples analysed in 2016 for tests (mostly included in LSCE portion), developments and various projects of the three partners.



MAGNUS: MAGNetism U-channels Software for cryogenic magnetometer

A. Van Toer and CliMag group

For its research activities in paleoclimate/paleoceanography, the CliMag group has developed the laboratory instruments and procedures for continuous high-resolution magnetic measurements of sedimentary sequences (using u-channels). In particular on our request, 2G Enterprises developed a small-access pass-through cryogenic magneto-meter equipped with high-resolution pick-up coils. This new instrument was delivered with no « satellites ». A “home-made” software for automatic measurements of various remanent magnetizations with this magnetometer had therefore been written. Over the last 25 years, it has progressively been improved and incremented with numerous sub-routines and multiple controls and warnings. Written as a macro Visual Basic for applications (VBA) in Excel, it became progressively too complex and the recent change to PC Windows 7 made its upgrade impossible.

A new version of the software « MAGNUS » has been developed in 2015-2016 in Visual Basic (.Net) for Windows 7, therefore, independent from Excel. This new software includes all the previous developments and warnings with a largely improved organization and important new elements:

- New ergonomic context for a simplified use
- New communication between electronics and computer

- Automatic correction for the unlocking of the electronics in case of abrupt changes in power supply
- Possibility of adjusting the software to the different parameters characterizing each magnetometer.

This unique development is highly valuable for the daily life in our laboratory where it is now routinely used. It also increases our national and international visibility as it can now be exported to numerous laboratories that have been interested for a long time in all included "tricks". It is also accompanied by a new version of the automatic data processing softwares as VBA for Excel 2011.



Fig. 1. Measurement window of MAGNUS with: on the right hand side the data progressively acquired and on the left the parameters of the undergoing treatment (e.g. core label, measured steps).



The new life of our 40-year old core repository

C. Wandres and A. Villedieu

(with the help of CliMag, Paleocean, GEDI and Geotrac groups)

Sedimentary cores have started to be stored 40 years ago at Gif-sur-Yvette, in the “cellar” located below the garden of the CNRS “château”. At that time, only part of what is now our core repository, was used for the storage but progressively, the space has been filled up, in particular since the launching in 1995 of the R.V. *Marion Dufresne II* and of its Calypso corer that allows to collect very long cores. This cellar is unique because it naturally maintains the sediment in perfect conditions for years. However, the storage of cores was not optimized. Other samples and containers started to accumulate. The cellar became largely messy and apparently saturated. A re-organization was critically needed.

A small group at LSCE led by Camille Wandres (AI BIATSS, CliMag group) and Anouk Villedieu (CDD, Paleocean group) accomplished an enormous work reorganizing, cleaning and optimizing the space. Temperature and humidity measured over a full year appear to be much more uniform in this

repository than in the space available in the underground of the building 701 at the Orme des Merisiers. The repository space was therefore kept for sediments and the other samples were moved to the 701. The storage of sediment cores was rationalized, old “forgotten” containers and not labeled old samples were thrown away. Space was cleaned and freed for new shelves receiving the cores piled up in the corridors.

The “new” core repository now allows an easy access to the stored sediment with free corridors and well-organized shelves. The room dedicated to the sampling is also cleaned. Additional space is now available to receive the cores that will be collected in the future during cruises organized by LSCE scientists.

This reorganization constitutes a remarkable improvement in the quality of the storage of our invaluable sedimentary archives. It further ensures the quality of sediment sampling, which is the essential step preceding laboratory measurements.

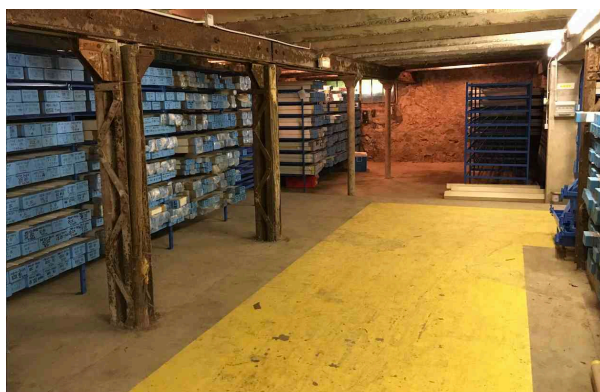


Fig. 1. Newly organized core repository